Origin of Precambrian Granulites from North-central China

by

Mark D. Boryta

Submitted in partial fulfillment
of the requirements for the degree of

Doctor of Philosophy in Geochemistry

Department of Earth and Environmental Sciences
New Mexico Institute of Mining and Technology
Socorro, NM
January 28, 1997

Acknowledgements

This research was sponsored in part by U.S. National Science Foundation grant INT-8802506 to K.C. Condie and by China National Science Foundation grant 4870147 to X.L. Qian of Peking University. Some support was also received from a New Mexico Tech research grant. Samples for INAA were irradiated at Sandia National Laboratories, Albuquerque, NM, and I appreciate the help of the reactor staff. Suggestions by my committee, Drs. Andrew Campbell, Kent Condie, David Norman and Maureen Wilks, have greatly improved this work.

Very special thanks are due to my advisor, Dr. Kent C. Condie, for his patience and oversight throughout the project. He cannot realize the positive effect of his wisdom and humor on me through the numerous digressions upon which I embarked, both intellectually and otherwise. I can only hope to repay him in part by exercising the vision of education that he imparted to me.

Special thanks are also due to Dr. David Johnson, whose longstanding and vocal belief in my abilities helped me through the "tunnel." Pat Mills watched over me as my guardian angel.

Jinzhong Liu was my silver-tongued partner in the field - without him, I would probably be stuck somewhere in Zhangjiakou waiting for permission from the provincial government. Xianglin Qian provided much-needed logistical support, as well as the occasional proper word in the proper ear.

Michael, Shirley, Joan, and Gerry all provided no small measure of support, both financial and moral. Thanks also to Nina, for giving me a life worth living, during my struggle and ever after.

Abstract

The northern border of the North China Craton is marked by a mountain chain composed in part of Late Archean/Early Proterozoic rocks. These rocks, including mafic dikes and sediments, have been metamorphosed to the granulite facies. The metamorphism was responsible for partial melting in the metasediments (khondalites) to form granitoids.

Chemical analyses of mafic dikes from the Hunyuanyao region in the central portion of this belt reveal three distinct groups of rocks. Group 1 dikes are metamorphosed tholeiitic basalts derived from a lithospheric mantle source region that was variably enriched in large ion lithophile elements (LILE). Group 2 dikes are chemically similar to norites and are derived from a light rare-earth element (LREE)-enriched refractory mantle source region. Group 3 dikes are metamorphosed high-Mg tholeiitic basalts that are chemically similar to modern mid-ocean ridge basalts. They are derived from a depleted mantle source region. The variability of mantle sources of the dikes is similar to that found in other granulite terranes, such as Scourie (Scotland), and indicates that the mantle had developed such heterogeneities by Late Archean time.

Khondalites (a suite of granulite-facies aluminous metasedimentary rocks), from the region between Hunyuanyao and Liangchen, are the equivalents of shales (sillimanite-garnet gneisses, SGG), siltstones, sandstones and/or graywackes (quartz-garnet gneisses, QGG) and tonalitic volcanic or volcaniclastic rocks (quartz-feldspar gneisses, QFG). Their protoliths are distinguished from paleosols based on lateral extent, thickness, and compositional similarities to modern and ancient shales such as PAAS. The provenance is interpreted to be chiefly composed of granitic material with minor basalt, but which did not include REE-fractionated material such as Archean tonalite. SGG have trace element signatures similar to sediments deposited near continental and oceanic island arcs, and QGG have chemical affinities to sediments deposited near a passive margin. These data suggest that the depositional environment of these sediments was similar to a modern back-arc basin.

In the Liangchen region, metamorphism of the khondalite suite has resulted in the production of granitoid magmas. The melt-forming reactions probably progressed from a muscovite dehydration melting reaction to a biotite dehydration melting reaction. The magmas are preserved in various stages of separation from restite material, as reflected by granitoid chemical compositions. Group 1 granitoids (granodiorites) have compositions similar to parent khondalites. Such similarity may have come about by incorporation of restite in the magma, as supported by the

degree of melting calculated for the group.. The Group 2 and 3 granitoids (granites) are derived by low degrees of melting and variable separation of residual minerals. Garnet appears to have controlled the heavy REE budget for these two groups, resulting in depletion of HREE as garnet was left behind in the residue. This separation is supported by the occurrence of garnet-rich schlieren.

Table of Contents

Table of Contents, continued

List of Figures

List of Figures, continued

List of Tables

Introduction

The granulite belt marking the northern boundary of the North China Craton (fig. 1) presents a geological situation that is ideal for studying the processes of crustal formation and differentiation at an important juncture in the history of the Earth. The granulite belt is of Late Archean/Early Proterozoic age (Qian et al., 1985) and contains a variety of rock types, including suites of mafic dikes, metamorphosed sedimentary rocks, and granitic intrusives that are derived from the sediments. Their preservation and the availability of structural and geochronological data provide an appropriate framework for this geochemical investigation.

There is much debate about the character of crustal formation and differentiation at the end of the Archean. Kröner (1991) and Davies (1995) review arguments that plate tectonic processes were common in the formation of crust in the Early Proterozoic, but that the Earth was probably too hot for such processes to have operated in the Early Archean.When and how the transition occurred remains a mystery that must be solved if we are to fully understand Earth processes and evolution.

Three geochemical studies are presented here, along with discussions on how their results bear on crustal evolution. The first is a study of the mafic granulites that appear as dikes cutting across the central portions of the granulite belt. The crust of the Earth grows by mafic contributions from the mantle, and the mantle from which crust has been extracted thus develops a suite of heterogeneities (components) (Wood, 1979; Pearce, 1983; Zindler and Hart, 1986; Hart and Zindler, 1989; Cattell and Taylor, 1990).

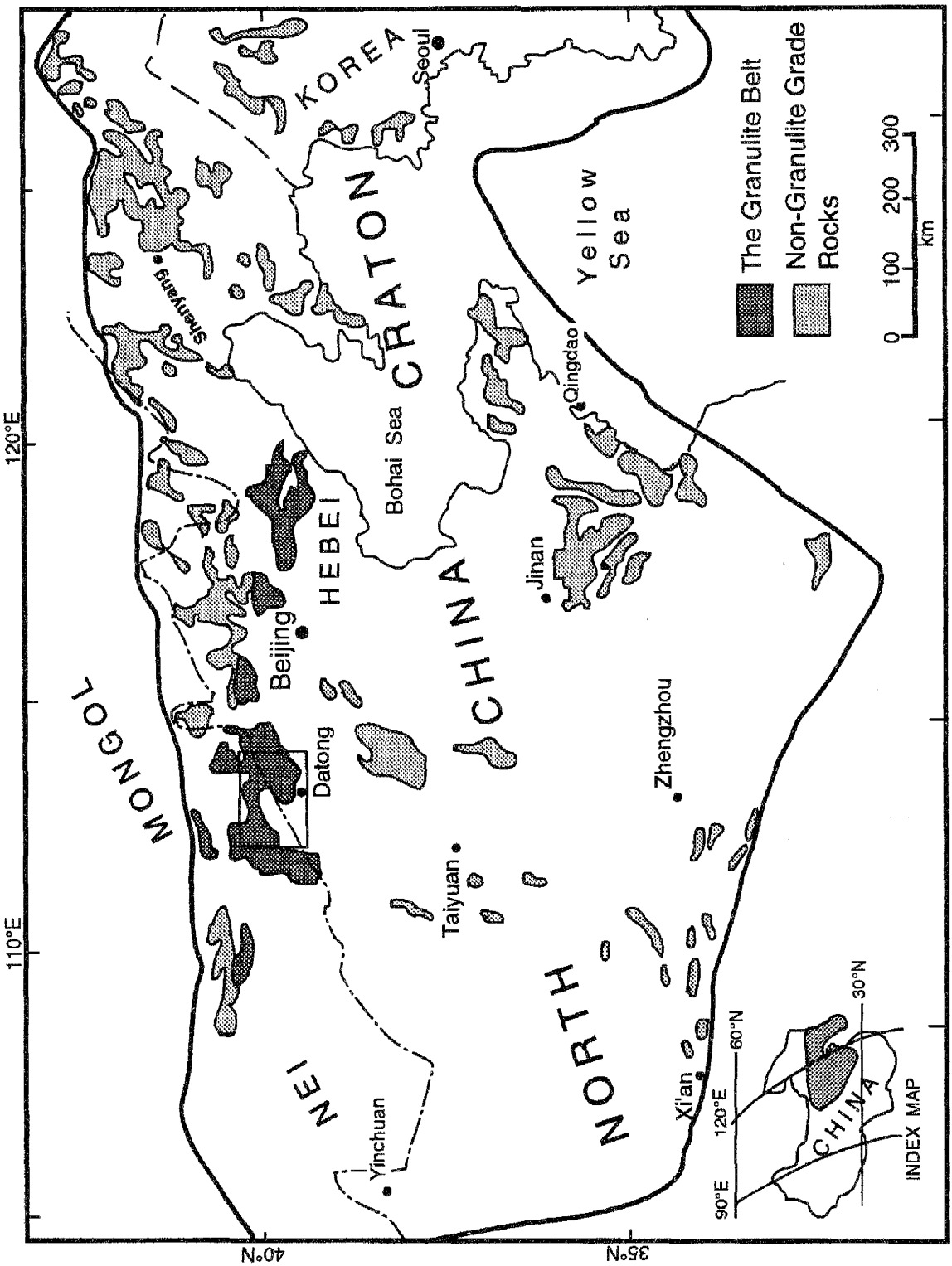

Figure 1: The North China Craton showing major exposures of Archean to Early Proterozoic rocks (after Condie et al., 1992). The boxed area is shown in detail in fig. 2.

The identification of mantle components and the timing of their development are important in understanding the evolution of the Earth. We can identify mantle components by geochemical modeling of the source from which mafic igneous rocks are derived. Geochemical variations in dikes of the granulite belt indicate that they are derived from differently-evolved compositions in the underlying mantle.

The second study is of compositional variations in a suite of Late Archean/Early Proterozoic metamorphosed sedimentary rocks. In general, weathering and sorting tend to alter the bulk chemical composition of sediments (Nesbitt et al., 1980; Stattegger, 1987; Condie et al., 1994; Gao and Wedepohl, 1995). Some elements are transported without fractionation from the source region to the site of deposition, however, and these elements may reflect the general composition of the region from which they are derived (Taylor and McLennan, 1985; Roser and Korsch, 1988; Condie and Wronkiewicz, 1988, 1990). By carefully examining the chemical character of sedimentary rocks, we can characterize the composition of the source from which they are derived. This, in turn, gives insight into crustal differentiation when we consider the geologic processes necessary to form the protoliths of those sediments. The variations in the compositions of metasedimentary rocks collected from the Nei Mongol granulite belt suggest that there are two separate source regions for the sediments: one source dominated by tonalite-trondhjemite-granodiorite gneiss (TTG), and another by a mixture of granite (*sensu stricto*) and mafic rocks, with little or no contribution from TTG.

The third investigation is a geochemical study of the transformation of the metasedimentary rocks into granitoids by partial melting. There has been a considerable

amount of work done on geochemical modeling of the origins of granitoid magmas, and the concept of the inclusion of residual material in the melt has become widely accepted (Wall et al., 1987; Wickham, 1987; Watt and Harley, 1993; Evans and Hanson, 1993). Most studies have focused on theoretical aspects of magmatic differentiation, while a few have considered experimental evidence. Few studies have dealt with detailed geochemical analyses of naturally-occurring samples of the three components involved in melting (source, segregated melt, and residue). The data presented herein support a model of granitoid magma generation in which residual minerals control key elemental distributions in the melt by various mechanisms.

Geologic Setting of the North China Granulite Belt

Late Archean/Early Proterozoic rocks are exposed throughout the North China Craton (Sino-Korean Paraplatform of Huang, 1978). The granulite belt forming its northern margin extends from eastern Hebei Province westward about 1000 km into Nei Mongol (fig. 1). It consists of highly metamorphosed volcanic and sedimentary supracrustal rocks and mafic and granitoid intrusives. The rocks within the belt have been divided into three groups; from east to west (and from oldest to youngest), these are the Qianxi Group, Miyun Group, and the Jining Group (Cheng, 1986). These are divided into five lithologic assemblages by Qian et al. (1985), as described below. The geologic relationships between the five assemblages remain unclear.

Assemblage I (lower part of the Qianxi Group), in the eastern part of the belt (eastern Hebei Province), comprises intercalated mafic to felsic granulites with local

pyroxene-bearing banded iron formation (BIF) and pods of ultramafic rock. Assemblage II (upper part of the Qianxi Group), exposed in western Hebei Province, comprises gray (tonalitic) gneisses and garnet-bearing two-pyroxene mafic and intermediate-felsic granulites associated with minor BIF. Ultramafic pods and lenses are small but abundant in Assemblage II. Assemblage III (lower part of the Jining Group), also called the *gray gneiss association*, occurs from northwestern Hebei Province to Datong (fig. 2). It consists of enderbitic to charnockitic gneisses with minor mafic granulite dikes and garnet-bearing quartzofeldspathic granulites. Assemblage IV (upper part of the Jining Group), hereafter termed the *khondalite suite*, comprises sillimanite-garnet-plagioclase gneisses with associated graphite-bearing quartzofeldspathic gneisses. This assemblage is in contact with the northwesternmost exposure of Assemblage III near Hunyuanyao (fig. 2). Westward (in the region near Liangcheng), evidence for a partial melting event that affected the khondalite suite is preserved. Association V (lowermost Wulashan Group) is exposed in the westernmost portion of the belt and consists of hornblende-(± biotite)-plagioclase gneisses with lenses of amphibolite, BIF, and marble. In this westernmost region, a 20-m-thick band of porphyroblastic (K-feldspar crystals up to 5 cm across) mylonite occurs in the center of the section. Association V is lithologically distinct from the khondalites, and the two assemblages are separated by about 100 km in which there are no outcrops of Precambrian rocks (fig. 1); hence, the geological relationships between them are not presently understood.

Rocks as old as 3.5 Ga (Sm-Nd model ages) occur in the eastern part of the granulite belt (Jahn and Zhang, 1984; Jahn et al., 1987; Jahn, 1990a, b), and the main

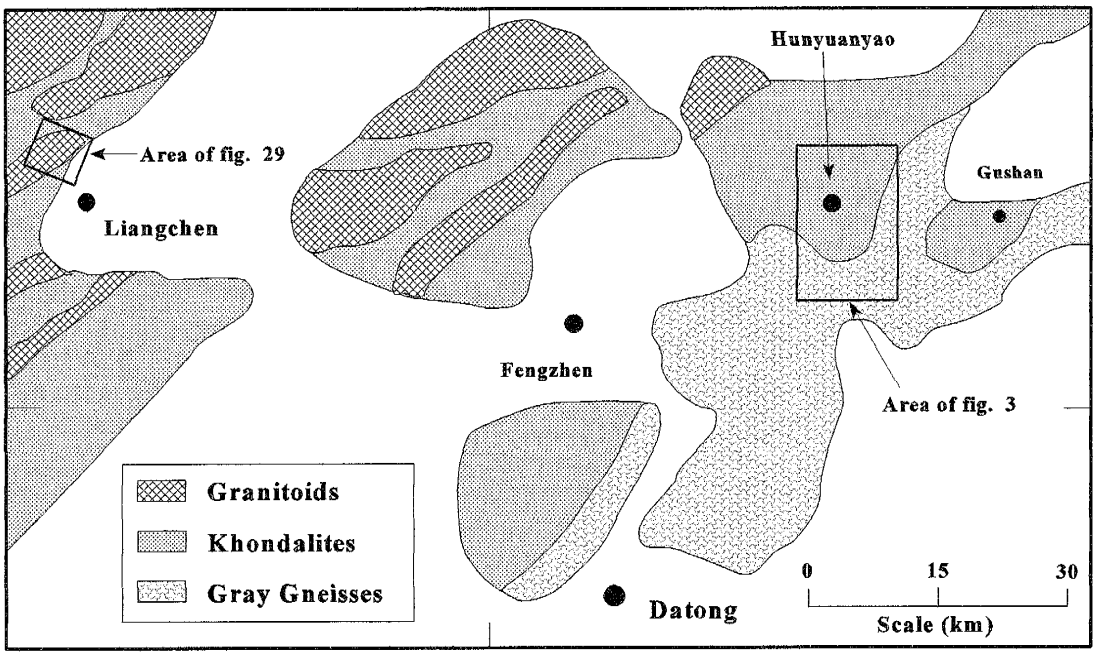

Figure 2: Generalized geology of the Datong area (after Condie et al., 1992). Mafic samples were collected from the Hunyuanyao area (box detail shown in fig. 3); granite samples were collected from area northwest of Liangchen (approximate box detail shown in fig. 29).

episode of metamorphism is dated at 2.6-2.3 Ga (Rb-Sr whole-rock and Sm-Nd model ages and U-Pb zircon ages) (Compston and Zhong, 1983; Jahn and Zhang, 1984; Liu et al., 1985). Preliminary Pb-Pb studies of single zircons collected from the Hunyuanyao-Datong area indicate metamorphic resetting between 2.45 and 1.96 Ga (J.J. Peucat, written comm., 1989).

Geothermobarometric studies of orthopyroxene-clinopyroxene and garnet-clinopyroxene pairs in felsic rocks indicate maximum temperatures and pressures of 770-790°C and 10-13 kb in the eastern part of the granulite belt (in eastern Hebei Province) and 770-920°C and 12-14 kb in the west (Datong-Hunyuanyao region) (Qian et al., 1985; Liu, 1989). Textural evidence for previous events has been obliterated.

Generalized Geology of the Study Areas

Rocks for this study were collected from the Hunyuanyao and Liangchen areas in the granulite belt north of Datong (fig. 2); sample locations in the Hunyuanyao area are shown in figure 3. (A detailed map for the Liangchen area is not available, but see fig. 19). Mafic samples were collected from the Hunyuanyao area northeast of Datong where the khondalite association is in contact with the gray gneiss association. Khondalites were collected from both the Hunyuanyao and Liangchen areas, and Precambrian granitic intrusives were collected from the Liangchen area.

The dominant rock types of the khondalite suite are sillimanite-garnet gneiss (SGG), garnet-biotite gneiss (QGG), and quartz-rich gneiss (QFG) in the approximate proportions 5:3:2, respectively (Condie et al., 1992). These are exposed in a continuous section at least 2 km thick. Throughout the region, incomplete outcrop exposure veils an accurate overall assessment, which may be further complicated by structural replication, hence this thickness is a minimum estimate. Individual SGG are banded in outcrop and up to 100 m thick, while the QGG thicknesses range from 10 cm to 3 m. QFG outcrops are usually small (<1 m), and thin lenses of marble are locally present. In the Liangchen region only, the khondalites are interlayered with granitic leucosomes and small plutons.

Qian et al. (1985) have interpreted the protoliths of the khondalite suite to have been deposited unconformably on the gray gneiss association. The relatively constant "stratigraphy" of the khondalites exposed near the contact with the gray gneisses in the Datong-Gehuyao area contrasts with the variability of rock types in the adjacent gray

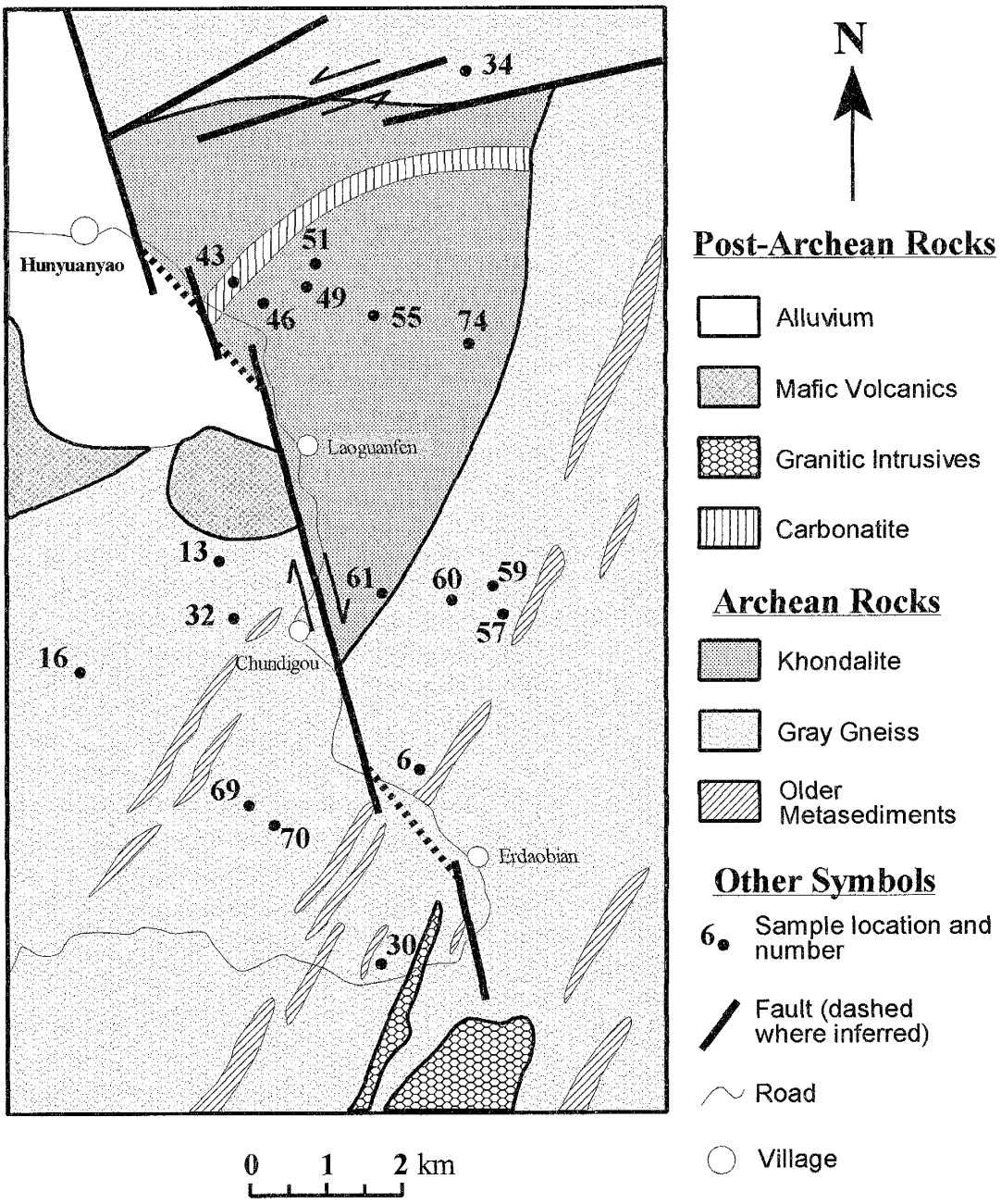

Figure 3: General geology (after Liu, 1989) and mafic granulite sample locations, Hunyuanyao region. Mafic dikes are oriented NE-SW, parallel to regional foliation; individual units are too small to be shown at this scale.

gneisses. This interpretation is consistent with a preliminary U-Pb zircon age of 3323±44 Ma from a single zircon collected from the gray gneisses near Sheijiango, about 60 km

east of Datong (Kröner et al., 1987), while preliminary, possibly metamorphic ages from single zircons collected from khondalites in the Datong-Hunyuanyao region are 1965±5 to 2450±4 Ma (J.J. Peucat, written comm., 1989). However, sedimentary structures indicative of the mode and direction of transport are nowhere preserved in the khondalites, and nowhere is the contact between these associations clearly exposed, so evidence for this interpretation remains equivocal.

In the Hunyuanyao area, a thin (1-2 m thick), highly sheared graphite-rich horizon marks the apparent base of the khondalite section. This horizon is being mined for the graphite. In the Gushan area (fig. 2), this "basal" graphite layer has been sheared into lenses that form some of the largest graphite deposits in northern China (Liu et al., 1989). These horizons have been interpreted as an original, continuous marker unit of the khondalite sequence (Qian et al., 1985). An alternative interpretation for their position is that the khondalite suite is thrust over the gray gneisses, and the graphite layers represent structural weaknesses that facilitated displacement. This latter interpretation is supported by the presence of nappe structures in retrograde granulites in the Zhangjiakou area to the east (in grey gneiss association; fig. 1), manifestations of an intense compressional event. The protoliths of the khondalite suite appear therefore to have been deposited unconformably on the gray gneiss association, and there may have been a small or large amount of displacement along the boundary subsequent to their deposition.

Near Liangchen in the west-central portion of the granulite belt (fig. 2), the granitoids of this study occur as small bodies up to 1 km across; they are conformable with, and intrude, the khondalite sequence. In this area, a few Precambrian mafic dikes

also intrude the khondalites. The khondalites and dikes contain mineral assemblages indicative of equilibration under granulite-facies conditions (see above). Nowhere are mafic dikes seen to intrude granitoid bodies. Khondalites appear banded and preserve an S-C structural fabric (Liu, 1989), indicating several pulses of deformation (see below). Metamorphism has induced incipient partial melting in the khondalites, and segregations of melt thicken as a quartz + feldspar leucosome develops (Plate 1). Thin pods and lenses of relatively inclusion-free garnet or sillimanite rarely are left as melanosomes; more often, however, these residual minerals are entrained in the melt. The proportion of melt in the khondalites increases toward the granitoid bodies. Within the granitoids, garnets may form glomerocrysts up to 1 cm across (Plate 2). Different granitoid bodies range from fine-grained equigranular (average grain size about 4 mm) to pegmatitic (with feldspar crystals approaching 5 cm in length). Compositional banding in the granitoids is much less well developed than in the khondalites. Feldspars show bent or broken cleavage traces (see Appendix D).

S-C foliation orientations suggest that one, or possibly two, Precambrian deformational events affected the rocks of the Datong region (Liu, 1989). Most mafic dikes in the Hunyuanyao area are oriented parallel to the primary foliation. Some dikes are straight and continuous, and others are folded along with the country rocks, perhaps indicating mafic intrusion at several times during metamorphism. Uplift to the present erosional level likely occurred during Mesozoic time when discordant granitoid intrusives (not sampled in this study) were emplaced.

Sampling and Analytical Techniques

Sampling was concentrated in the Hunyuanyao and Liangchen areas where detailed structural data are available (Liu, 1989). Extreme care was taken to avoid fractured and weathered surfaces. Samples were crushed in a chipmunk jaw crusher, ground between porcelain plates to the size of sand or finer, and the sample was split. The splits used for INAA and major element analyses were further ground to a fine powder with an agate mortar and pestle. The split from which XRF trace element analyses are derived was further ground using a tungsten-carbide TEMA mill.

Major and trace elements Y, Zr, Nb, Rb, Sr, and Ni were determied by X-ray fluorescence (XRF) using an automated Rigaku 3064 XRF spectrometer coupled with a PDP-11 computer and in-house software at the New Mexico Bureau of Mines and Mineral Resources in Socorro. Two techniques were involved, following the methods of Norrish and Hutton (1969) and Norrish and Chappell (1977). Fusion disks were prepared for major-element analyses, and pressed powder pellets were prepared for trace-element analyses. Precision and accuracy for XRF are <10% for most elements and <15% for all elements (Boryta, 1988).

Trace elements Cs, Th, U, Sc, Cr, Co, Hf, Ta, La, Ce, Nd, Sm, Eu, Tb, Yb, and Lu were determined by instrumental neutron activation analysis (INAA) using methods similar to those described by Jacobs et al. (1977) and Gibson and Jagam (1980). 200-300 mg of sample powder were sealed in polyethylene vials and irradiated in the Annular Core Research Reactor facility at Sandia National Laboratories in Albuquerque, New

Mexico. Gamma-ray counts were conducted from 7-12 days and from 35-45 days following irradiation using twin coaxial intrinsic Ge-crystal detectors and and Nuclear Data 581 analog-to-digital converters coupled with a Vax WorkStation 3100. Data processing was completed using an updated version of TEABAGS (Trace Element Analysis By Automated Gamma-ray Spectroscopy) (Lindstom and Korotev, 1982). After flux gradient corrections were applied (Chappell and Hergt, 1989), precision and accuracy for INAA are <5% for most elements and <10% for all elements (Boryta, 1988).

Part I: Origin and Source of Precambrian Mafic Dikes of the Northern Border of the North China Craton

Introduction

Mafic dikes occur in a variety of tectonic settings related to crustal extension. Sigursson (1987) has shown that Icelandic mafic dikes may be emplaced by lateral propagation from magma chambers located at high levels in the crust. Mohr (1987) and Condie (1996) have argued that, despite probable crustal contamination, certain elemental ratios of mafic dikes can be used under certain circumstances to constrain the chemical composition of their source. To understand the evolution of the earth's mantle, Weaver and Tarney (1980, 1981a,b), Sheraton and Black (1981), Tarney and Weaver (1987), Bernard-Griffiths et al. (1987), and Sheraton et al. (1990) have investigated the geochemical characteristics of Precambrian mafic granulites. These workers have shown that small-scale heterogeneities in the subcontinental lithosphere (i.e., dike sources) were distinct in the early Precambrian.

In order to constrain the chemical composition and variation of the Archean mantle beneath the northern margin of the North China Craton, samples were collected from granulite-facies mafic dikes from the Hunyuanyao area of Nei Mongol.

General relationships

In the Hunyuanyao area (fig. 3), dikes crosscut both the khondalite suite and gray gneiss associations. The dikes generally parallel the regional foliation, trending roughly NE. Outcrops of dikes are chiefly small, partly covered by loess, and sometimes sheared

into lenses, and hence it is impossible to determine ages of dikes relative to one another in the field. Contacts vary from sharp to indistinct, but relationships to country rock, preserved through granulite-facies metamorphism, indicate that the dikes are intrusive. This origin is different from that interpreted for the Archean mafic granulites in eastern Hebei Province (Qianxi Group), whose protoliths were probably extrusive volcanic flows (Jahn and Zhang, 1984; Jahn, 1990b). However, the Hunyuanyao and eastern Hebei mafic rocks have similar ranges in major and trace element compositions. Minimum absolute ages for the suite are set by the age of the granulite metamorphism at 1.9-2.4 Ga (J.J. Peucat, written communication, 1989). Dikes vary in thickness from 5 cm to 1 m; only dikes thicker than 40 cm were sampled for chemical analyses.

Petrography

The dikes are divided into three groups based chiefly on their rare-earth element distributions; major elements and petrographic analyses support these groupings, but show significant overlap among the groups. Thin sections reveal that the dikes are recrystallized under lower granulite-facies conditions (Appendix A) and have undergone local amphibolite-facies retrogression. Most samples contain granoblastic plagioclase and two pyroxenes; quartz and olivine are missing in the samples. Reddish-brown biotite is minor in most samples. Slightly to moderately sericitized plagioclase is found in four samples.

Group 1 dikes (10 samples) are the most common (Plate 3a, b), and have equigranular granoblastic textures, suggesting that the minerals developed under upper

amphibolite- to granulite-facies conditions. They contain plagioclase (An_{45-55}) (35-50%) that is sometimes slightly sericitized. Clinopyroxene (20-40%) is always more abundant than orthopyroxene (0-20%). In most samples, reddish-brown or brownish-green hornblende (10-30%) has partially replaced pyroxenes. In a few samples, hornblende is partially replaced by minor reddish-brown biotite. In one sample (30), up to 35% chlorite has replaced pyroxene and hornblende. Opaque minerals and apatite are present in all samples; one sample (69) also contains rare zircon. Sample 43 contains subequal proportions of plagioclase (35%), clinopyroxene (30%), and olive-brown hornblende (30%), which has replaced pyroxene. Minor reddish-brown biotite (5%) has partially replaced hornblende. This sample contains trace amounts of opaque minerals and apatite; epidote occurs as small granules along fractures.

Group 2 dikes (4 samples, Plate 4a, b) contain abundant brownish-green or reddish-brown hornblende (25-50%) and varying proportions of plagioclase (10-45%) and clinopyroxene (5-45%). Textures are equigranular granoblastic. One sample (55) contains 20% orthopyroxene and only a trace of plagioclase. Hornblende typically replaces pyroxene, and a few hornblende grains are partially replaced by biotite. Plagioclase grains are equant. Anorthite content was not determined because most grains show pericline or complex twinning and bent cleavage traces. Opaque minerals are abundant, and some of them are exsolved from retrograde hornblende. Apatite is present in all four samples, and zircon is notably absent.

Group 3 dikes (2 samples, Plate 5a, b) are the only dikes that contain garnet (10-25%). The textures are equigranular granoblastic, although garnet porphyroblasts are

elongated parallel to a weakly developed foliation. Other major minerals are plagioclase (20-25%; anorthite content determination precluded by sericitization), clinopyroxene (30-45%), and orthopyroxene (10-15%). Sample 46 also contains 10% brown hornblende and almost 5% combined biotite and chlorite, which are formed at the margins of pyroxene grains. Sample 49 contains thin chlorite veinlets. Opaque minerals and apatite are present in trace amounts, and again, zircon is absent.

Samples from two dikes that were analyzed do not fit in any of the above groups. Sample 6 consists of 50% dark brownish-green hornblende, 35% plagioclase (An_{55}), and 12% diopside. This sample has about 2% opaque minerals and up to 1% apatite. The abundance of apatite is reflected in its high P_2O_5 concentration (1.05%). Sample 61 contains about 50% zoned plagioclase (cores = An_{55}, rims = An_{45}), 40% clinopyroxene, and 10% orthopyroxene. This sample contains no hornblende. Exsolution lamellae are present in some of the clinopyroxene grains. Orthopyroxene occurs as tabular laths. Trace minerals include minor biotite (replacing pyroxene), opaque minerals, and apatite.

Alteration

The equant rather than euhedral shapes of the hornblende in the dikes suggests a metamorphic rather than igneous origin for this mineral (Sheraton et al., 1990). The equigranular granoblastic textures and plagioclase + hornblende + two-pyroxene (± garnet) mineral assemblages found in most of the dikes indicate recrystallization at granulite-facies conditions. Nearby, metapelitic rocks also contain mineral assemblages indicative of granulite-facies conditions, including the assemblage K-feldspar +

sillimanite + quartz + plagioclase (Condie et al., 1992). The lack of muscovite in the metapelites, the very slight sericitization of plagioclase and the rare presence of retrograde chlorite in the mafic dikes suggests that retrogressive fluids were localized rather than pervasive. Therefore, the assemblage hornblende + plagioclase ± diopsidic clinopyroxene ± hypersthene in mafic rocks is likely the result of metamorphic recrystallization at lower granulite-facies conditions.

Relatively anhydrous granulite-facies metamorphic assemblages can result from either of two processes. One process is the elevation of temperatures and pressures, which causes hydrous phases (e.g., muscovite and biotite) to become unstable; liberated H_2O-rich fluid can cause melting in the nearby felsic gneisses or carry away soluble ions. Escape of H_2O (dehydration) generally results in a decrease in the concentrations of large-ion-lithophile elements (LILE: Na, K, Rb, Cs, Pb, Th, and U) (Weaver and Tarney, 1983). Another process involves the influx of a CO_2-rich fluid phase, which lowers the activity of an H_2O-rich fluid. This process has been identified in granulites from southern Norway (Touret, 1971) and southern India (Condie et al., 1982; Allen et al., 1985). Influx of CO_2 can also mobilize the high field-strength elements (HFSE: Ti, Y, Zr, Nb, Hf, and Ta) and LREE (Mysen, 1979; Wendlandt and Harrison, 1979) as soluble carbonate complexes.

If a relatively pervasive influx of a CO_2-rich fluid were responsible for granulite mineral assemblages, several features would be manifest in the rocks (Newton, 1987): 1) the dehydration of amphibole to form orthopyroxene; 2) an abundance of CO_2-rich fluid inclusions in quartz; 3) coexistence of lower-grade rocks with hypersthene-bearing

granulites, implying passage of a CO_2-rich fluid along localized zones; 4) variable LILE depletion; 5) depletion of CaO, FeO, Fe_2O_3, and MgO and slight enrichment in SiO_2; and 6) enrichments in Ta, Nb, Cr, Co, and Sc and depletions in REE and Y. In the samples collected for this study, hornblende is abundant, and rare fluid inclusions appear to be H_2O-rich. The grade of metamorphism is uniform and there is no evidence for incipient charnockitization in surrounding felsic gneisses. In addition, the depletions in major elements and changes to HFSE (predicted in numbers 5 and 6 above) are not observed. When compared to unaltered mafic igneous rocks (Beswick and Soucie, 1978), the major element distributions (with the exception of Na) appear to have remained immobile during metamorphism (fig. 4).

The only feature consistent with a local influx of a CO_2-rich fluid is the observed variability in LILE concentrations (especially Cs, Rb, Th, and U). Such variability of incompatible elements cannot be generated by igneous fractionation processes alone (e.g., Lundstrom et al., 1994). Dikes of this study (for which U contents are above the lower limit of detection) have an average Th/U ratio of about 2.8, but samples 59 and 61 have a ratio of 7.1. Keppler and Wyllie (1990) showed that U can be removed preferentially to Th in the presence of CO_2-rich fluids. However, the samples in this study having U concentrations below the limit of detection also have low Th contents, and samples with high Th/U ratios have average U but high Th contents. Overall, results suggest that CO_2 was only locally (if at all) important in causing dehydration reactions in the Hunyuanyao area. The extreme depletions of LILE are thus attributed to metamorphic dehydration processes.

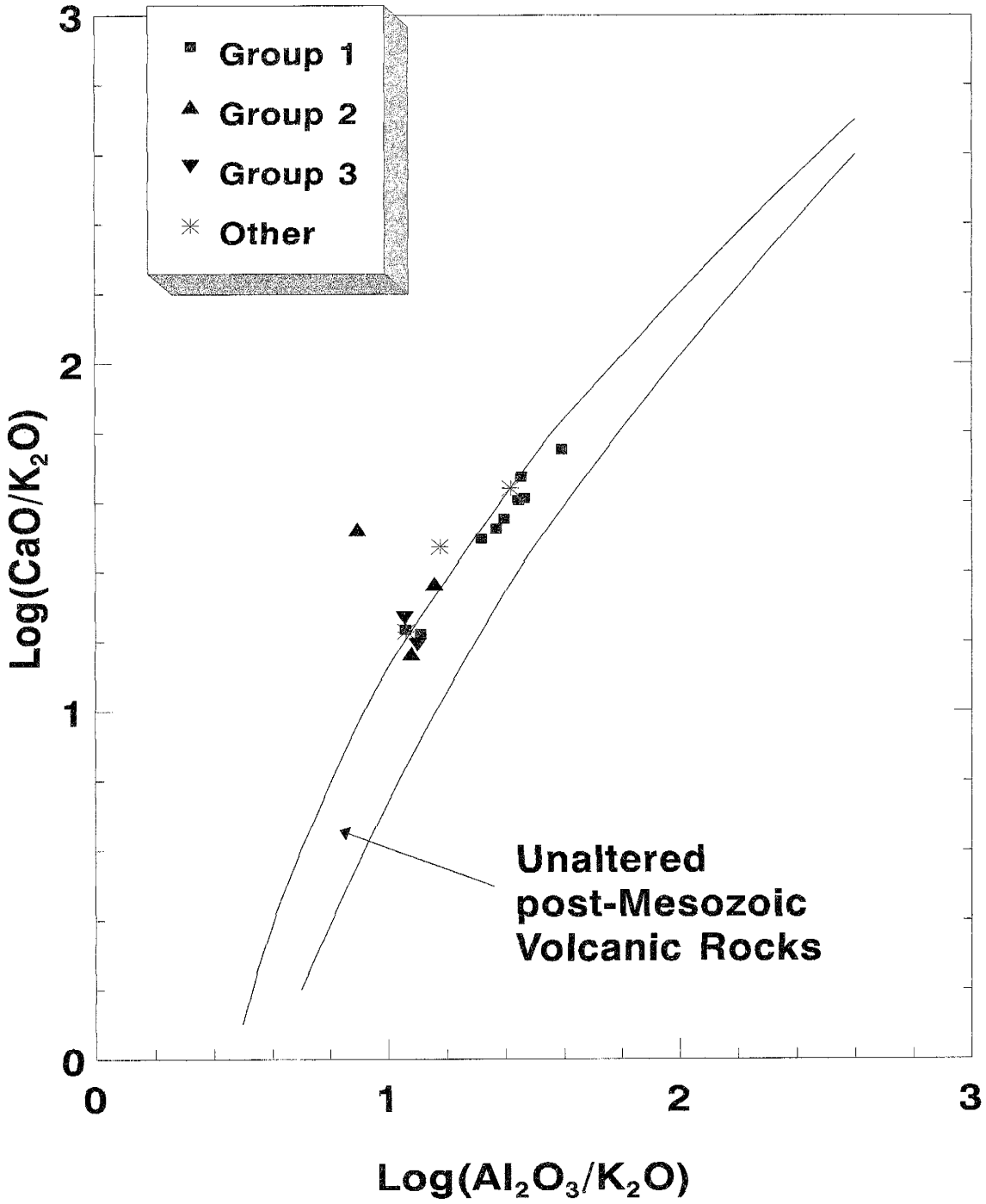

Figure 4: Alteration screen (Beswick and Soucie, 1978) shows similarity in composition between Hunyuanyao mafic dikes (this study) and relatively unaltered post-Mesozoic volcanic rocks.

Major Element Distributions

Major- and trace-element data are presented in Table 1. Group 1 dikes are tholeiitic and show a small range in SiO_2 content (47-51%). CaO decreases (11.3-9.3%), TiO_2 and Fe_2O_3T increase (0.72-1.9% and 12.0-17.4%), and SiO_2 and Al_2O_3 (fig. 5) remain approximately constant with decreasing Mg number.

Group 2 dikes are compositionally similar to norites or basaltic komatiites (after Jensen, 1976), but there is no petrographic evidence for relict cumulus olivine or spinifex texture. This group is characterized by high Mg numbers (67-76), intermediate Fe_2O_3T (10.7-15.6%), and low TiO_2 (0.5-0.6%) contents. Sample 55 has high CaO (14.4%), Mg number of 76.1, and low Al_2O_3 (6.2%), features consistent with the dike's abundance of clinopyroxene: this sample contains about 50% clinopyroxene and only a trace amount of plagioclase. Samples 59 and 60 have high Na_2O and K_2O (4.6-5.6%, and 1.16-1.55%, respectively). These high abundances suggest that element remobilization may be important in these dikes; petrographic evidence supports this contention (Appendix A). Sample 59 contains 2-3% magnetite that is exsolved from Fe-rich hornblende during retrograde growth of Fe-poor hornblende. Sample 60 contains plagioclase that is more extensively sericitized than the other samples.

Group 3 dikes are geochemically similar to high-Mg tholeiites. Mg numbers (both 58) and other major element distributions overlap with those of Group 1 (fig. 5).

Sample 6 has anomalously low SiO_2 content (40.8%) and high Fe_2O_3T, TiO_2, MgO, CaO, and P_2O_5, presumably reflecting the abundances of hornblende, Fe-Ti oxides,

Table 1: Major and trace element data for mafic dikes, Hunyuanyao region, Nei Mongol, China

	Group 1 dikes									
	13	16	30	32	34	43	51	57	69	70
SiO_2	50.49	50.47	49.83	50.21	49.87	50.11	48.92	50.04	47.38	51.03
TiO_2	0.97	1.79	1.48	0.91	0.77	0.79	1.29	0.80	1.83	0.86
Al_2O_3	13.01	12.91	12.92	14.30	13.98	13.66	12.84	13.66	12.38	13.33
Fe_2O_3T	13.87	15.56	15.76	12.48	12.21	10.60	14.97	12.08	16.38	13.07
MnO	0.21	0.24	0.25	0.18	0.21	0.16	0.23	0.20	0.40	0.21
MgO	6.45	5.46	5.89	6.01	8.20	8.23	6.38	7.37	7.41	7.92
CaO	10.35	9.16	10.21	10.97	11.11	10.99	10.52	10.77	11.25	11.01
Na_2O	4.09	3.28	3.02	4.37	3.24	4.27	3.71	4.46	2.43	1.88
K_2O	0.43	0.92	0.48	0.45	0.33	1.09	1.03	0.54	0.40	0.59
P_2O_5	0.11	0.21	0.16	0.12	0.08	0.10	0.12	0.10	0.15	0.09
Rb	11.2	29.4	6.3	10.4	6.3	14.9	10.4	10.1	6.1	11.7
Cs	0.2	0.36	0.16	0.1	0.18	nd	0.18	0.19	0.19	0.32
Sr	199	216	174	215	144	293	283	224	173	152
Pb	15	18	14	15	14	16	22	16	20	17
Th	0.65	2.57	0.24	0.64	0.47	1.57	0.54	0.55	0.09	0.76
U	nd	0.67	nd	nd	nd	0.6	nd	nd	nd	nd
Sc	48.8	48.7	48.6	49	48.8	47.8	58.9	47.9	55.5	52
Cr	92	82	74	66	166	143	168	192	68	181
Co	61	53	58	59	59	44	70	60	53	0.61
Ni	54	50	33	42	69	36	61	67	47	48
Y	24.4	41.6	35	23.3	17.8	19.1	37.4	21.1	47.6	21.4
Zr	68	130	98	73	51	55	89	64	106	56
Nb	5.4	7.7	7.3	5.0	4.2	7.2	8.9	4.9	12.1	5.0
Hf	2.2	5.77	2.76	1.96	1.52	1.57	3.29	1.65	4.66	1.64
Ta	0.22	0.54	0.38	0.23	0.11	0.59	0.35	0.13	0.98	0.21
La	7.1	18.5	8.0	7.5	5.0	11.0	16.3	7.4	11.6	7.1
Ce	15.7	39.3	20.5	16.8	12.4	28.4	43.8	15.1	29.9	17.9
Sm	2.9	5.9	3.9	2.9	2.2	3.8	6.6	2.4	6.1	2.8
Eu	0.95	1.72	1.30	1.00	0.77	1.06	2.01	0.86	1.72	0.90
Tb	0.6	1.12	0.87	0.59	0.41	0.59	1.13	0.46	1.28	0.51
Yb	2.14	3.61	3.3	2.07	1.74	1.64	4.37	1.81	4.58	2.01
Lu	0.38	0.61	0.57	0.38	0.3	0.28	0.73	0.31	0.76	0.33
Mg#	51.2	44.2	45.7	52.1	60.2	75.5	49.0	57.9	50.5	57.7
$(La/Yb)_N$	2.01	3.11	1.47	2.20	1.74	4.06	2.26	2.48	1.53	2.14
Eu/Eu*	0.90	0.82	0.89	0.95	0.99	0.84	0.89	1.01	0.77	0.92
Ti/Zr	85.5	82.5	90.4	74.7	90.5	86.1	86.9	74.9	103.5	92.1
La/Zr	0.10	0.14	0.08	0.10	0.10	0.20	0.18	0.12	0.11	0.13
Zr/Nb*	18.2	14.2	15.2	18.7	27.3	5.5	15.0	29.0	6.4	15.7
Zr/Y	2.79	3.13	2.80	3.13	2.87	2.88	2.38	3.03	2.23	2.62
Ta/Yb	0.10	0.15	0.12	0.11	0.06	0.36	0.08	0.07	0.21	0.10

nd: not detected or not determined. Fe_2O_3T: total Fe as Fe_2O_3. Mg#: MgO/(MgO + FeO), in molecular percent, where FeO = 0.79 Fe_2O_3T. $(La/Yb)_N$: La/Yb normalized to chondritic

Table 1: Major and trace element data for mafic dikes, continued.

	Group 2				Group 3		Other	
	44	55	59	60	46	49	6	61
SiO_2	48.9	49	48.48		48.47	47.69	40.76	49.41
TiO_2	0.53	0.53	0.48		0.95	0.82	1.62	0.96
Al_2O_3	10.3	5.97	14.9		14.52	14.67	11.64	13.71
Fe_2O_3T	14.14	11.69	10.33		13.51	12.8	16.55	13.41
MnO	0.2	0.2	0.17		0.25	0.22	0.21	0.21
MgO	14.79	16.57	9.57		8.55	7.76	12.17	7.47
CaO	9.13	13.92	9.95		9.81	13.03	12.58	12.5
Na_2O	1.31	1.32	4.24		2.47	1.76	2.71	1.76
K_2O	0.66	0.7	1.14		1.06	1.18	0.71	0.48
P_2O_5	0.03	0.1	0.75		0.1	0.07	1.05	0.08
Rb	13.8	27.94	14.08	26.91	38.72	48.11	6.5	11.05
Cs	0.49	0.79	0.16	nd	0.48	0.28	nd	1.14
Sr	35	225	291	790	524	777	514	174
Pb	23	16	11	10	32	15	19	18
Th	1.93	1.25	2.48	0.22	0.37	nd	0.77	5.52
U	0.46	0.49	0.35	nd	0.31	nd	nd	0.78
Sc	28.1	69.6	36.5	35	52.4	50.4	42.9	56.4
Cr	1370	768	567	141	357	307	162	351
Co	97	80	53	47	63	59	67	52
Ni	637	300	183	136	97	122	72	82
Y	14.3	13.7	13.9	14.6	28.1	16.7	31.2	20.3
Zr	46	54	50	51	51	37	57	52
Nb	4.9	4.6	4.5	3.7	4.9	4.3	7.9	4.4
Hf	1.33	1.4	1.37	1.18	1.46	0.93	1.79	8.05
Ta	0.16	0.09	0.16	0.11	0.14	0.11	0.18	3.11
La	8.4	11.3	16.4	12.6	3.2	1.4	25.3	24
Ce	18.4	29.4	29.9	30.8	8.3	4.7	79	45.8
Sm	2.2	4.2	2.2	2.7	2.6	1.8	15.8	7.5
Eu	0.55	1.16	0.71	0.81	0.86	0.77	4.42	0.58
Tb	0.4	0.33	0.32	0.36	0.64	0.5	1.34	2.52
Yb	0.91	0.83	1.38	1.37	2.8	2.04	1.74	7.91
Lu	0.16	0.14	0.24	0.23	0.51	0.34	1.46	1.44
Mg#	70.2	76.2	67.6		58.8	57.8	74.4	68.8
$(La/Yb)_N$	5.59	8.25	7.20	5.57	0.69	0.42	8.81	1.84
Eu/Eu*	0.71	1.04	0.99	0.95	0.85	1.06	1.03	0.18
Ti/Zr	69.1	58.8	57.6		112	133	170	111
La/Zr	0.18	0.21	0.33	0.25	0.06	0.04	0.44	0.46
Zr/Nb*	16.9	35.3	18.4	27.3	21.4	19.8	18.6	1.0
Zr/Y	3.22	3.94	3.60	3.49	1.81	2.22	1.83	2.56
Ta/Yb	0.18	0.11	0.12	0.08	0.05	0.05	0.10	0.39

meteorite. Eu* = $(Sm_N^2 \times Tb_N)^{1/3}$, where Sm_N and Tb_N are normalized to chondritic meteorite. Nb* = Ta × 17.

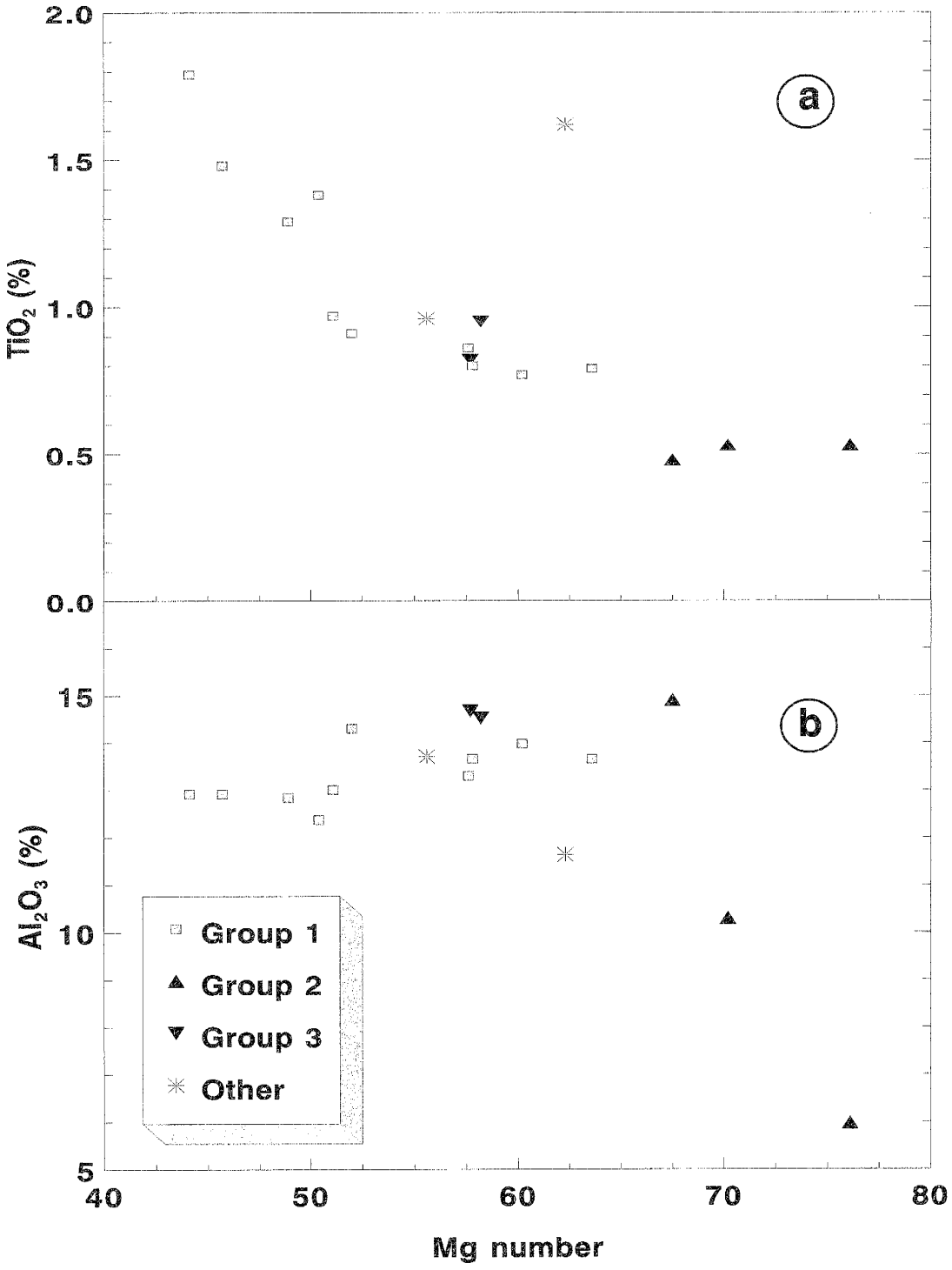

Figure 5: Mg number vs. (a) TiO_2 and (b) Al_2O_3 for mafic dikes.

and apatite. Sample 61 has major element abundances similar to Group 3 dikes, except for its notably lower K_2O content (0.46%).

Rare Earth Element (REE) Distributions

Chondrite-normalized REE distributions of Group 1 dikes (fig. 6a, b) are flat or gently sloping. LREE are slightly enriched ($(La/Yb)_N$ = 1.5-2.5); samples 16 and 43 are more LREE-enriched than the other samples with $(La/Yb)_N$ = 3.1 and 4.1, respectively (Table 1). Most of these have small or negligible negative Eu anomalies (Eu/Eu* = 0.9-1.0); Eu anomalies tend to become larger with decreasing Mg number (fig. 7).

Group 2 dikes are enriched in LREE ($(La/Yb)_N$ = 5.6-8.2, fig. 8a). Most have negligible Eu anomalies (0.95-1.04), but sample 44 has Eu/Eu* = 0.71. The four samples fall into two subgroups on the basis of HREE contents: samples 44 and 55 have slightly more fractionated HREE than samples 59 and 60.

The two Group 3 dikes have LREE-depleted distributions ($(La/Yb)_N$ = 0.69 and 0.42), similar to NMORB, and abundances are 10-20 × chondrites (fig. 8b). One sample (49) has a slightly positive (1.06), and the other (46) has a negative Eu anomaly (0.85).

Sample 6 has an unfractionated LREE but HREE-depleted pattern (fig. 9) with no Eu anomaly. Sample 61 has a flat REE pattern and an extreme negative Eu anomaly (fig. 6e; Eu/Eu* = 0.18).

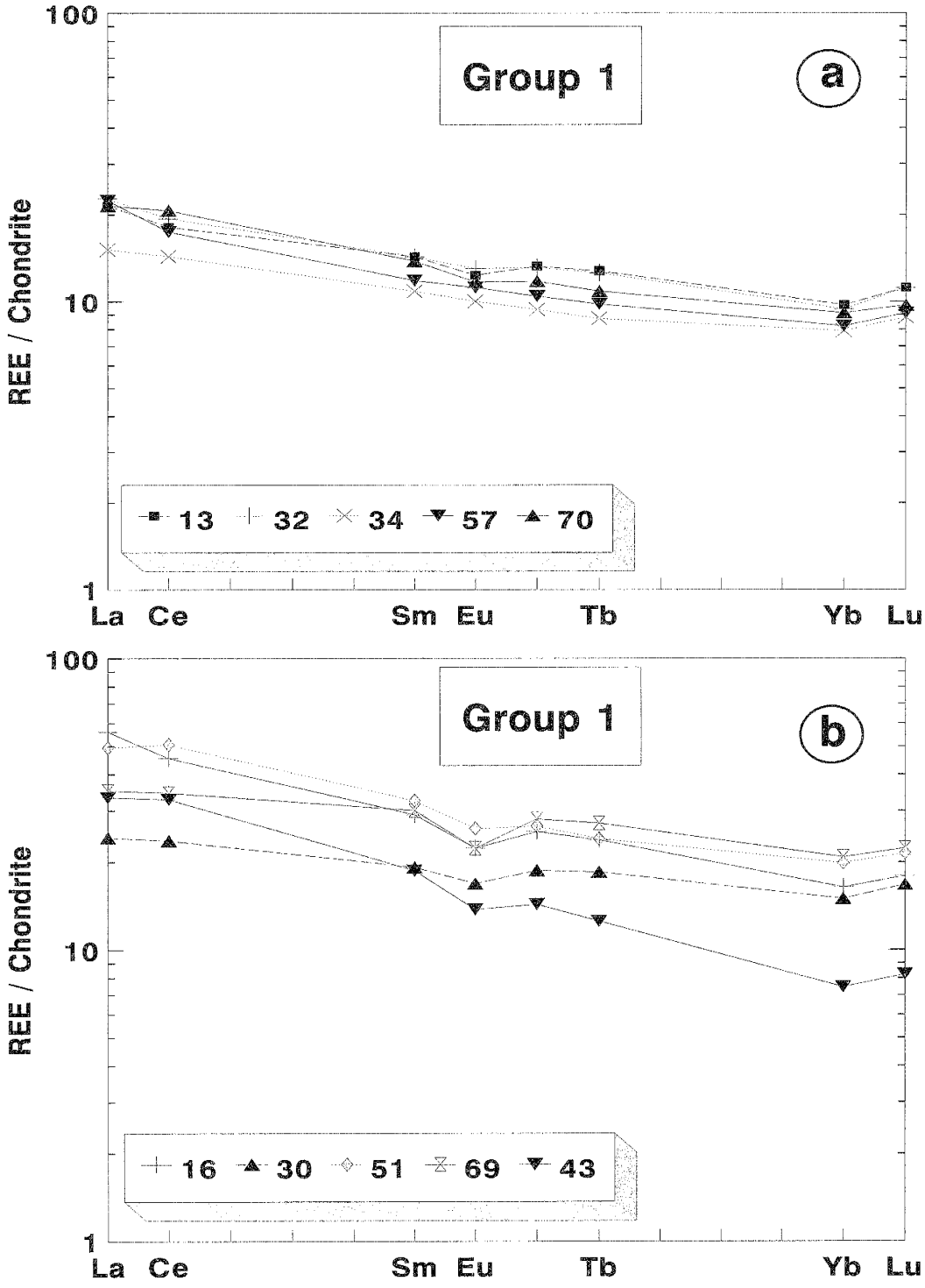

Figure 6: Rare-earth element distributions in Group 1 dikes, normalized to chondritic meteorite. Note: Gd data point is calculated using the formula $Gd_N = (Sm_N \times Tb_N^2)^{1/3}$.

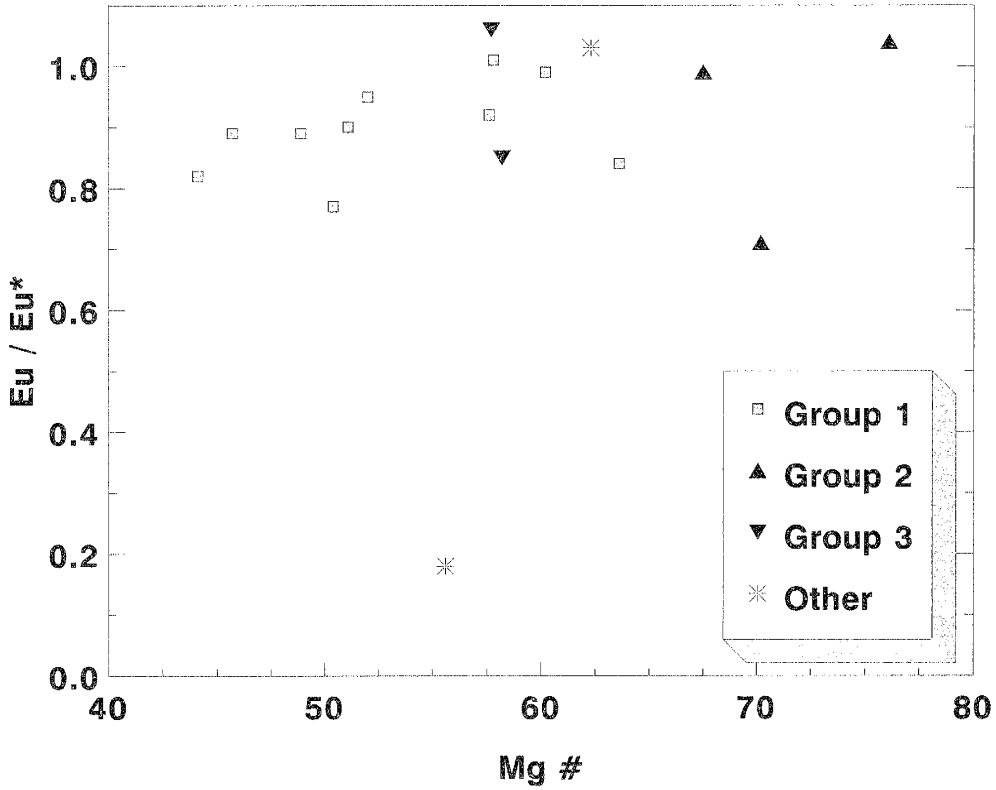

Figure 7: Mg number vs. Eu/Eu* for mafic dikes.

Large-Ion Lithophile Elements (LILE): Rb, Cs, Sr, Pb, Th, U

Group 1 dikes have generally low Rb concentrations relative to other groups of this study, (6-12 ppm, except sample 16 with 29 ppm and sample 43 with 15 ppm). Cs concentrations are also lower, ranging between 0.10 and 0.36 ppm, but Sr concentrations are moderate (144-293 ppm), as are Pb (14-22 ppm). Low Th concentrations (0.09-2.57 ppm) are positively correlated with Rb (fig.10). U concentrations are generally below the limit of detection.

Group 2 dikes have higher Rb concentrations (14-28 ppm). Cs and Sr concentrations are highly variable for the small sample population analyzed (0.16-0.79 ppm and 35-790 ppm, respectively). Pb concentrations are moderate (10-23 ppm), and U

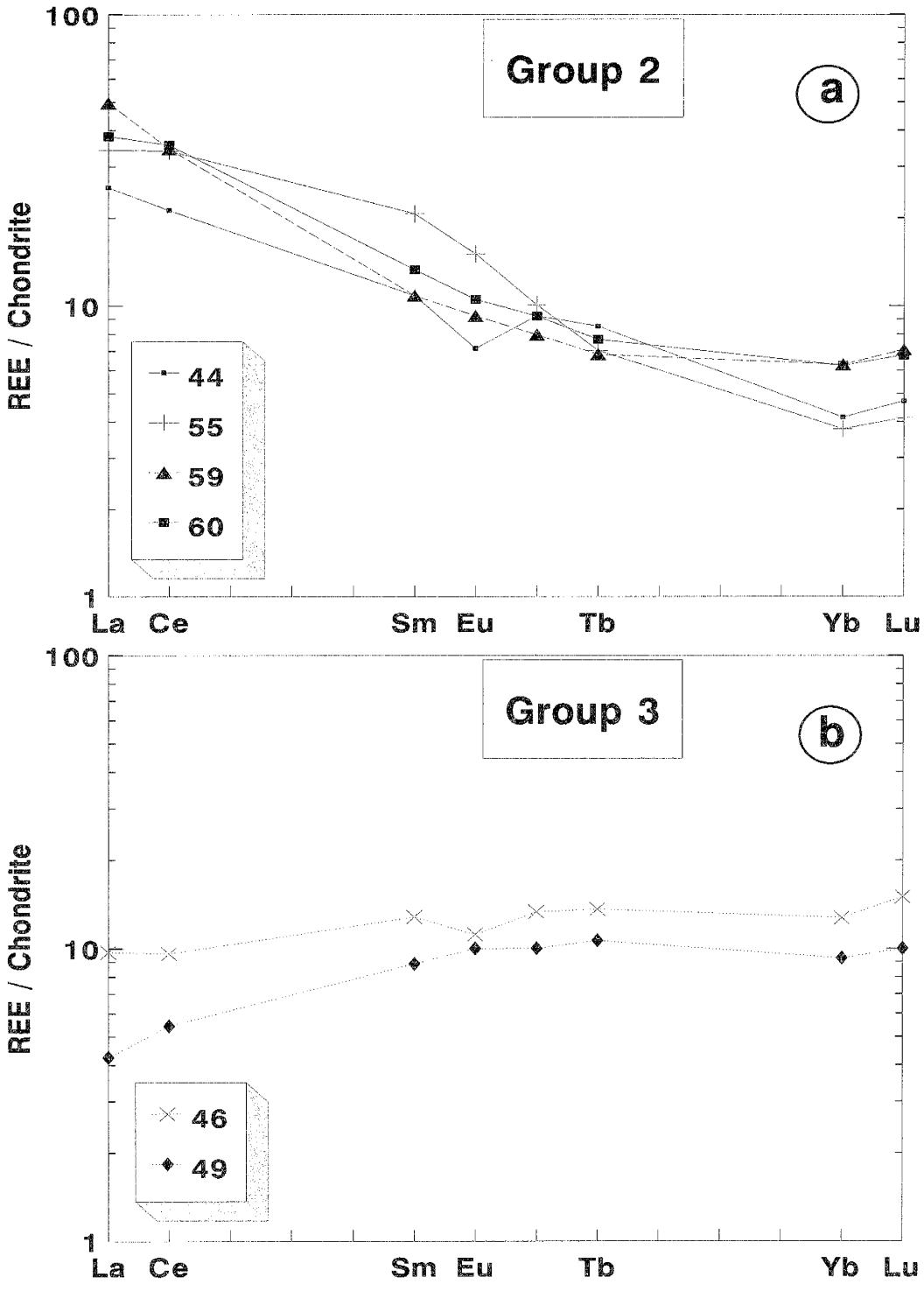

Figure 8: Rare-earth element distributions in (a) Group 2 and (b) Group 3 dikes, normalized to chondritic meteorite. Note: Gd data point is calculated as in fig. 6.

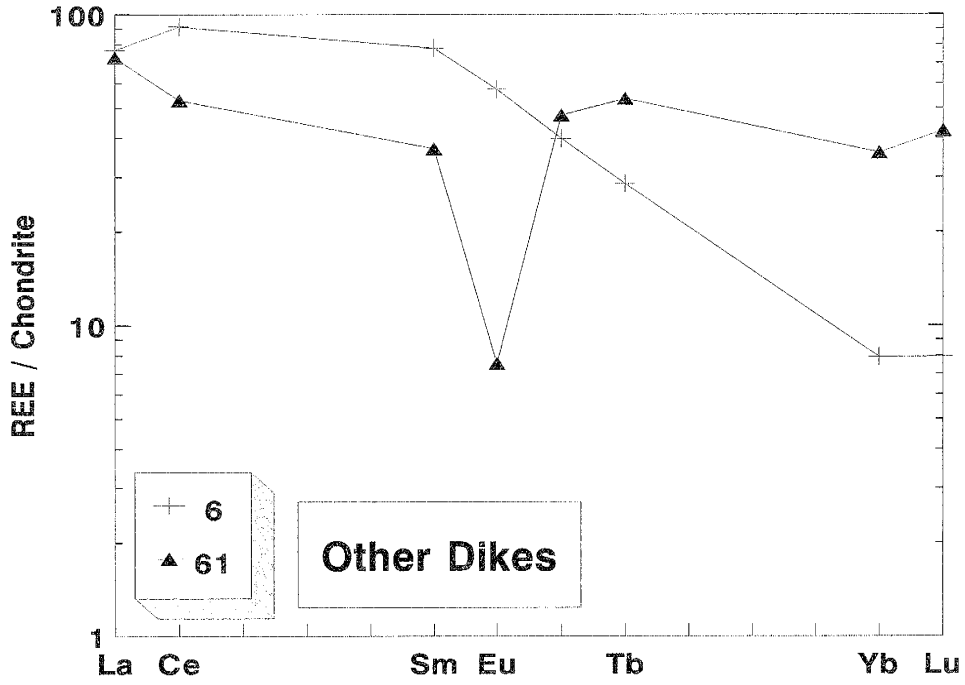

Figure 9: Rare-earth element distributions in other mafic dikes, normalized to chondritic meteorite. Note: Gd data point is calculated as in fig. 6.

contents are detectable (0.35-0.49 ppm). Th concentrations are generally higher than those of Group 1 (1.25-2.48), although sample 60 has only 0.22 ppm. However, the positive correlation between Rb and Th is not manifest (fig. 10).

Rb concentrations of the two Group 3 dikes are higher than the other groups (39-48 ppm), as are Cs and Sr concentrations (0.28-0.48 and 524-777 ppm, respectively; see also fig. 12b). Pb concentrations are again moderate (15, 32 ppm) and Th and U concentrations are low but detectable in one sample, but below detection in the other.

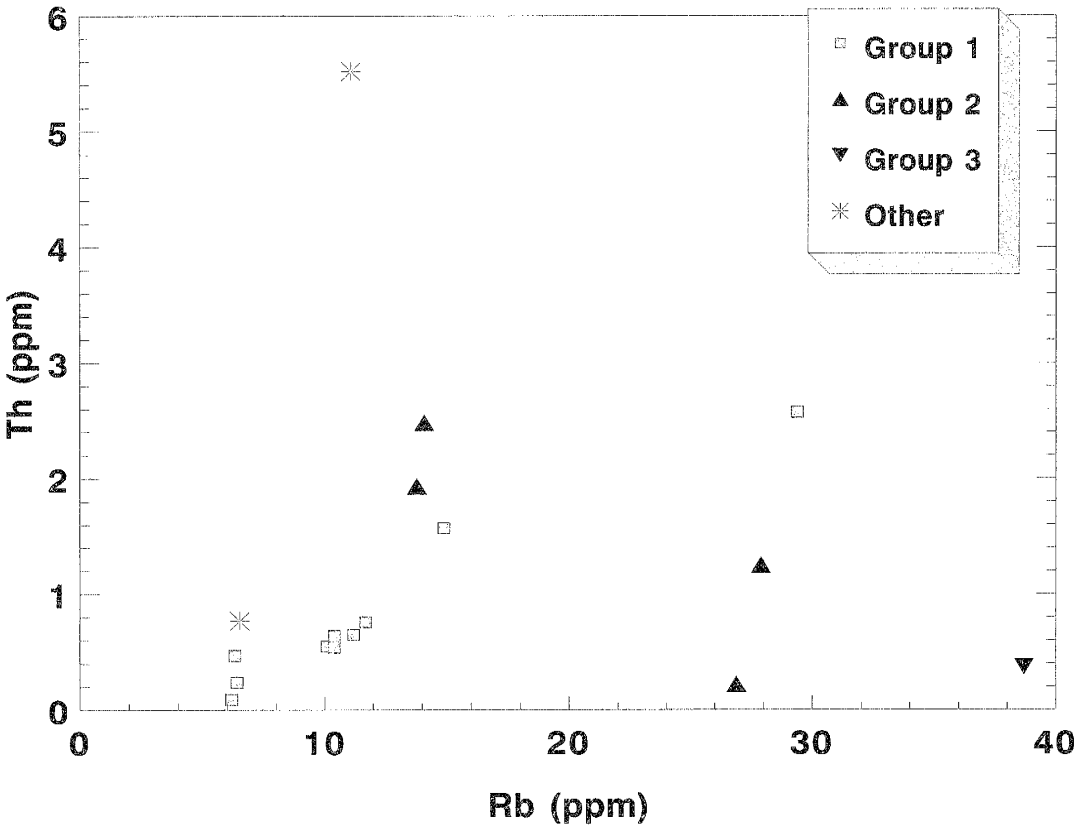

Figure 10: Concentrations of Rb vs. Th for mafic dikes.

High Field-Strength Elements (HFSE) and Transition Metals

Group 1 dikes have higher HFSE (Y, Zr, Nb, Hf, Ta) and significantly lower transition-metal (Sc, Cr, Co, Ni) contents (Table 1; fig. 11a,b) than the other two groups. This group is low in Ta and Ti (except sample 69, which has a slight positive Ta-Nb* anomaly, and 43, which has a positive Ti anomaly, fig. 11a) relative to PM-normalized abundances of LILE and REE. The inconsistent relationship of Nb with Ta may be caused by Nb concentrations at or below the limit of detection by XRF (measured Nb concentrations are presented in Table 1). To avoid this problem in comparisons and graphical presentations, Nb data were recalculated from Ta data assuming Nb* = Ta × 17 (Condie, 1996). Enrichments in HFSE and REE are coupled with depletions of Sr and P.

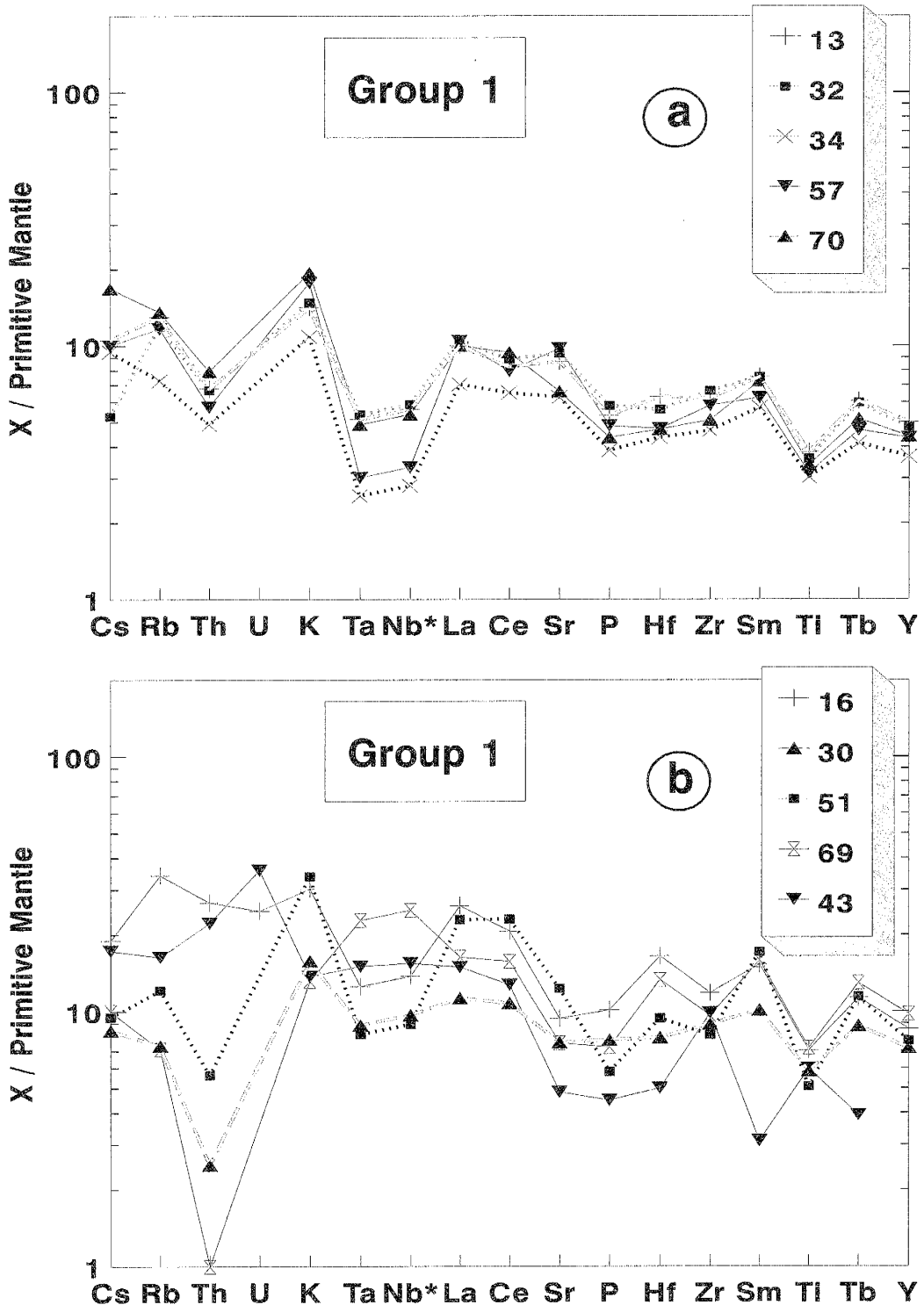

Figure 11: Concentrations of elements in Group 1 dikes normalized to Primitive Mantle (Wood, 1979). Elements are arranged from left to right in order of decreasing incompatibility in mafic magmas.

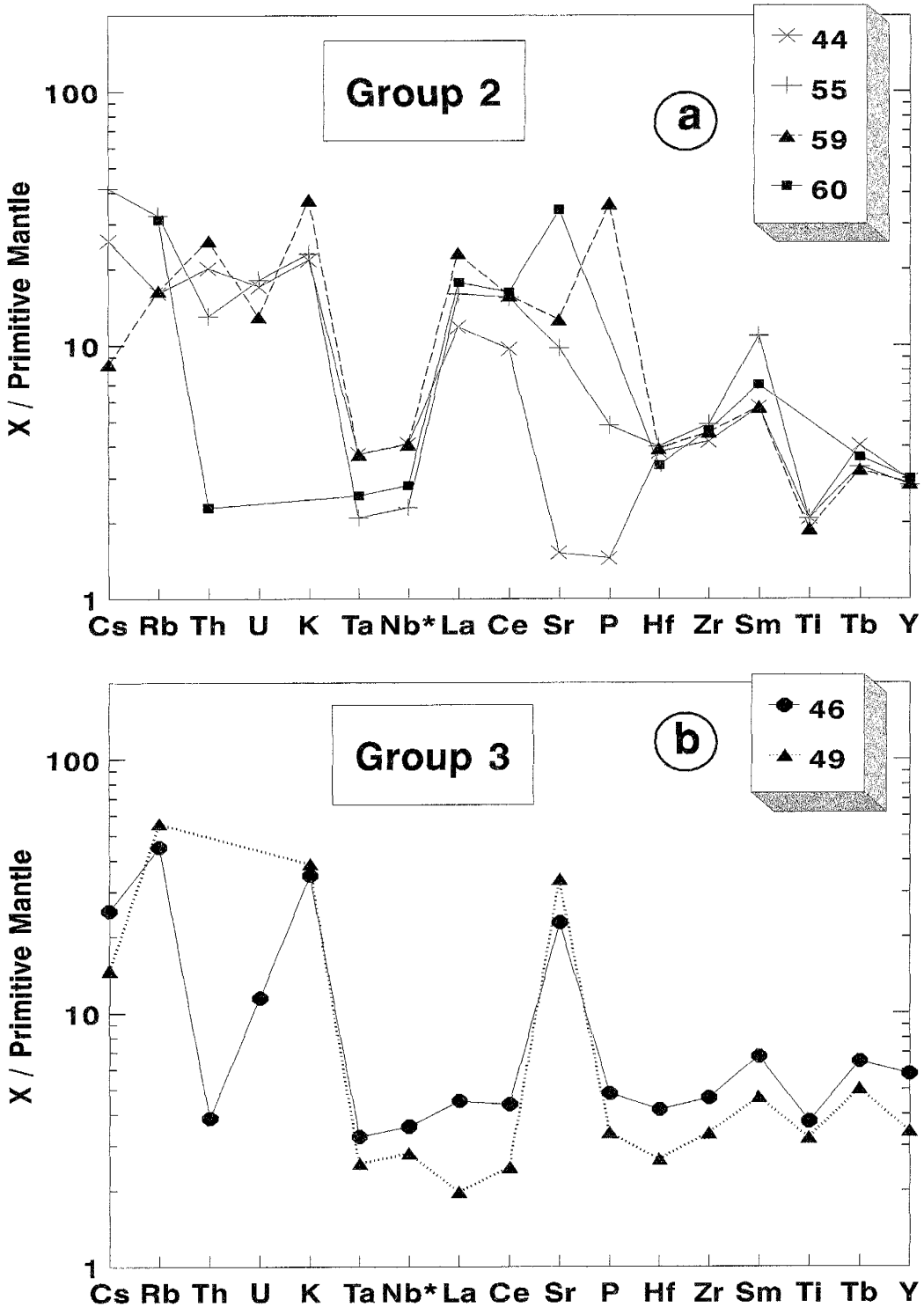

Figure 12: Concentrations of incompatible elements in (a) Group 2 and (b) Group 3 mafic dikes normalized to Primitive Mantle (Wood, 1979). (See also fig. 11)

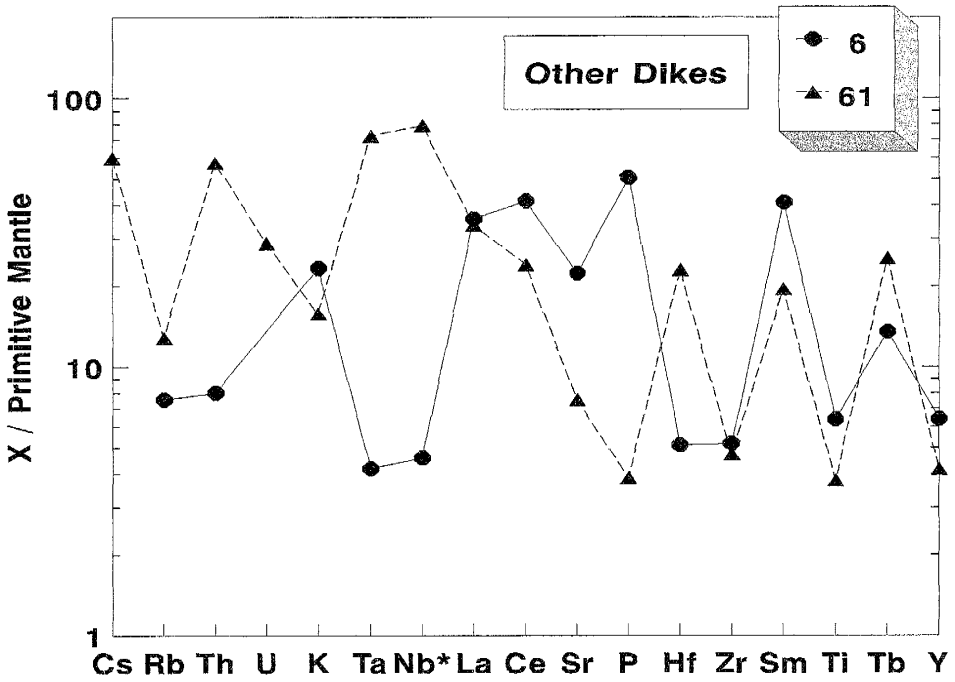

Figure 13: Concentrations of incompatible elements in other mafic dikes normalized to Primitive Mantle (Wood, 1979). (See also fig. 11)

High Zr/Nb* (5.5-30) and intermediate Ti/Zr, Zr/Y, La/Zr, Ta/Yb, and $(La/Yb)_N$ separate this group from the others (Table 1). Sample 43 has lower Zr/Nb* and higher Ta/Yb, La/Zr, and $(La/Yb)_N$ than the other dikes in this group.

In comparison, Group 2 dikes have lower Zr (45-55 ppm) and other HFSE concentrations (fig. 12a). Like Group 1 dikes, Group 2 dikes show significant depletions in Ta and Ti relative to LREE. This group is also characterized by lower Ti/Zr than the other dikes (60-73), but Zr/Nb* ratios are intermediate and Zr/Y, Ta/Yb, La/Zr and $(La/Yb)_N$ ratios are consistently higher than the other two groups.

The concentrations of HFSE and transition metals of Group 3 dikes overlap between Groups 1 and 2 . This group does not have the marked Ta depletion of the other

two groups (fig. 12b). Ti/Zr ratios are high (115-140) compared with Group 1 and 2 dikes, but other ratios (Zr/Nb*, Zr/Y, La/Zr, and Ta/Yb) are low.

HFSE and transition-metal contents of sample 6 are similar to those of Group 1. This sample also has low Ta and Sr contents. Sample 61 has Hf and Ta contents that are anomalously high (8 and 3.1 ppm, respectively; fig. 13). Other HFSE and transition metal contents are similar to those of Group 1 dikes. Ratios of incompatible elements (Table 1) are significantly different for these two samples than for the other groups. Sample 6 has high Ti/Zr and La/Zr despite its average Zr content. Zr/Nb* is similar to Group 1 but Zr/Y is similar to Group 3. Sample 61 has Ti/Zr similar to Group 3, but other ratios are much higher than those of Group 3. La/Zr and Ta/Yb are significantly higher in sample 6 than in any other dike analyzed for this study.

Discussion

Geochemical Models

The three groups of dikes differ sharply in their geochemical characteristics, implying that they are not cogenetic. Understanding the processes that operated to produce the dike suites is important before any constraints can be placed on mantle source compositions.

Fractional crystallization (FXL) and combined assimilation/fractional crystallization (AFC) processes have been evaluated for the Nei Mongol dikes. Details for models, including distribution coefficients and model parameters, are given in Appendix B. In figure 14, Ni is plotted against $(La/Yb)_N$ ratio for the three groups of dikes, and calculated trends are shown for fractional crystallization and various AFC models (DePaolo, 1981). Group 2 dikes are similar geochemically to norites or basaltic komatiites (note their especially high Ni contents, Table 1); therefore, geochemical models use a komatiitic starting liquid composition ($(La/Yb)_N = 0.76$, Ni = 2000 ppm) and the fractionating assemblage involves olivine and spinel. Models use a rate of assimilation to fractional crystallization (Ra/Rc) of 0.40 for komatiite (as recommended by Huppert and Sparks, 1985). Compositions of model assimilates include the bulk continental crustal estimate (B) of Taylor and McLennan (1985), an average Archean tonalite (T), and an average khondalite (S) from rocks exposed in the area (see Appendix B). Compositions for rocks from the surrounding gray gneiss association, into which

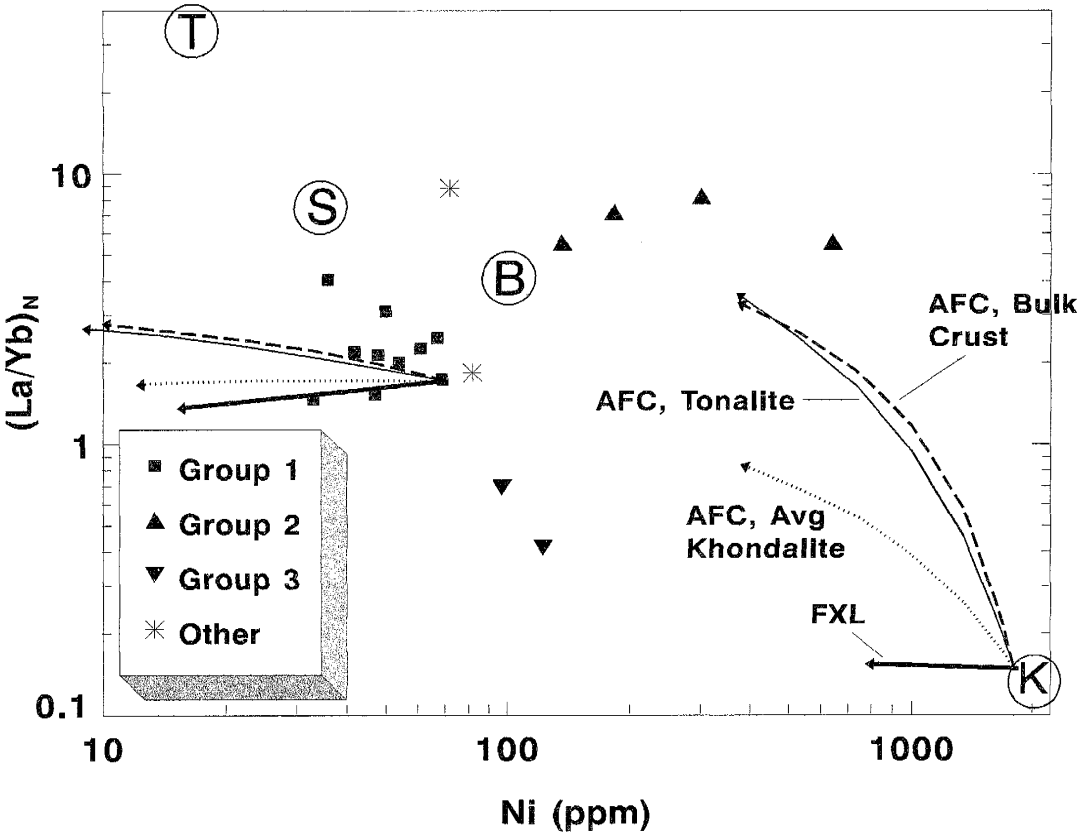

Figure 14: Ni vs. $(La/Yb)_N$ for Hunyuanyao mafic dikes, with trends calculated by geochemical modeling using sample 34 as a starting composition for Group 1 dikes and a model komatiite (circled K) for Group 2 dikes. Models (discussed in text) include fractional crystallization (FXL, thick solid line) and combined assimilation/fractional crystallization (AFC). Compositions of AFC model assimilates for both dike groups are Bulk Crust (circled B; Taylor and McLennan, 1985; dashed lines), average Archean tonalite (circled T; Condie, personal communication; thin solid lines) and average khondalite (circled S; Condie et al., 1992 and this study; dotted lines). Length of each model arrow represents 40% crystallization.

some of the Hunyuanyao dikes are intruded, are similar (Liu, 1989) to the bulk crustal estimate of Taylor and McLennan (1985).

Models are also presented for the Group 1 dikes. Sample 34 was chosen as a starting liquid composition because of its high Mg# and transition metal contents and low and flat REE distributions. It also has no Eu or Sr anomalies (figs. 6a and 11a) and thus represents the most primitive sample in the group. (Sample 43 has a slightly higher Mg# but lower transition metal contents and more fractionated REE distributions and so

is considered less likely to represent the most primitive magma in this group.) A lower Ra/Rc = 0.25 is chosen for Group 1 AFC models because the temperature of basaltic magma is lower than that of komatiite, hence basaltic magma's lessened ability to assimilate crustal materials (Huppert and Sparks, 1985). The trends in major elements with Mg# (fig. 5a, b) are consistent with magma compositions controlled by fractionation of a mafic mineral assemblage (olivine, pyroxenes, calcic plagioclase). Magnetite (or chromite) must fractionate to remove Cr in the more evolved dikes.

The enrichment of incompatible elements and ratios (e.g. Hf, Zr, Y, and $(La/Yb)_N$) relative to primitive mantle (Table 1 and figs. 11 and 14) in Group 1 dikes cannot be explained by FXL. Even 50% FXL of the assemblage olivine + clinopyroxene + plagioclase + magnetite (in the proportions 10:20:70:0.1) does not explain these enrichments (fig. 14). The HFSE enrichments could result from open-system FXL (in which mafic phases continue to deplete Mg and transition metals).

Assimilation of HFSE-enriched crustal material could explain some of the variation in incompatible trace element ratios, especially if the parental magma were more capable (Ra/Rc > 0.25) of assimilating crustal material (i.e., had a higher temperature) than basalt. However, the variations could equally reflect heterogeneity in a mantle source in which HFSE and LREE have been variably enriched (Wood, 1979; Pearce, 1983; Zindler and Hart, 1986; Hall and Hughes, 1990). It is impossible to test further between these two hypotheses using the present data, but the latter is favored in light of the difficulty in fractionating La from Yb (fig. 14) using reasonable values of Ra/Rc.

In contrast to Group 1 dikes, Group 2 dikes show little variation in incompatible element concentrations and ratios (e.g., Zr, $(La/Yb)_N$), whereas compatible elements such as Ni and Cr vary by an order of magnitude (Table 1). Fractionation of light from heavy REE is also more pronounced in Group 2 than in Group 1 (figs. 8a and 14). The high Mg# and transition metal contents of Group 2 dikes are consistant with crystallization of a Cr-bearing phase. In addition to olivine, chromite has been identified as an important phase in komatiitic lavas from Newton Township, Ontario (Cattell and Arndt, 1987). Crystallization of olivine and Cr-spinel are required to produce the dramatic changes in Ni and Cr in the Group 2 dikes (fig. 14). However, none of the minerals that crystallize from mafic or ultramafic melts (olivine, pyroxenes, plagioclase, or spinel) can fractionate the REE sufficiently to match the Group 2 data. Furthermore, while the markedly low Sr and P contents of sample 44 may reflect crystallization/removal of plagioclase and apatite, the high Sr content of sample 60 appears to indicate *accumulated* plagioclase. Hence, strictly FXL models cannot explain all of the variation in Group 2 dikes. Crustal assimilation models also fail to account for the compositional variation seen in Group 2. While assimilation of Archean tonalite could cause the enrichment in LREE, it would also cause enrichments in other incompatible elements (Sr, Ta, Hf, Zr, etc.) that are not observed. Hence, the variation in compositions of Group 2 dikes appears to be controlled chiefly by crystallization of olivine and chromite with accumulation or crystallization of plagioclase, as well as by heterogeneities in the mantle source.

Group 3 dikes are significantly different from Group 1 and 2 dikes in terms of incompatible element ratios such as Ti/Zr, Ta/Yb, La/Zr, and Zr/Y. Consequently, Group

3 dikes cannot be related by FXL or crustal contamination to Groups 1 or 2. The strongly positive Sr anomalies (fig. 12b) may indicate accumulation of plagioclase; however, only sample 49 has a corresponding positive Eu anomaly. Due to the small sample population, modeling was not attempted for these samples.

Mantle Sources

Petrographic data and compositional variations (e.g., figs. 10-12) support the contention that K, Rb and Th and related LILE may have been mobilized in a few of the dikes (e.g., samples 30, 69, and 60) during metamorphism. Hence, the distributions of these elements are suspect in characterizing the mantle sources of granulite-facies dikes.

The major- and trace-element data described above suggest that the Hunyuanyao dikes were derived from at least three distinct mantle sources. Group 1 dikes have PM-normalized distributions showing an overall slight enrichment in more-incompatible over less-incompatible elements (fig. 11a, b). Variable depletion in P (relative to LREE/HFSE, fig. 11a, b) is probably related to removal of apatite. The depletions in Ta and Ti, present in all of Group 1 (except sample 69, which has a positive Ta anomaly), are thought to be related to the removal of a Ta-Nb*-Ti- (TNT) rich phase (spinel?); such depletions are generally interpreted to reflect a subduction zone component (Pearce, 1983; McCulloch and Gamble, 1991; Karsten et al., 1996) in the source.

Figure 12a shows that the element distributions of Group 2 dikes are distinct from those of Group 1 dikes. The Ta-Nb* depletion is more significant, and overall enrichments in Hf, Zr, Tb and Y relative to primitive mantle are less than in Group 1. It

is also clear that the LREE are significantly enriched over other HFSE relative to primitive mantle. Variable Sr and P anomalies probably reflect removal and/or accumulation of plagioclase, apatite and monazite during cooling of the dikes.

Group 3 dikes have PM-normalized patterns showing that more-incompatible elements are less enriched than less-incompatible elements (fig. 12b); their REE distributions and incompatible element abundances are similar to modern NMORB and they appear to have been derived from a similar depleted source The strong positive Sr anomalies are probably the result of accumulation of plagioclase, although corresponding positive Eu anomalies are not observed (fig. 8b).

The other dikes have highly variable PM-normalized distributions (fig. 13). Sample 6 is enriched in Sr and LREE relative to HFSE, and sample 61 shows a positive Ta anomaly and a decoupling of Hf from Zr that is probably a result of analytical error.

Th/Ta and La/Yb ratios are useful in constraining mantle sources (Condie, 1996) because of the near-equal incompatibility of these elements in processes of mafic differentiation. On such a diagram (fig. 15), Group 1 dikes generally fall on a mixing line between primitive or depleted mantle and upper continental crust. (Three samples plot below the mixing line, suggesting possible local Th depletion during metamorphism.) The samples plot much closer to the DM/PM end of the mixing line, further supporting

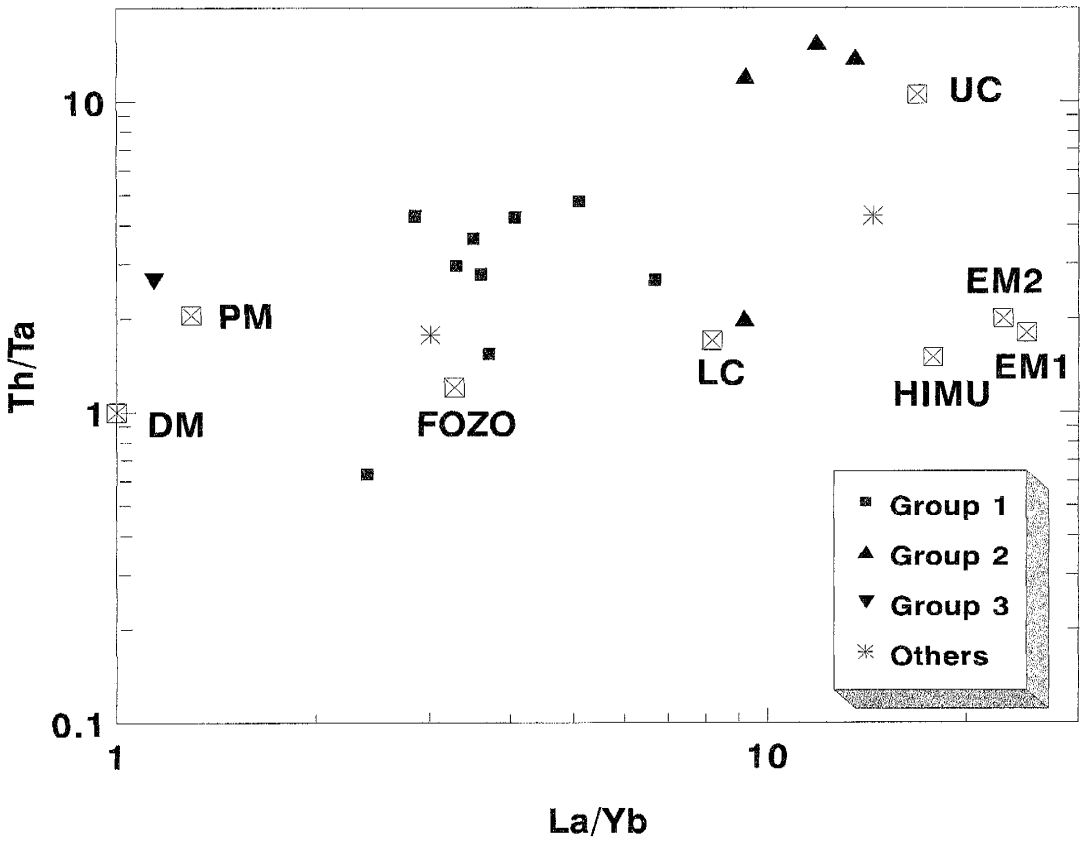

Figure 15: Incompatible element ratios of Hunyuanyao mafic dikes. Typical mantle source compositions include depleted mantle (DM), primitive mantle (PM), lower mantle plume component (FOZO), high U/Pb (HIMU), and enriched mantle sources (EM1 and EM2); typical sources of contamination include lower and upper continental crust (LC and UC, after Condie, 1996). Group 1 dikes probably result from mixing between DM/PM and UC (see also fig. 14); Group 2 dikes require a different source; and Group 3 dikes (one sample) are likely derived from a DM source. FOZO, HIMU and EM sources are probably insignificant contributors to Hunyuanyao magmas.

the contention that the actual proportion of assimilation of crustal material must be low, and favoring a primitive mantle source that is variably enriched in LILE.

Group 2 dikes (except sample 60, whose Th was probably depleted during metamorphism, see above) plot near upper crustal material on figure 15. Their compositions clearly preclude a felsic origin, and Condie (1996) has interpreted mafic magmas with near-upper crustal Th/Ta and La/Yb ratios (and especially those coupled with low Ta, Th and Rb contents) to be derived from a source involving Archean

subcontinental lithosphere. This source must be refractory to produce melts with the high Mg numbers of Group 2. The source must also either be enriched in LREE or contain residual garnet to produce the high La/Yb ratios of these dikes.

Only one dike from Group 3 has a detectable concentration of Th; it plots near a PM or DM source, further supporting derivation from a depleted mantle source.

Comparisons with Mafic Dikes from Other Granulite Terranes

Comparisons of the Hunyuanyao area dikes with those from other high-grade terranes can give us a better understanding of the evolution of the Precambrian mantle. Although comprehensive Th, Ta, La, and Yb (and many other elements) data for many terranes are not available, Ta data can be estimated from Nb data (if given) as discussed above, and Yb can be estimated from Y, due to the geochemical similarities of these elements (Condie, 1996).

One of the best studied of Precambrian mafic dikes is the Scourie dike complex of Scotland (Weaver and Tarney, 1981b). The Scourie samples include four dike suites defined by Weaver and Tarney (1981b): picrites, norites, olivine gabbros, and dolerites (here termed tholeiites). Hunyuanyao Group 1 dikes have REE distributions similar to Scourie tholeiites, and Group 2 dikes have compositions similar to the Scourie norites (fig. 16). Hunyuanyao Group 1 and 2 dikes and Scourie tholeiites and norites all have enriched LREE distributions, high transition-metal contents, and relatively low HFSE concentrations. On PM-normalized diagrams, the norites are strikingly similar to Group 2 dikes in terms of Ta and Ti depletions as well as enrichments in LREE relative to HFSE.

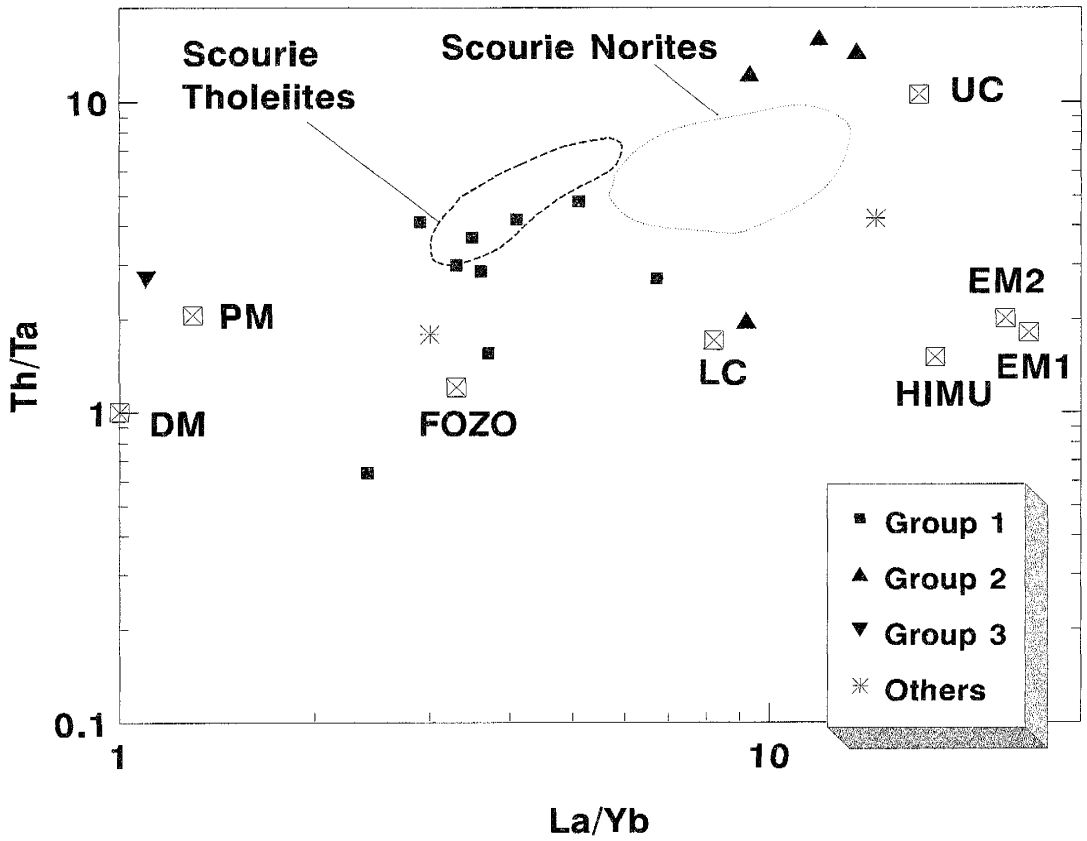

Figure 16: Incompatible element ratios of Hunyuanyao mafic dikes compared with Scourie norites and tholeiites (dolerites; Weaver and Tarney, 1981b). Mantle sources as in fig. 15.

Although broadly similar, the Scourian tholeiites are more enriched in LILE and in LREE, relative to HFSE, than Group 1 dikes. Mafic rocks with compositions similar to modern NMORB are present in the Hunyuanyao area (Group 3 dikes) but are absent in the Scourie dikes (Weaver and Tarney, 1981b); Scourie picrites and olivine gabbros have no counterpart in the Hunyuanyao area.

Scourie tholeiites have been interpreted to have been derived from an undepleted mantle source in the subcontinental lithosphere that has been enriched in incompatible elements (Weaver and Tarney, 1981b; Tarney and Weaver, 1987), just as dikes from Group 1 of this study. However, Group 1 dikes are distinguished from Scourie tholeiites

in that mixing with a FOZO or HIMU component (which may represent the residual slabs recycled into the mantle at subduction zones (Saunders et al., 1988)) is not evident (Condie, 1996). Scourie norites appear to be derived from a more refractory source (than that of the tholeiites) that has been enriched in incompatible elements and especially in LILE (Condie, 1996; Tarney and Weaver, 1987), and the same conclusion is reached for Group 2 dikes.

The Hunyuanyao rock associations may be correlated with granulites in eastern Hebei Province (EHP) on the basis of metamorphic ages, and chemical compositions (Jahn and Zhang, 1984; Jahn et al., 1987; data presented herein). Concentrations of most major elements in mafic dikes overlap between the two regions, except that Al_2O_3 contents of EHP dikes are higher, and TiO_2 and Fe_2O_3T are lower, than Hunyuanyao dikes. Dikes from both regions in China have low Zr, Y, and Nb contents and Zr/Y ratios and high CaO and La/Zr. Transition metal contents are similar, and LILE ratios such as Rb/Sr and K/Rb are highly variable in dikes from both regions. REE distributions, however, are slightly different: HREE contents are lower in EHP mafic granulites, resulting in higher $(La/Yb)_N$ (average 4.1) and Eu/Eu* approaches unity (average 0.95), while Hunyuanyao dikes average 3.4 and 0.91 for these ratios, respectively. The reasons for these discrepencies are unclear, but it should be noted that examples of each of the three dike groups defined in this paper can also be found in the EHP dikes described by Jahn et al. (1987). These similarities support the assumption that the Hunyuanyao and eastern Hebei portions of the North China granulite belt are related, and mafic rocks of both regions may be derived from similar mantle sources.

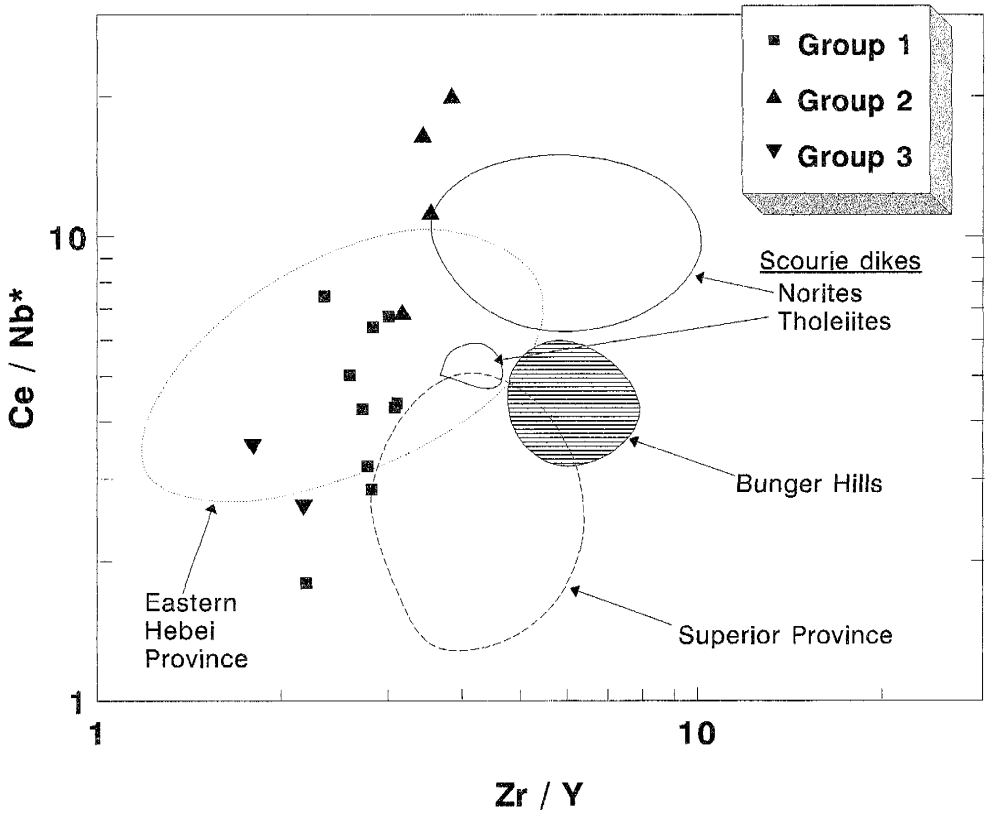

Figure 17: Comparison of incompatible element ratios Ce/Nb* and Zr/Y of Hunyuanyao mafic dikes with dikes from various Precambrian terranes: Scourie norites and tholeiites (Weaver and Tarney, 1981b), Bunger Hills, Antarctica (Sheraton et al., 1990), eastern Hebei Privince (Jahn and Zhang, 1984; Jahn et al., 1987), and the Superior Province (Condie et al., 1987).

In Figure 17, trace element ratios from the Hunyuanyao dikes are compared with those from mafic dikes of granulite grade from the EHP, Scourie and other Archean/Early Proterozoic terranes, including mafic rocks from the southern Superior Province (Condie et al., 1987), and the Bunger Hills of East Antarctica (Sheraton et al., 1990). Although the dikes from the southern Superior Province include analyses of Archean (Matachewan) through Middle Proterozoic (Abitibi) dike swarms, they still form a compact population(fig.17) that is separate from the China data. The Superior dikes have relatively flat to gently sloping distribution patterns on primitive mantle-normalized diagrams (Condie et al., 1987), with moderate Sr and Ti anomalies and no

Ta-Nb anomalies. Overall enrichments in incompatible elements are greater in the Superior dikes than in the granulite dikes from China. Mafic granulites from the Bunger Hills (BH) (Sheraton et al., 1990) are geochemically distinct from those of this study. BH dikes span a range of compositions, from tholeiitic to picritic and alkalic. All of the BH samples have anomalously high P_2O_5 contents coupled with high HFSE and LILE contents, and CaO is much lower than in the dikes from China. Unlike the EHP rocks, Fe_2O_3T contents of BH dikes are similar to the Hunyuanyao area dikes. Data on HREE are not available for BH dikes, but LREE are enriched above dikes from the other areas. Small to negligible depletions in Nb and Ti relative to REE are unlike the Chinese mafic dikes, and indicate derivation from more enriched subcontinental lithosphere.

The Bunger Hills and Superior Province dikes have Ce/Nb ratios that are lower, on the whole, than dikes with similar Zr/Y from other areas. Also, most of the dikes from China have Zr/Y ratios lower than the Scourie or Bunger Hills dikes of similar Ce/Nb* (fig. 17).

The dike suites from each of the granulite terranes discussed above are interpreted to be derived from multiple mantle source regions by the original investigators. The Scourie tholeiites and norites are derived from two distinct mantle sources (Weaver and Tarney, 1981b), and the dikes from the Superior Province, the Bunger Hills, and eastern Hebei Province are all derived from at least three distinct mantle source regions in each area (Jahn and Zhang, 1984; Condie et al., 1987; Jahn et al., 1987; Sheraton et al., 1990). Within a geographic area there are large variations in trace element ratios such as Ce/Nb, Th/Nb, La/Yb, and Zr/Y, but distinctions between

different regions are obvious (fig. 17). These results suggest that mantle heterogeneities beneath regions on the order of 10^4 km^2 were common by the Late Archean.

Conclusions to Part I

1. Three petrographically and geochemically distinct groups of Late Archean/Early Proterozoic mafic dikes, metamorphosed to the granulite grade, occur in a small geographic area (about 60 km^2) near Hunyuanyao along the northwestern boundary of the North China craton. Their field occurrences are nondistinctive.

2. Dikes from Group 1 are metamorphosed tholeiitic basalts with flat to slightly LREE-enriched REE distributions. The trends shown by their HFSE and transition-metal contents and Mg numbers suggest that fractional crystallization processes were most important in controlling their compositions. Group 1 dikes originated in a variably-enriched lithospheric mantle and involved a small degree of mixing with upper continental crust or Archean subcontinental lithosphere.

3. Group 2 dikes are chemically similar to norites, with elevated Cr and Ni contents and relatively high Mg numbers. They are strongly enriched in LREE but not in other HFSE. They were derived by high degrees of melting of a LREE-enriched refractory mantle source followed by crystallization of olivine and chromium spinel.

4. Groups 1 and 2 are strongly depleted in Ta relative to other incompatible elements, which reflects retention of TNT phase(s) in their mantle sources. The mantle source of Group 2 dikes also probably contains residual garnet.

5. Group 3 dikes are chemically similar to high-Mg tholeiites. The depleted LREE, low TiO_2 and other HFSE contents, and lack of a Ta-Nb anomaly suggest they were derived from a depleted mantle source similar to that of modern MORB. La/Yb ratios preclude any significant involvement of HIMU or FOZO mantle components in these samples.

6. Mantle source heterogeneities preserved in the Hunyuanyao area on a small scale could also be part of a larger, distinctive mantle that existed beneath the entire North China granulite belt. This mantle was chemically similar to portions of the mantle beneath the Scourie terrane of Scotland, but had lower concentrations of HFSE than the mantle beneath the Bunger Hills of East Antarctica.

Part II: Geochemical Evidence for the Origin of Khondalites, Nei Mongol, China

Introduction

The term khondalite applies to a suite of metamorphosed aluminous sediments consisting of garnet-quartz-sillimanite rocks intercalated with garnetiferous quartzites, graphite schists and marbles (Walker, 1902). This assemblage has long been interpreted to represent the metamorphosed equivalent of platform sediments (e.g., Shackleton, 1976), although Dash et al. (1987) have more recently interpreted them as residual soils. Recrystallization under granulite-facies conditions tends to obliterate relict textures that might distinguish the protolith as sedimentary. Such a distinction might be made on the basis of geochemical characteristics; however, geochemical distinction is probably not possible between paleosols and pelites derived from intensely weathered terranes. Nanda and Pati (1989) have pointed out that outcrops of khondalites are usually not fresh, but instead are weathered to a brownish-red color, discouraging sampling for chemical analyses. Therefore, extensive modern studies of the geochemistry of khondalites are rare, exceptions being those by Barbey et al. (1982) on khondalites from Lapland (major elements and transition metals), and by Dash et al. (1987) on khondalites from Orissa, India.

This study was undertaken to characterize the geochemical nature of khondalites from a little-known terrane in the Datong area (figs. 1, 2) of Nei Mongol, China. Geological relationships are detailed under the heading *Generalized Geology of the Study Areas* above. Major and trace element data are used to constrain the compositions of

crustal components from which the khondalites are derived. In addition, the Nei Mongol khondalites are compared with data from other khondalites as well as modern and ancient residual soils in order to test the chemical distinctions between the two hypotheses for the origin of khondalites.

Petrographic features

Samples collected and analyzed by the author are denoted with a prefix of K; other samples (those with a J prefix) were collected and analyzed by Liu Jinzhong. Modal abundances of the K samples are summarized in Table 2, and detailed petrographic analyses are listed in Appendix C. Three groups are recognized, based on modal abundances and trace element distributions: sillimanite-garnet gneisses (SGG), quartz-garnet gneisses (QGG) and quartz-feldspar gneisses (QFG).

The SGG (Plate 6a, b) contain 20-30% quartz, up to 50% plagioclase, 30-50% perthitic K-feldspar, up to 5% biotite, up to 15% sillimanite, and 10-30% garnet. Grain sizes of the dominant minerals vary greatly, with garnet porphyroblasts approaching 5 cm across; quartz and feldspars are usually 1-4 mm in size. Trace minerals include zircon, apatite, opaque minerals, and sphene. Biotite defines a marked foliation, and sillimanite is generally found in the foliation planes. Quartz grains show undulose extinction, and feldspars have bent or broken twin planes; these features reflect a late stage of deformation, probably in response to uplift of the terrane. Feldspars are generally slightly to moderately sericitized (highly sericitized samples were not included in this study).

Table 2: Modal averages and ranges in the three principal khondalite groups from the Datong region. Subgroup of SGG are excluded from averages.

	Sill-Gar Gneiss (SGG)	Qtz-Gar Gneiss (QGG)	Qtz-Fsp Gneiss (QFG)
No. of samples*	15 (8)	5 (3)	4 (1)
Quartz	27 (15-35)	62 (50-70)	30 (20-40)
Plagioclase	14 (tr-40)	19 (7-27)	26 (10-30)
K-feldspar	27 (5-60)	10 (3-20)	41 (30-50)
Biotite	2 (tr-5)	1 (tr-2)	2 (tr-4)
Sillimanite	11 (5-20)	tr	-
Garnet	18 (5-40)	7 (5-10)	tr (0-5)
Opaque Minerals	tr	tr	tr
Apatite	tr	tr	tr
Sphene	tr	tr	tr
Zircon	tr	tr	tr

* Number of samples described in Appendix D is given in parentheses; remainder of petrographic descriptions are given by Liu (1989).

Sample K62 contains very little quartz, but is composed of 60% perthitic K-feldspar, 30% garnet, 5% sodic plagioclase and 1% biotite.

The QGG (Plate 7a, b) are usually fine-grained and equigranular, comprising mostly quartz (50-70%, stretched into lenses; undulose and recrystallized grains are common) and plagioclase (10-30%; An_{45} composition could be determined for only one sample, K23). Perthitic K-feldpar composes 5-20%, garnet 5-10% and biotite ranges up to 2%. Sillimanite is rare in the QGG. Trace minerals include zircon, apatite, opaque minerals, and sphene.

The QFG are fine- to medium-grained equigranular rocks with compositional banding resulting from the segregation of biotite in thin horizons. The QFG have mineral proportions that are slightly different from the SGG; most significantly, sillimanite occurs in only trace amounts in the QFG. Quartz usually makes up about 30%, with 10-30% plagioclase, 30-50% perthitic K-feldspar, 2-4 % biotite, and up to 5% garnet. Accessory phases include zircon, apatite, opaque minerals, and sphene. Textures are similar to the SGG, with foliations weakly developed. Again, most feldspar is slightly to moderately sericitized, and quartz shows undulose extinction. Feldspar twins are commonly bent or broken.

Geochemical Results

Major Elements

Major and trace element data are given in Table 3. The major element contents are diverse within each group but are distinct among groups.

SiO_2 contents in SGG range from 54-71%, and show a negative correlation with Al_2O_3. Al_2O_3 contents are high (14-21%) (fig. 18a; for comparison, post-Archean average Australian Shale (PAAS; Taylor and McLennan, 1985) is plotted on this and subsequent diagrams); TiO_2 ranges from 0.5-1.0%. Fe_2O_3T varies between 6-11% (fig. 18b), averaging about 8% and MgO shows a restricted range of 2.0-3.2%. CaO is generally low with most samples containing 0.5-1.5% (fig. 18c). Na_2O and K_2O are more variable, ranging from 0.5-4.0% and 0.9-7.0%, respectively.

Table 3: Major and trace element data for khondalites from the Datong region.

	Sillimanite-Garnet Gneisses									
	k11	k20	k42	k48	k62	k64	k65	k77	J3	J6
SiO_2	71.24	66.05	61.36	63.17	54.17	61.64	69.04	64.54	60.68	62.27
TiO_2	0.70	0.82	0.71	0.79	0.78	0.71	0.63	0.59	0.70	0.92
Al_2O_3	15.77	17.38	19.31	16.94	20.38	19.26	15.97	17.84	20.40	19.91
Fe_2O_3T	6.42	7.35	6.87	8.59	10.70	7.32	7.21	6.40	8.83	8.83
MnO	0.05	0.06	0.04	0.10	0.08	0.05	0.05	0.04	0.09	0.09
MgO	2.39	2.36	2.11	3.11	3.32	2.47	2.28	2.22	2.85	3.12
CaO	0.51	0.51	1.11	1.00	1.52	0.69	0.47	2.00	0.45	0.56
Na_2O	0.71	0.92	2.25	3.30	2.51	2.54	0.89	3.06	0.53	0.70
K_2O	3.16	4.13	6.08	3.02	6.73	6.00	3.67	3.24	3.67	3.13
P_2O_5	0.06	0.07	0.06	0.06	0.06	0.06	0.06	0.07	0.20	0.29
LOI	0.30	0.29	0.14	0.05	0.60	0.25	0.40	0.97	2.59	0.45
TOTAL	101.32	99.93	100.03	100.13	100.85	100.99	100.65	100.96	100.99	100.27
Rb	102	149	227	70	172	254	160	97	179	112
Sr	137	117	181	229	252	159	135	235	112	157
Ba	732	727	773	785	1064	746	687	564	776	879
Th	12.9	9.2	6.0	11.6	5.4	12.6	13.4	8.9	13.5	13.9
Zr	193	180	141	229	151	155	137	135	176	182
Hf	7.4	5.2	4.9	8.5	6.6	4.8	5.3	4.4	nd	nd
Nb	7.8	9.6	3.8	14.6	21.2	9.2	8.3	8.8	18.6	21.2
Ta	0.88	0.57	0.60	1.05	1.35	0.57	0.73	0.66	nd	nd
Y	33	36	31	52	43	32	27	29	53	19
La	45	38	38	46	41	37	40	38	57	54
Ce	90	73	62	91	69	77	86	80	103	101
Nd	38	26	23	39	23	35	35	37	50	49
Sm	7.37	6.37	6.45	7.60	5.55	7.20	7.34	6.30	9.56	7.62
Eu	1.29	1.26	1.31	1.54	1.68	1.11	1.18	1.30	1.52	1.43
Gd	nd	nd	nd	nd	nd	nd	nd	nd	8.93	5.48
Tb	1.04	0.93	0.91	1.40	1.37	0.94	0.99	0.83	1.37	0.65
Yb	3.41	3.27	3.11	4.60	4.75	3.71	3.24	3.25	6.22	2.10
Lu	0.53	0.48	0.49	0.72	0.77	0.56	0.48	0.49	0.99	0.35
Sc	16	19	18	21	30	20	17	17	29	12
V	95	103	95	122	121	109	102	92	110	146
Cr	107	128	131	134	157	136	125	102	12	131
Co	11	18	15	17	15	13	15	14	nd	nd
Ni	18	44	14	15	17	28	17	25	41	69
CIW*	89.0	88.4	77.6	70.5	75.1	78.5	88.0	67.7	94.4	93.1

* CIW is the Chemical Index of Weathering, $Al_2O_3/(Al_2O_3 + CaO + Na_2O) \times 100$, using molecular ratios; CaO is that remaining after apatite is subtracted assuming all P_2O_5 is in apatite (after Harnois, 1988).

Table 3: continued

	Sillimanite-Garnet Gneisses								
	J13	J15	J16	J28	k21	J2	J23	J24	J30
SiO_2	65.43	65.34	53.84	62.45	60.20	65.78	68.66	67.90	61.98
TiO_2	0.65	0.89	0.96	0.58	1.36	0.70	0.74	0.32	0.86
Al_2O_3	18.12	18.54	24.43	16.11	19.72	17.92	13.98	15.12	15.76
Fe_2O_3T	7.91	9.18	11.47	7.17	5.85	4.95	7.22	7.85	11.91
MnO	0.08	0.13	0.14	0.07	0.08	0.09	0.13	0.12	0.14
MgO	2.43	2.73	3.31	2.56	2.16	1.60	2.70	2.36	3.95
CaO	0.78	0.39	0.74	1.37	4.35	2.04	1.93	1.41	3.17
Na_2O	0.65	0.49	1.79	3.90	3.91	3.25	2.23	1.88	1.34
K_2O	2.45	2.95	2.80	3.59	0.90	3.32	0.91	3.32	1.08
P_2O_5	0.11	0.16	0.18	0.24	0.04	0.14	0.15	0.16	0.19
LOI	1.13	0.87	0.77	1.92	1.38	0.97	1.55	1.04	1.35
TOTAL	99.74	101.67	100.43	99.96	99.94	100.13	100.20	101.48	101.73
Rb	112	88	75	64	12	67	nd	82	43
Sr	107	83	139	242	622	451	241	329	184
Ba	930	815	843	859	210	1052	351	1273	349
Th	19.2	nd	nd	nd	0.4	13.6	nd	1.0	nd
Zr	182	219	261	239	50	181	407	274	298
Hf	nd	nd	nd	nd	1.8	nd	nd	nd	nd
Nb	38.7	6.1	5.1	34.5	9.8	3.0	11.1	10.7	46.0
Ta	nd	nd	nd	nd	1.14	nd	nd	nd	nd
Y	32	48	48	35	23	44	44	71	53
La	79	45	40	41	16	71	45	31	14
Ce	139	69	60	70	31	121	70	39	24
Nd	61	33	26	36	8	48	24	13	14
Sm	10.0	6.67	7.61	6.50	2.61	5.50	4.20	3.89	3.68
Eu	1.70	1.35	1.46	1.30	1.38	2.58	1.33	1.69	1.14
Gd	8.04	7.59	9.85	5.32	nd	4.76	6.53	6.79	4.34
Tb	1.04	1.17	1.46	0.91	0.59	0.91	1.22	1.44	0.97
Yb	3.42	5.13	5.35	4.13	2.59	4.26	5.00	9.19	6.58
Lu	0.51	0.83	0.91	0.59	0.44	0.62	0.90	1.48	0.94
Sc	19	nd	nd	17	15	21	nd	31	29
V	52	133	187	117	112	35	138	87	223
Cr	263	266	245	319	47	38	157	109	390
Co	nd	nd	nd	nd	9	nd	nd	nd	nd
Ni	27	13	43	117	14	30	53	21	136
CIW	89.1	94.2	86.4	65.9	58.1	67.3	67.2	74.1	67.7

nd = not determined or not detected.

Table 3: continued

	Quartz-Garnet Gneisses					
	k23	k45	k47	J25	J26	J27
SiO_2	83.55	82.76	78.81	81.40	82.81	82.41
TiO_2	0.53	0.43	0.25	0.29	0.46	0.47
Al_2O_3	8.73	8.73	11.43	9.64	8.77	9.70
Fe_2O_3T	2.77	2.76	3.19	2.58	3.09	2.26
MnO	0.04	0.03	0.04	0.08	0.08	0.09
MgO	0.87	1.12	1.27	1.16	0.76	0.58
CaO	1.52	1.41	1.41	0.81	1.37	1.14
Na_2O	1.41	1.47	1.96	1.75	1.30	1.65
K_2O	0.89	0.89	1.71	0.92	0.50	0.50
P_2O_5	0.05	0.05	0.05	0.07	0.05	0.08
LOI	0.27	0.19	0.36	0.99	0.76	1.59
TOTAL	100.62	99.83	100.47	99.69	99.95	100.47
Rb	25	21	57	13	10	26
Sr	183	178	189	112	104	106
Ba	213	182	357	127	41	62
Th	5.6	2.4	8.1	7.5	nd	11.8
Zr	298	188	116	181	439	519
Hf	8.2	6.0	4.1	nd	nd	nd
Nb	3.3	1.4	2.8	18.4	31.0	29.2
Ta	0.32	0.55	0.50	nd	nd	nd
Y	24	21	27	18	28	36
La	30	25	27	24	28	28
Ce	64	53	56	48	61	66
Nd	29	22	24	24	28	30
Sm	5.61	4.52	4.47	4.75	4.99	5.74
Eu	0.90	1.03	0.93	0.82	0.92	0.80
Gd	nd	nd	nd	4.07	4.49	5.43
Tb	0.82	0.67	0.62	0.62	0.72	0.90
Yb	2.69	2.05	2.39	1.80	3.43	3.81
Lu	0.46	0.34	0.36	0.27	0.52	0.58
Sc	7	7	7	5	8	7
V	28	39	29	17	17	21
Cr	76	65	32	94	143	131
Co	5	4	4	nd	nd	nd
Ni	7	12	6	19	19	31
CIW	63.8	64.2	66.8	69.7	66.0	67.9

Table 3: continued

	Quartz-Feldspar Gneisses					
	k38	J1	J19	J20	J21	J22
SiO_2	71.03	73.64	56.58	71.44	71.63	64.24
TiO_2	0.33	0.16	0.69	0.47	0.31	0.40
Al_2O_3	15.54	14.96	17.37	13.50	14.43	18.83
Fe_2O_3T	1.96	1.00	4.67	1.96	3.26	1.91
MnO	0.03	0.05	0.09	0.06	0.04	0.09
MgO	0.84	0.19	4.88	1.17	0.35	0.51
CaO	1.78	1.18	5.83	1.28	1.40	3.26
Na_2O	3.17	4.05	1.25	2.61	3.06	5.65
K_2O	4.85	5.05	3.07	6.25	5.75	1.36
P_2O_5	0.12	0.30	0.16	0.17	0.21	0.17
LOI	0.36	0.70	5.21	0.67	0.34	0.74
TOTAL	100.00	100.70	99.80	99.58	100.78	96.80
Rb	149	nd	178	150	258	16
Sr	375	782	178	299	3091	589
Ba	806	582	738	1315	236	390
Th	16.2	nd	nd	nd	nd	nd
Zr	128	71	192	70	317	74
Hf	3.3	nd	nd	nd	nd	nd
Nb	3.2	7.5	8.1	24.2	33.3	20.0
Ta	0.34	nd	nd	nd	nd	nd
Y	11	nd	12	3	7	5
La	41	nd	52	196	63	26
Ce	88	nd	89	330	104	36
Nd	38	nd	36	137	43	14
Sm	6.42	nd	6.39	17.41	5.43	1.81
Eu	0.98	nd	1.70	2.21	1.63	1.60
Gd	0.00	nd	4.47	7.32	4.04	1.16
Tb	0.38	nd	0.64	0.29	0.38	0.12
Yb	1.06	nd	0.90	0.85	0.83	0.72
Lu	0.13	nd	0.26	0.09	0.14	0.17
Sc	5	nd	nd	nd	6	nd
V	46	10	152	41	36	23
Cr	54	37	153	31	236	24
Co	3	nd	nd	nd	nd	nd
Ni	10	8	84	37	80	34
CIW	65.6	64.9	58.6	68.5	67.1	56.0

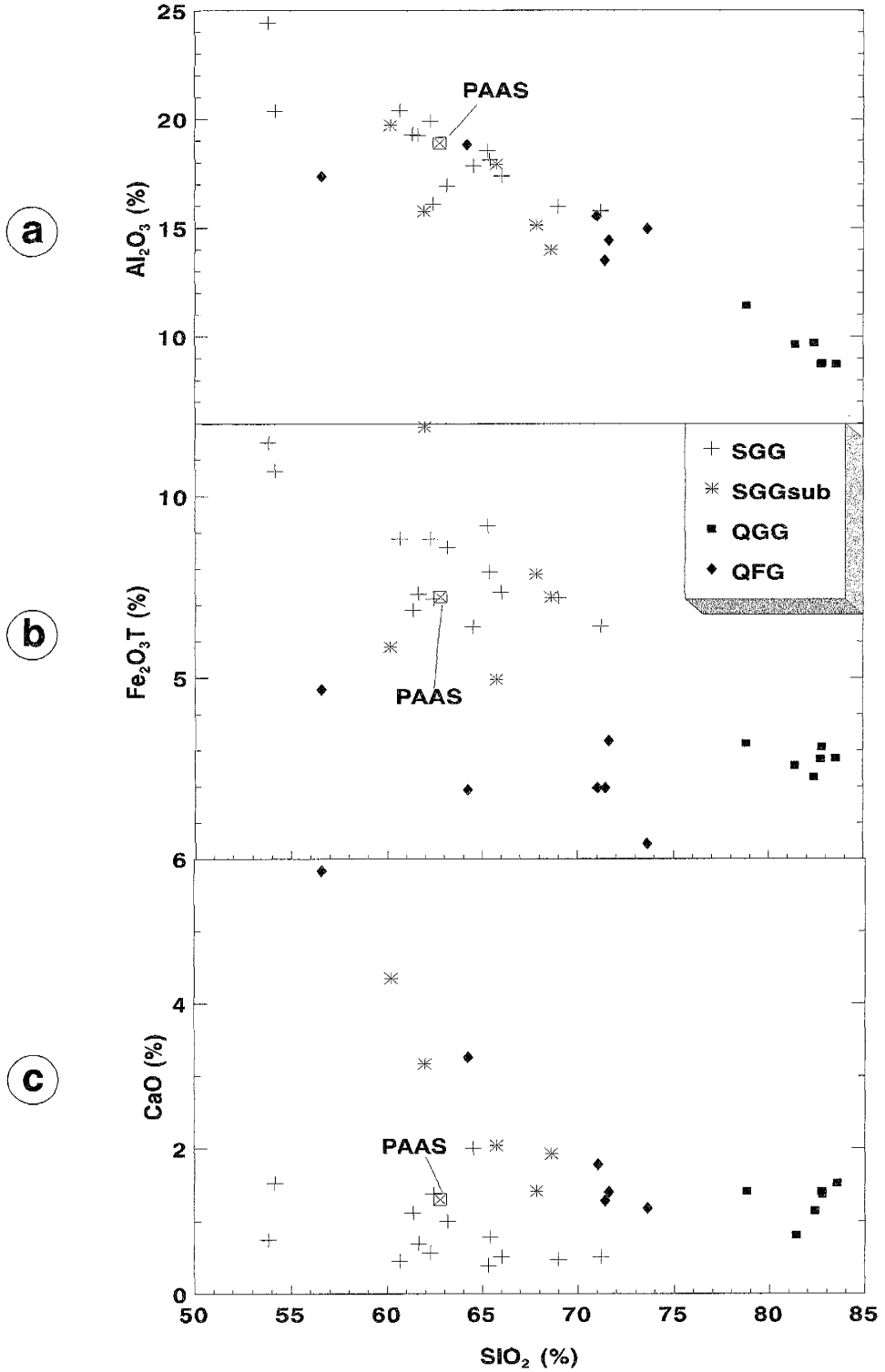

Figure 18: Major element distributions for Datong area khondalites and PAAS (post-Archean average Australian shale; Taylor and McLennan, 1985).

A subgroup of SGG, made up of five sillimanite-garnet gneisses (K21, J2, J23, J24, and J30), is chemically distinct from the main group (e.g., fig. 18c). These samples have intermediate SiO_2 contents (60-68%), but CaO ranges from 5-12% and shows a strong negative correlation with SiO_2. The range in most major elements (Al_2O_3, Fe_2O_3T, MgO, Na_2O) is similar to that in the SGG, but K_2O contents tend to be lower.

The high modal quartz content in the six QGG samples results in high SiO_2 contents that range from 79-84%. As a result of quartz dilution, most other major elements have low concentrations: Al_2O_3 (8.7-11.4%, fig. 18a), TiO_2 (0.25-0.53%), Fe_2O_3T (2.3-3.2%, fig. 16b), and MgO (0.6-1.3%). This is supported by the modal abundance data (Table 2). CaO and Na2O are not lower in QGG than in SGG due to this effect, a feature controlled by their respective modal plagioclase contents (20-25%). It is probable that the SGG and QGG form one continuous population that may not be adequately represented due to incomplete sampling.

The QFG are distinguished from the others by low TiO_2 (0.3-0.5%), Fe_2O_3T (1.9-3.3%, fig. 18b), and MgO (0.35-1.2%), moderate Al_2O_3 (13.5-18.8%, fig. 18a), and high CaO (1.4-3.3%, fig. 18c). Na_2O and K_2O are generally much higher than in SGG, ranging from 2.6-5.6 and 1.4-6.3%, respectively; K_2O/Na_2O varies from 1.0-2.5, except for sample J22, in which $K_2O/Na_2O = 0.24$. One sample (J19) has anomalously high MgO (4.88%) and CaO (5.83%); its TiO_2 and Fe_2O_3T contents are also slightly higher than the others in this group (0.69% and 4.7%, respectively), while SiO_2 is anomalously low (56.6%).

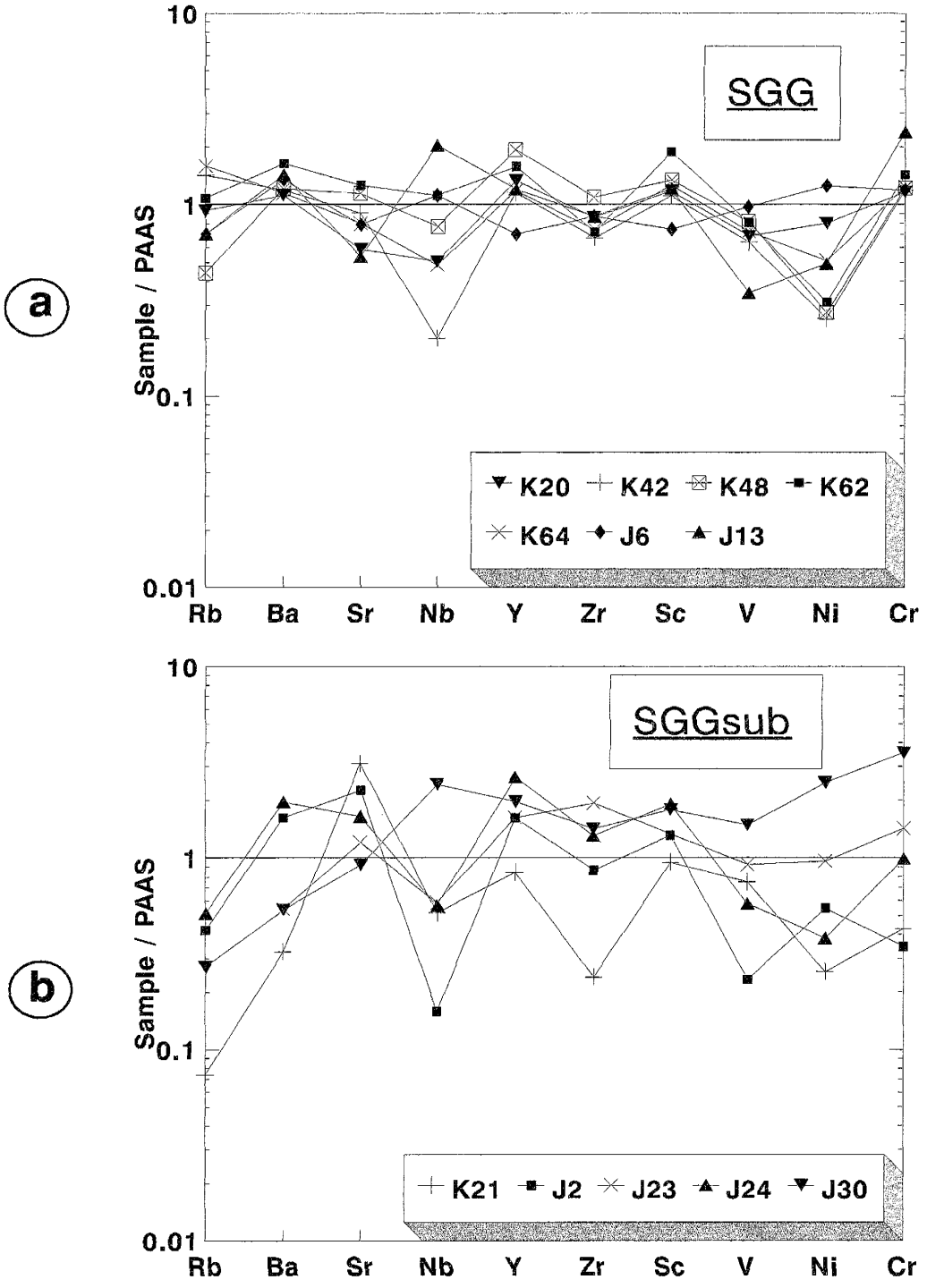

Figure 19: LILE (Rb, Ba, Sr), HFSE (Nb, Y, Zr) and transition metal (Sc, V, Ni, Cr) distributions for (a) representative SGG and (b) subgroup of SGG, norrmalized to PAAS (Taylor and McLennan, 1985). SGG are strikingly similar to average shales.

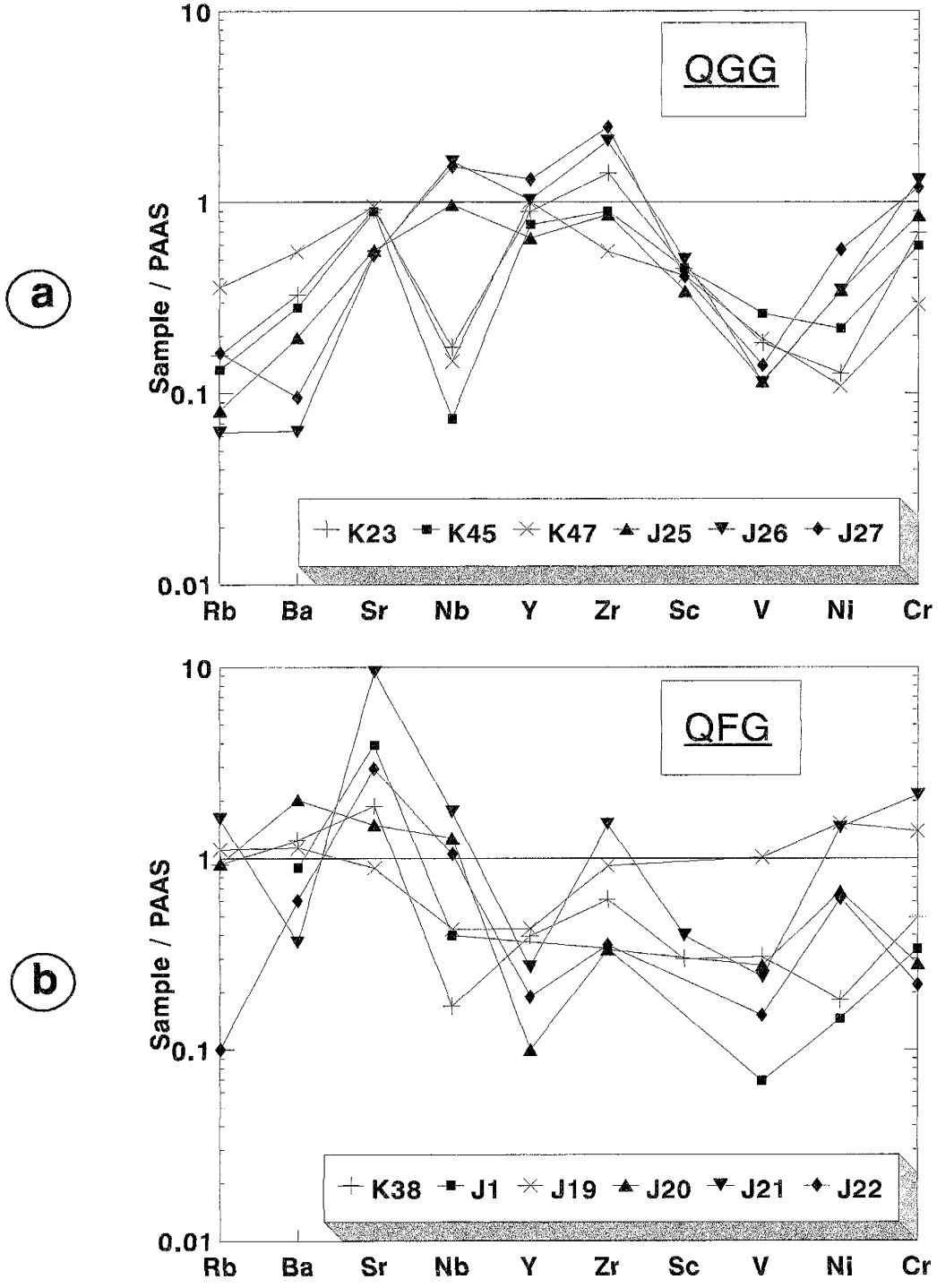

Figure 20: LILE (Rb, Ba, Sr), HFSE (Nb, Y, Zr) and transition metal (Sc, V, Ni, Cr) distributions for (a) QGG and (b) QFG, norrmalized to PAAS (Taylor and McLennan, 1985). Note depletions in Rb, Ba, Sc, V and Ni in QGG.

Large-Ion Lithophile Elements (LILE)

LILE concentrations among the khondalites are related to quartz dilution: modal quartz shows a negative correlation with total LILE. The SGG have significant variations in LILE (Rb, Th, Ba, Sr, etc.) abundances, as expected considering the variation in major elements and modal compositions. Average concentrations are similar to PAAS (fig. 19a). Rubidium contents range from 25-250 ppm; Sr from 80-300 ppm; Th from 5-20 ppm; and Ba from 250-1000 (most cluster between 650-850 ppm). Samples in the subgroup of SGG (fig. 19b) tend to have more variable LILE concentrations: Rb ranges from 12-82 ppm, Sr from 184-622 ppm; Th from 0.4-13.6 ppm; and Ba from 210-1273 ppm.

LILE contents in QGG samples are much lower than in the SGG (Table 3) and PAAS (fig. 20a). The QFG have more variable LILE concentrations than the other groups (Table 3; fig. 20b). Barium varies from 240-1300 ppm, Rb from 16-260 ppm, and Sr from 180-780 ppm (sample J21 has Sr content of 3100 ppm).

Rare Earth Elements (REE)

The SGG have REE distributions that are markedly similar to Phanerozoic shales (Gromet et al., 1984; Taylor and McLennan, 1985) with enriched LREE (~100× chondrite), only slightly fractionated HREE (~20× chondrite) and significant Eu anomalies (Eu/Eu* ranges from 0.43-0.78, fig. 21). Sample J13 is somewhat enriched in LREE relative to the other samples, with La = 250× chondrite); J6 has slightly lower HREE (Yb and Lu about 10× chondrite).

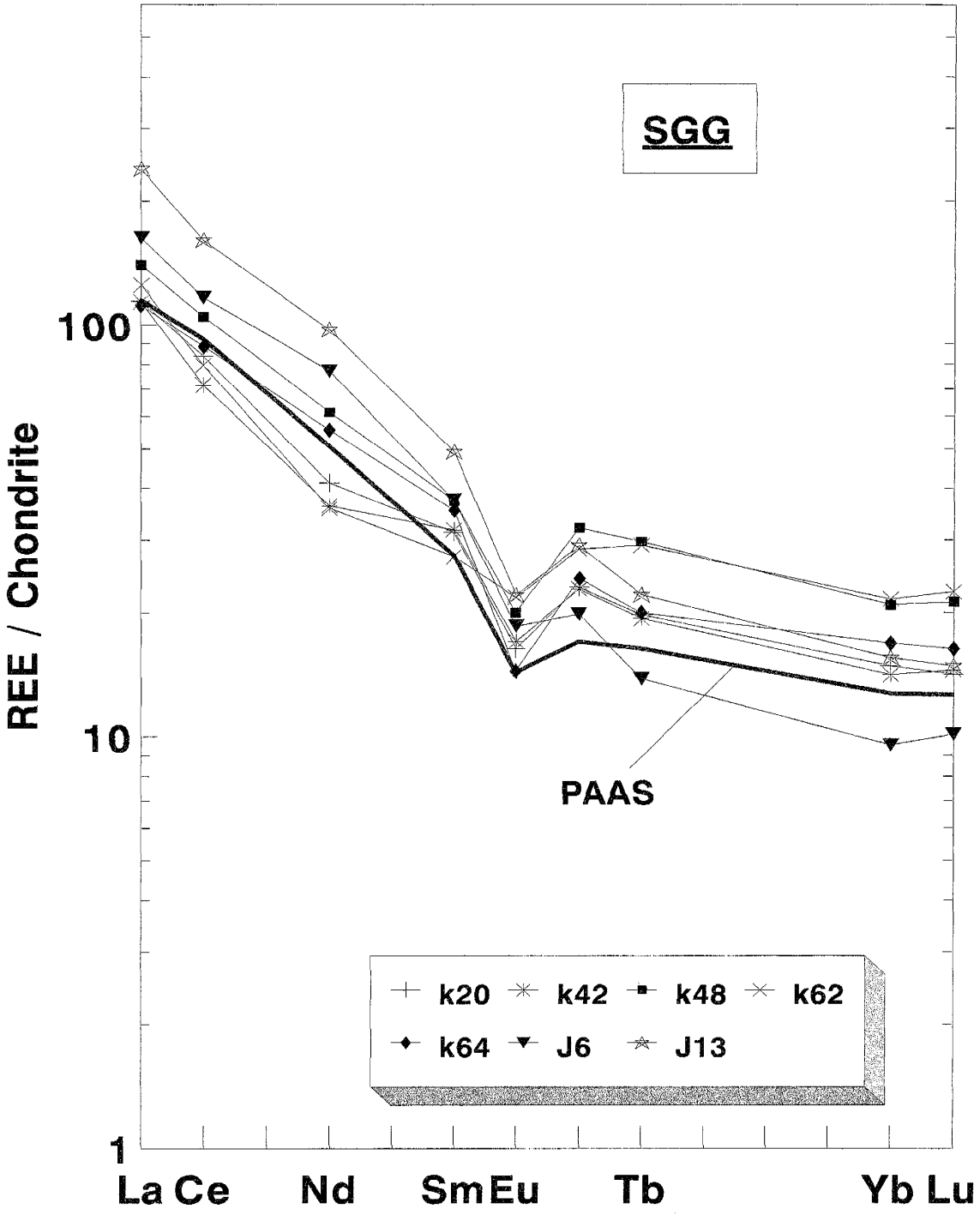

Figure 21: REE distributions for representative SGG, normalized to chondritic meteorite; PAAS for reference. Note that Gd value is calculated (see fig. 6).

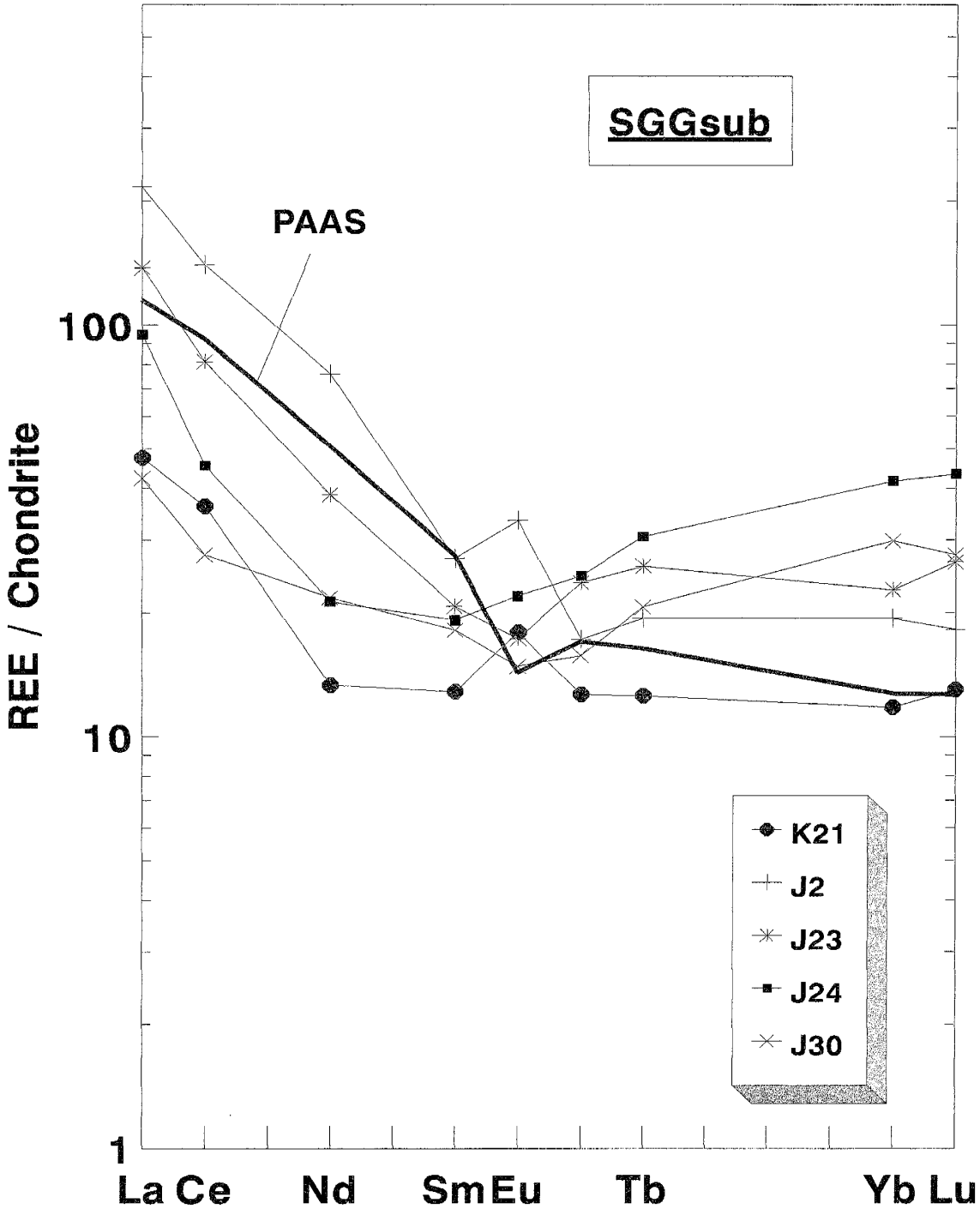

Figure 22: REE distributions for subgroup of SGG, normalized to chondritic meteorite; PAAS for reference. Note that Gd value is calculated (see fig. 6).

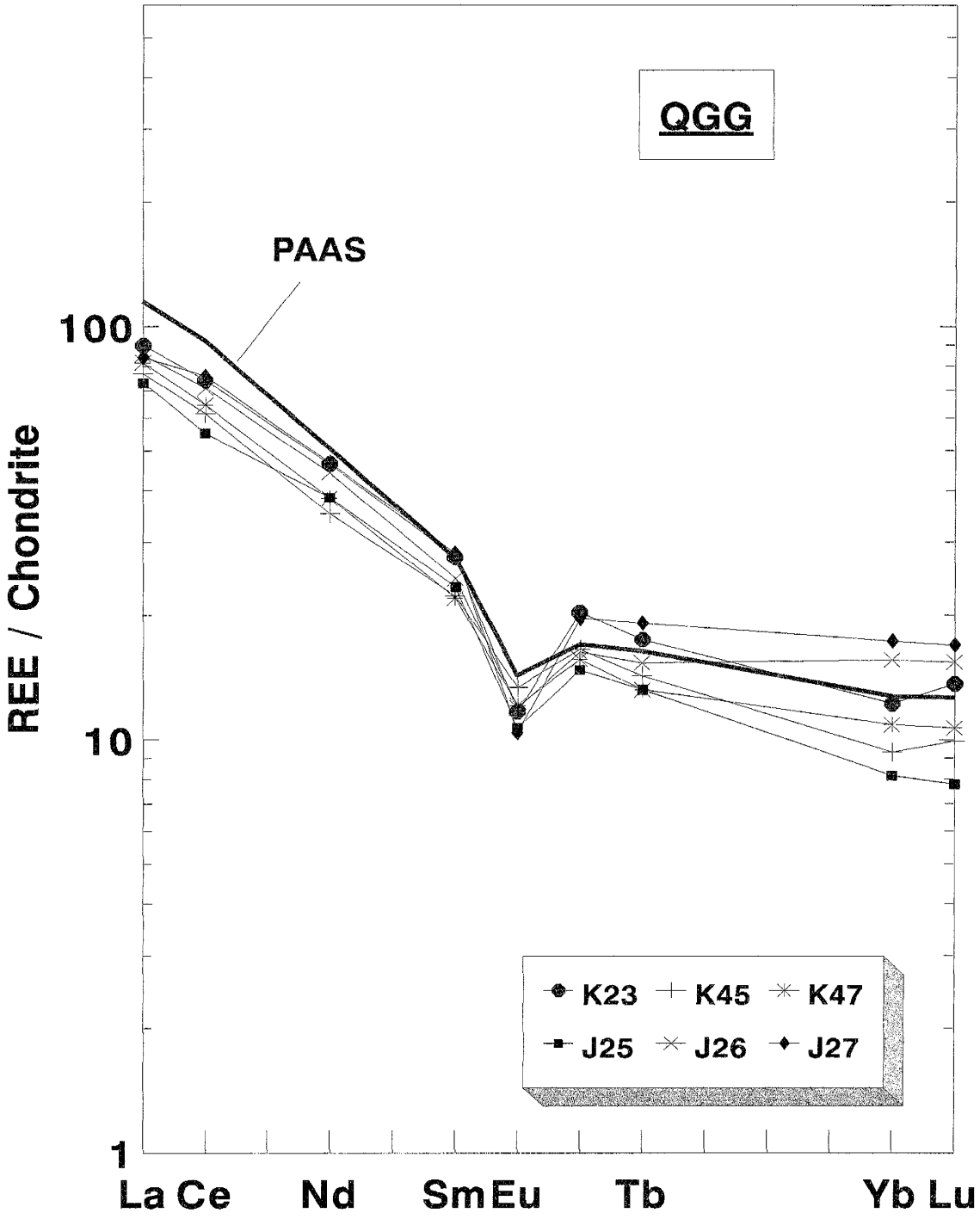

Figure 23: REE distributions for QGG, normalized to chondritic meteorite; PAAS for reference. Note that Gd value is calculated (see fig. 6).

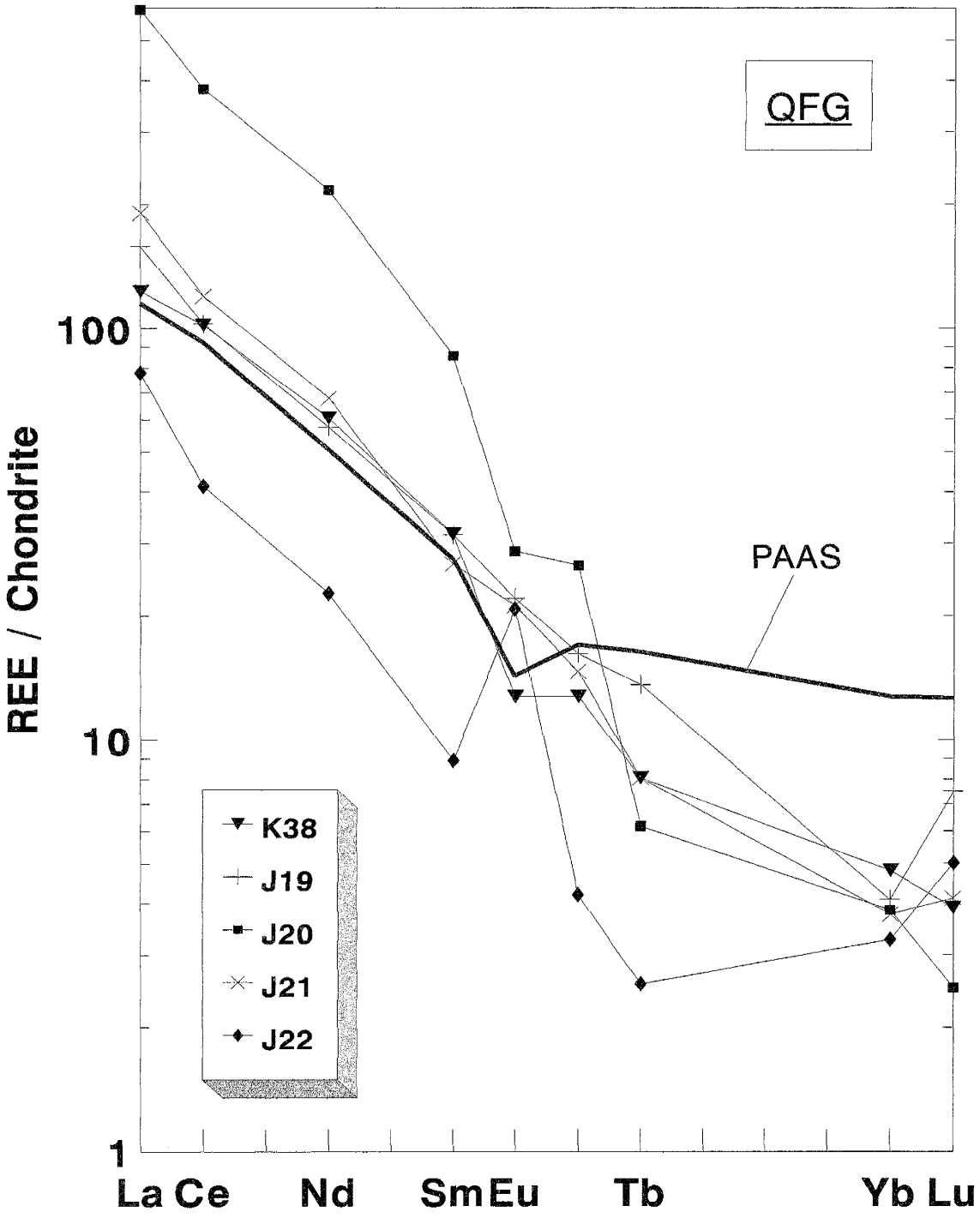

Figure 24: REE distributions for QFG, normalized to chondritic meteorite; PAAS for reference. Note that Gd value is calculated (see fig. 6).

The five samples in the SGG subgroup also have more variable REE distributions (fig. 22). Three have relatively flat HREE distributions and positive Eu anomalies (K21, J2 and J23) and two have U-shaped patterns (J24 and J30) similar to some other Early Archean metasediments (Taylor et al., 1986; Boak and Dymek, 1992). It would appear that different phases are controlling the light and heavy REE in these latter samples. Although zircon can be responsible for marked enrichments in HREE, the only slightly elevated Zr contents in these samples do not support this interpretation (McLennan, 1989; Condie, 1991a). Enrichment in garnet is also not responsible for the high HREE, as these samples have modal garnet abundances similar to the other SGG.

The QGG have REE distributions that are also similar to the SGG and PAAS, but with slightly lower REE concentrations (fig. 23). As with the SGG, Eu anomalies are significant (Eu/Eu* = 0.43-0.70). These striking similarities suggest that the REE were contained in similar mineral phases in the protoliths of both types.

The QFG have REE distributions (fig. 24) that contrast markedly with those of the SGG and QGG. HREE are low (2-4× chondrite) and REE are highly fractionated ($(La/Yb)_N$ = 24-51, with one sample = 154, compared with 5-17 in the SGG and QGG), with little or no Eu anomaly. Sample J22 has total REE contents that are markedly lower than the others in this group, and also a strong positive Eu anomaly. These steep REE patterns are similar to those of Archean TTG (tonalite-trondhjemite-granodiorite) (Jahn and Zhang, 1984; Martin, 1987) and also to those of enderbites found in the gray gneiss association east of Datong (Liu, 1989).

High Field Strength Elements (HFSE) and Y

The SGG have concentrations of HFSE (Zr, Hf, Nb, Ta) and Y (Table 3) that are similar to PAAS (fig. 19). Zr shows a narrow range of concentration, from 130-260 ppm. Hf varies between 4.4-8.4 ppm for the eight samples with data, and correlates with Zr content (Zr/Hf ≈ 29), suggesting that zircon controls the concentrations of these elements. Nb varies in SGG samples by an order of magnitude (3.8-30 ppm), although most samples contain 5-15 ppm Nb. Ta varies between 0.57-1.35 ppm for the K-samples (Ta data are not available for the J-samples), and correlates with the Nb data (Nb/Ta ≈ 13).

HFSE concentrations of QGG samples are also similar to PAAS (fig. 20a), but these samples show a much larger range in Zr contents than the SGG. Zr and Hf concentrations are again correlated, indicating zircon control. Nb is depleted relative to Y in three samples.

Most QFG samples are strongly depleted in HFSE (Nb excluded) relative to SGG, QGG, and PAAS (fig. 20b). Zr varies from 70-190 ppm, except in sample J21 (320 ppm Zr). Hf and Ta data are available for only one sample (K38). Nb contents vary from 3.2-33 ppm.

Transition Metals

Transition metal (V, Sc, Co, Cr, Ni) contents of SGG samples are similar to PAAS except for moderate depletion in Ni (fig. 19). V contents generally vary from 95-190 ppm, but sample J13 contains only 52 ppm. Sc contents vary from 12-30 ppm. Only

eight samples were analyzed for Co, which varies from 11-18 ppm. V, Co, and especially Sc vary consistently with Fe_2O_3T and TiO_2, suggesting that they are contained in Fe-Ti oxide phases. Cr contents vary from 110-320 ppm, with most samples having about 150 ppm; sample J3 contains only 12 ppm Cr. Ni varies from 15-130 ppm, with most samples containing about 25 ppm; Ni is not well correlated with Cr, and neither Cr nor Ni correlate with Fe or Ti.

Transition metal contents are much lower in QGG samples than in PAAS (fig. 20a), with V and Ni showing the greatest depletion. V varies from 17-40 ppm while Sc varies only from 5-8.0 ppm. Co is present in concentrations of about 4 ppm. Cr varies from 32-140 ppm, and Ni from 7-31 ppm.

The QFG also have low concentrations of transition metals relative to the other groups and PAAS (fig. 20b), although analyses for Sc and Co are not comprehensive. V contents range from 10-50 ppm, except for sample J19 which has 150 ppm V. Cr variations are similar to those of V; sample J19 contains 150 ppm Cr, but sample J21 contains 236 ppm Cr, and is not coupled with high V or Ni.

Discussion

Protolith

Khondalites have traditionally been assumed to represent the metamorphosed equivalents of aluminous or clay-rich sediments, i.e. shales, and related sediments. This interpretation has been called into question by Dash et al. (1987) and Dash and Bowes

(1991) who have proposed that the khondalites exposed in Orissa, India are the metamorphosed equivalents of deeply weathered soils. These authors have compared the geochemical data from their khondalites to average crustal estimates and to modern deeply-weathered soil profiles from Brazil. However, the major element criteria they used are not definitive in distinguishing between residual soils and sediments derived from erosion of deeply weathered terranes (e.g., the ternary diagram of SiO_2-Al_2O_3-Fe_2O_3T was proposed by Moore and Dennen (1970) to distinguish quartzites, arkoses, graywackes, and shales - not soils). Most investigations of the geochemistry of paleosols (e.g., Schau and Henderson, 1983; Zbinden et al., 1988; Holland et al., 1989; Rainbird et al., 1990) rely on geologic data in addition to chemical composition to distinguish them as such (Condie et al., 1992). Such evidence includes the following.

1) Khondalite suites typically have some form of stratigraphy preserved (Barbey and Cuney, 1982; Dash et al., 1987; Nanda and Pati, 1991). In the Datong region, khondalite units are found to be interlayered on the scale of meters, with individual layers remaining traceable for kilometers along strike despite their metamorphic grade (Condie et al., 1992). While some structural repetition on a regional scale is probable, there is no evidence for deformation being responsible for layering that occurs on the scale of outcrops. Paleosols generally do not perserve such pervasive layering (see (2) below).

2) Ancient paleosols commonly have thicknesses ranging from 1-10 m. Modern paleosols from the Amazon Basin, referred to by Dash et al. (1987), are surprisingly thick at 100 m (Kronberg et al., 1979). Nanda and Pati (1991) have reported that the thickness

before tectonism of the Orissa khondalite suite must be a few tens of kilometers, and thus the inference of a paleosol protolith is unrealistic. As pointed out by Nanda and Pati (1991), Dash et al. (1987) have called upon only one stage of development for the deeply weathered soil that is the proposed protolith for the Orissa khondalites.

Considering (1) and (2), the thicknesses, intercalation, and extent of exposed khondalite suites are probably the result of sedimentary or volcanic/volcaniclastic processes rather than *in situ* weathering.

3) Metamorphic equivalents of unweathered bedrock have not been identified in khondalite terranes. The preservation of stratigraphic horizons implies that the contact of the paleosol with its unweathered bedrock might also be preserved; in the Orissa region and others, no such parent is exposed (Dash et al., 1987; Nanda and Pati, 1991; Condie et al., 1992).

4) The overall chemical compositions of high-Al khondalites ($Al_2O_3 > 12\%$) in this study and in that of Barbey et al. (1982) are consistently similar to Phanerozoic shales and siltstones. This constancy further suggests well-mixed sedimentary protoliths. Paleosols form by *in situ* weathering of bedrock. Both bedrock composition and intensity of weathering are variable. The result is a paleosol with highly variable composition (Kronberg et al., 1979; Zbinden et al., 1988; Rainbird et al., 1990; Condie et al., 1992).

For these reasons it is likely that the khondalites from the Datong region as well as those from Lapland and Orissa are not metamorphosed paleosols. An alternative interpretation for the origin of the Orissa khondalite suite is that the Al-rich portion of the suite represents sediment that has been derived from a deeply weathered source

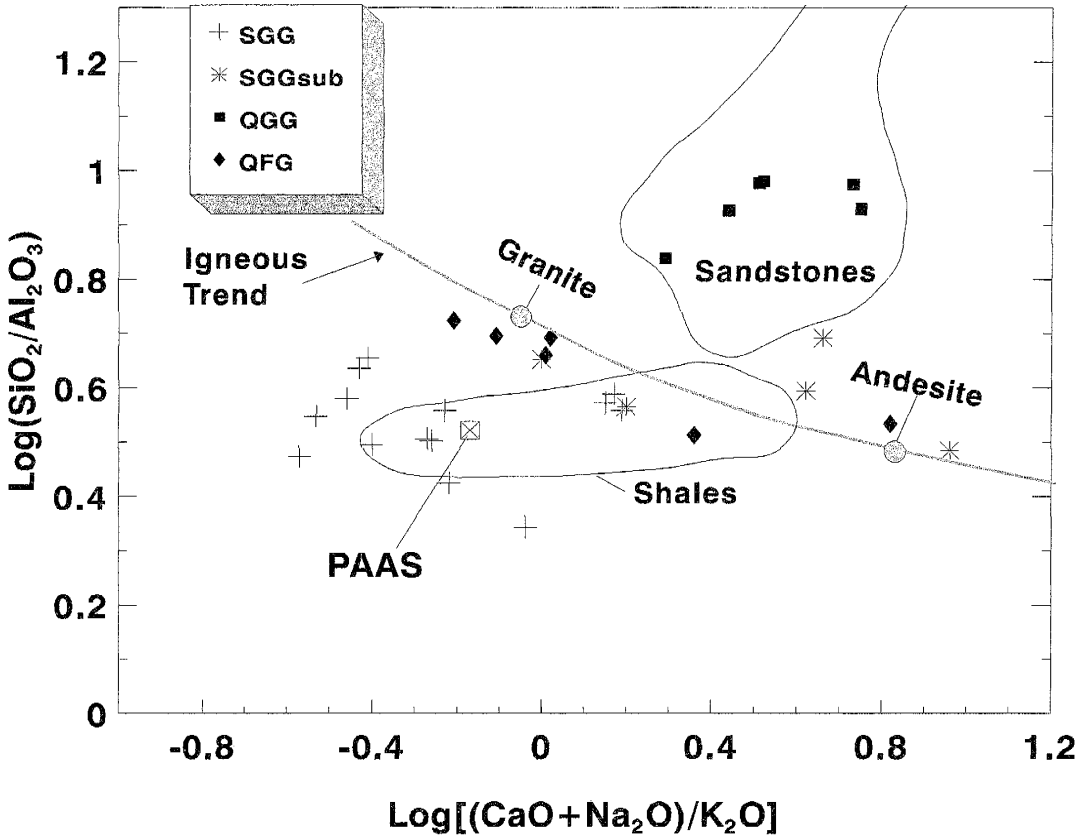

Figure 25: Plot of log [(CaO + Na_2O) / K_2O] vs. log (SiO_2 / Al_2O_3) (Garrels and MacKenzie, 1971) for khondalites from the Datong area, showing similarities of SGG to shales and PAAS and of QGG to arkoses and graywackes (sandstone field). QFG define a trend subparallel to the igneous trend, indicating a strong igneous influence in their protoliths.

region (Condie et al., 1992). The SGG from the Datong region also may have had shale and feldspathic sandstone or siltstone precursors. A relatively small proportion of a given khondalite suite may have igneous precursors, as proposed here for the QFG of the Datong region.

Support for shale and sandstone protoliths is further demonstrated in figure 25, in which the SGG appear to be similar to average shales and the QGG plot in the field of sandstones.

The protoliths of the QFG are difficult to ascertain. Boryta (1988) and Boryta and Condie (1990) were able to show that many of the "meta-arkosic" rocks from the Central Zone of the Limpopo Belt were actually orthogneisses, but they had a larger sample population than the six samples of this study. However, it is reasonable that the QFG represent metamorphosed igneous (or volcaniclastic) rocks of Archean tonalitic (or tonalite-trondhjemite-granodiorite, TTG) composition because of their steep REE patterns and negligible Eu anomalies (Condie, 1981a, b; Arkani-Hamed and Jolly, 1989). Contact relations do not preserve definitive evidence distinguishing between an intrusive, volcanic or volcaniclastic origin, nor can such origins be distinguished by chemical analysis alone. The transitional nature of a few of the samples suggests that the suite is, at least in part, metasedimentary in origin; the presence of small negative Eu anomalies in some of the samples may document the input of some granitic material (Gao and Wedepohl, 1995). In figure 25 the QFG plot sub-parallel to an igneous fractionation trend, which supports an igneous (or volcaniclastic) origin.

Composition of the Source Region

In order to use the compositions of the khondalites to constrain the composition of their sedimentary provenances, we must understand the degree of weathering of source material prior to their deposition. Studies of modern weathering show that Na, Ca and Sr are rapidly depleted during chemical weathering and that such elements as Al, Ti, and Zr are relatively enriched (Kronberg et al., 1979; Wronkiewicz and Condie, 1987; Condie et al., 1994). Harnois (1988) has proposed a Chemical Index of Weathering that

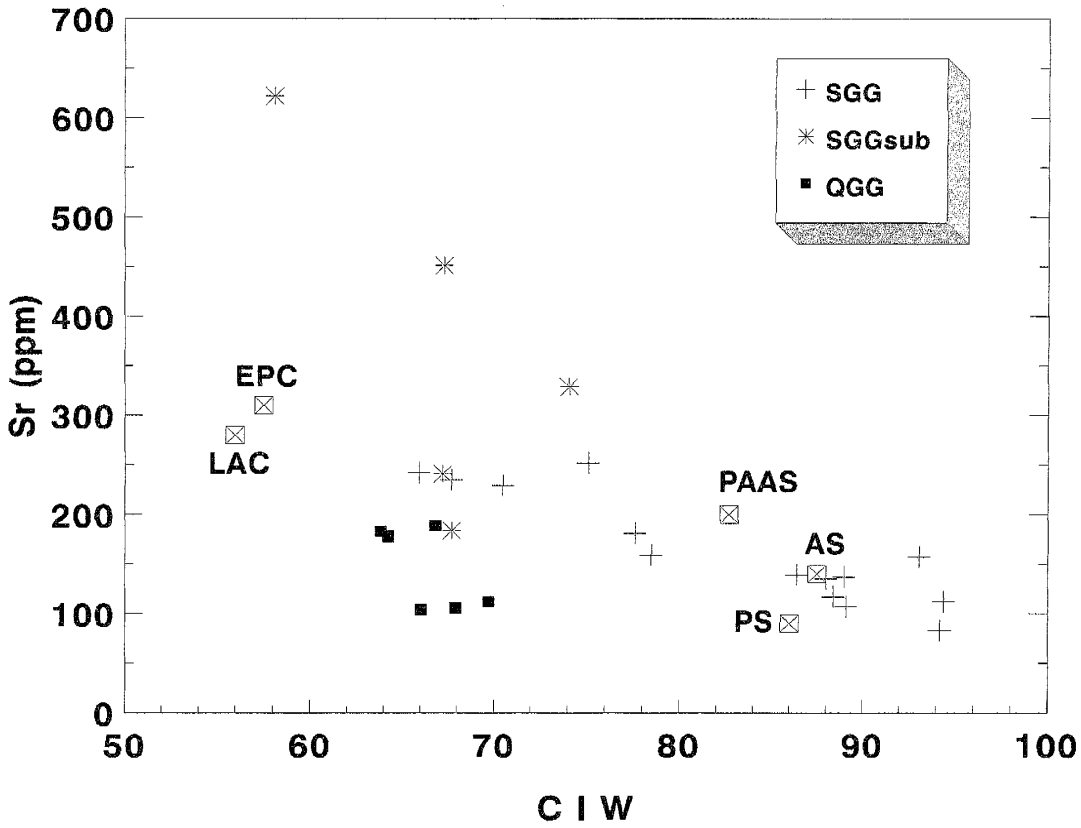

Figure 26: Sr vs. Chemical Index of Weathering (CIW) indicates the degree of weathering of source regions. CIW = $\{[Al_2O_3 / (Al_2O_3 + CaO + Na_2O)] \times 100\}$ using molecular ratios (after Harnois, 1988). CaO is that remaining after apatite is subtracted assuming all P_2O_5 is in apatite. PAAS, post-Archean average Australian shale (Taylor and McLennan, 1985). AS and PS, average Archean and Early Proterozoic shales; LAC and EPC, average Late Archean and Early Proterozoic upper continental crust (Condie et al., 1992).

uses the major elements Al_2O_3, CaO and Na_2O as a measure of the intensity of weathering of sedimentary material. These elements are thought to be nearly immobile during metamorphism of the Datong khondalites. Fresh granitic rock tends to have CIW values of 50-65, while CIW values of intensely-weathered paleosols (laterites) are around 95 - 100 (Harnois, 1988; Gao and Wedepohl, 1995). Reference points, including average Late Archean Crust (LAC) and Early Proterozoic Crust (EPC) and average Archean and Proterozoic shales (AS and PS) (Condie et al., 1992), and PAAS (Taylor and McLennan,

1985), serve to demonstrate that as continental crust undergoes progressive weathering, CIW increases and Sr, which is concentrated in feldspar, decreases. In figure 26, the SGG show an inverse correlation between CIW and Sr. This correlation suggests that the SGG are derived from progressively weathered sedimentary rocks (Wronkiewicz and Condie, 1987; Condie et al., 1992). The QGG plot below the trend of the SGG; quartz dilution has probably resulted in lower Sr, but does not affect the CIW values of these samples.

Certain trace elements (e.g., REE, HFSE) are transported directly from the source to sedimentary basin without being fractionated; that is, the REE pattern of a shale directly mimics that of the bulk composition of its source region (Taylor and McLennan, 1985; Gao and Wedepohl, 1995 and references therein). This is because those elements (REE, HFSE) are either housed in minerals (such as zircon, apatite, allanite, and monazite) which are resistant to both chemical and mechanical weathering processes, or are adsorbed on clay minerals (this occurs with transition metals, REE), and thus have minimal residence times in surface waters. The REE distributions of shales thus reflect that of the source from which they are derived.

The SGG and QGG have REE patterns (figs. 21-23) with negative Eu anomalies ($Eu/Eu^* = 0.4\text{-}0.8$) and $(Gd/Yb)_N$ ratios (1-2) that are similar (fig. 27) to those of Phanerozoic cratonic terrigenous sediments (shales; McLennan, 1989). These negative Eu anomalies are larger and $(Gd/Yb)_N$ ratios smaller than corresponding values in either Archean or Proterozoic upper continental crust (Condie, 1991a; Condie et al., 1992). Archean TTG sources have considerably higher $(Gd/Yb)_N$ ratios (≥ 2) and negligible Eu anomalies, implying that TTG, such as the Late Archean enderbite and TTG terranes

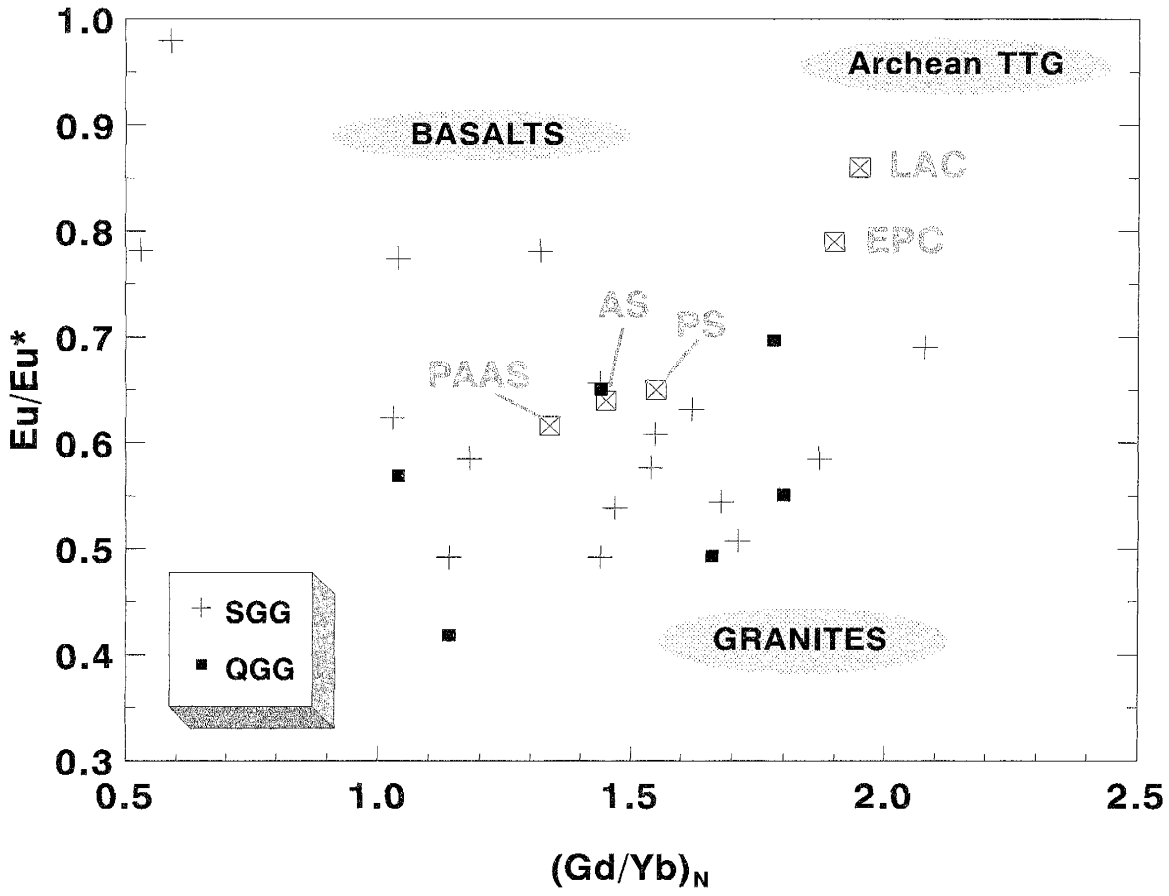

Figure 27: Eu/Eu* vs. $(Gd/Yb)_N$ showing distribution of SGG and QGG from the Datong region. SGG subgroup is not differentiated from the main group on this diagram, but SGG subgroup samples with high Eu/Eu* (>1: K21, J2, J24) are not plotted. The fields for Basalts, Granites and Archean TTG are placed on the figure where the compositions of Late Archean and Early Proterozoic examples of these rocks fall (Condie et al., 1992). PAAS, post-Archean average Australian shale (Taylor and McLennan, 1985); AS and PS, average Archean and Early Proterozoic shales; LAC and EPC, average Late Archean and Early Proterozoic upper continental crust (Condie et al., 1992).

making up the northern margin of the North China craton (Liu, 1989), were not major contributors to the basin in which the khondalite protoliths were deposited.

The protoliths of SGG and QGG may be derived from dominantly granitic sources with some basaltic input. Although Archean komatiites (or norites, see Mafic Dike section) may have been present in small amounts in the sediment source regions,

the low Ni and Cr contents in the SGG and QGG precludes them from being important contributors.

Constraints on Tectonic Setting

Geochemical data favor two contrasting origins for the Datong area khondalites. On discriminant diagrams such as those proposed by Bhatia (1983) and Bhatia and Crook (1986), QGG are most similar to graywackes deposited in cratonic or passive margin basins, while SGG are similar to those deposited in continental island arc or active continental margin settings (fig. 28). However, the appropriateness of these diagrams for the interpretation of tectonic settings of sedimentary rocks other than graywackes is questionable, and it is not clear that the Datong khondalites represent metamorphosed graywackes.

An important constraint is placed on the tectonic setting by the presence of the QFG. These gneisses have equigranular textures and variable thicknesses, ranging from 10 cm to 2-3 m. Contacts with the surrounding gneisses are sharp and conformable. These features and the widespread lateral distribution of the QFG leave open the possibility that the QFG may be volcanic or volcaniclastic horizons, or tonalitic intrusive sills (Condie et al., 1992). If the QFG are of volcanic or volcaniclastic rather than intrusive origin, as suggested by their lateral extent, then they may represent fallout from eruptions from nearby continental-margin arc systems (Condie et al., 1992). Arc and back-arc basin successions of similar age to the Datong khondalites occur at several localities along the southern boundary of the North China Craton (Sun et al., 1988,

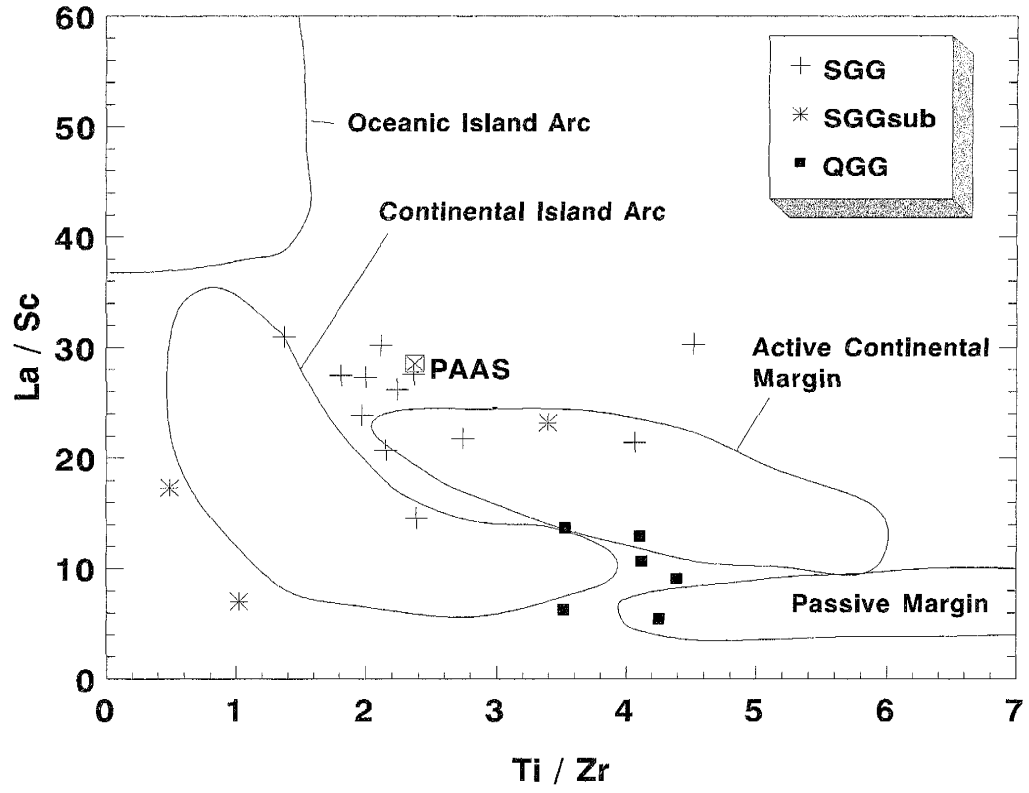

Figure 28: Khondalite distribution of La/Sc vs. Ti/Zr (Ti in ppm). PAAS, post-Archean average Australian shale (Taylor and McLennan, 1985). Fields represent average graywacke compositions found in each tectonic environment (after Bhatia and Crook, 1986)

1990). These authors have proposed that the Early Proterozoic rocks exposed in the Zhongtiao Mountains in southern Shanxi Province represent an ancient convergent margin arc of the North China craton.

An interpretation consistent with available data and tectonic discrimination diagrams is that the region north of Datong represents a Late Archean or Early Proterozoic back-arc basin, perhaps something like the modern Japan Sea. Material was shed into this basin from two sides, resulting in two distinct conpositions of sediments. The QGG are derived from the passive continental margin side, and the SGG are derived from the active continental margin or continental arc. Deposition of the khondalite suite

could be coeval with volcanic activity in the Zhongtiao Mountains, which may be responsible for the deposition of the QFG.

Conclusions to Part II

1. The khondalite suite exposed in the granulite belt marking the northern edge of the North China craton includes the metamorphosed equivalents of shales (SGG), siltstones or sandstones (QGG), and tonalitic volcanic or volcaniclastic rocks (QFG).

2. The protoliths of the khondalites are not paleosols, as proposed for khondalites of the Eastern Ghats region by Dash et al. (1987).

3. Khondalites from the Nei Mongol granulite belt are similar in many respects to those of Lapland reported by Barbey et al. (1982), and to many of those reported by Dash et al. (1987), suggesting that khondalite associations may represent metamorphosed pelitic successions derived from moderately to highly weathered source regions. The variability of trace elements can be used to constrain the compositions of the source regions.

4. Based on major and trace element data, the provenance of these rocks had granitic with minor basaltic material as important constituents, and komatiitic material was not significant.

5. The tectonic setting in which the sediments were deposited is speculative, but one interpretation is a back-arc basin bordering a passive continental margin, such as the present-day Japan Sea between northern China and Japan.

Part III: Geochemistry and Differentiation of Granitoids

Introduction

Our understanding of the bulk chemical composition of the Earth's crust relies in part on geochemical models for intracrustal differentiation (Bickle, 1990). Intracrustal differentiation occurs when heating during regional metamorphism of the lower to middle crust induces partial melting of that crust. There is a vast array of conditions that pertain to this process, known as anatexis, including those of temperature and pressure, mineralogical and chemical compositions of rocks, availability of fluids, composition of fluid, etc. (for overviews, see Ashworth and Brown, 1990; Rubie and Brearley, 1990; Pitcher, 1993; Wilson, 1993; McDermott et al., 1996). These conditions affect the manner in which the chemical composition of the resulting melt relates to that of the source because they affect the participation of various minerals in the melting process.

In the previous sections we have assumed that REE are transferred from the source with little or no fractionation. In the case of granitoid genesis, this is not a valid assumption (Evans and Hanson, 1993; Barbey et al., 1995; Johannes et al., 1995). The least understood aspect of incipient melting in granitoid systems is the degree to which the various phases in the source transmit their chemical signatures to the melt (Condie and Sinha, 1996). Trace minerals such as zircon, monazite and apatite often host the majority of the REE in granitoids (Watson and Harrison, 1984; Taylor and McLennan, 1985; Wall et al., 1987; Watt and Harley, 1993; McDermott et al., 1996), and REE are

framework elements in some of these minerals [e.g., monazite has the general formula (Ce, La, Nd, Th)(PO_4, SiO_4)]. Experimental work and studies of natural systems have shown that these phases do not consistently participate in melting reactions (e.g., Watson and Harrison, 1984; Watt and Harley, 1993; McDermott et al., 1996).

The study of granitoid genesis in the Liangchen region was undertaken to test our understanding of the geochemical aspects of anatexis. By modeling the melting process to fit the observed compositions of the source and melt, we should be able to better understand the transfer of geochemical signatures from source to melt. The compositions of the granitoids are compared with granitoids from known tectonic regimes in an effort to constrain the environment in which they formed.

Results

Field Relationships

Khondalites crop out in the Liangchen area (figs. 2, 29). They are intruded by sparse Precambrian mafic dikes (too small to be indicated in the map area of fig. 29) that contain mineral assemblages identical to those found in the Hunyuanyao area. Khondalites are banded and often preserve an S-C structural fabric, indicating at least two deformational events (Liu, 1989). The mineral assemblage found in the khondalites (Qtz + Plg + Ksp + Bio + Sill + Gar, Part II) is typical of shales metamorphosed under granulite-grade conditions. At lower grades of metamorphism, muscovite is an abundant mineral in shales; thus metamorphism probably induced dehydration of muscovite to

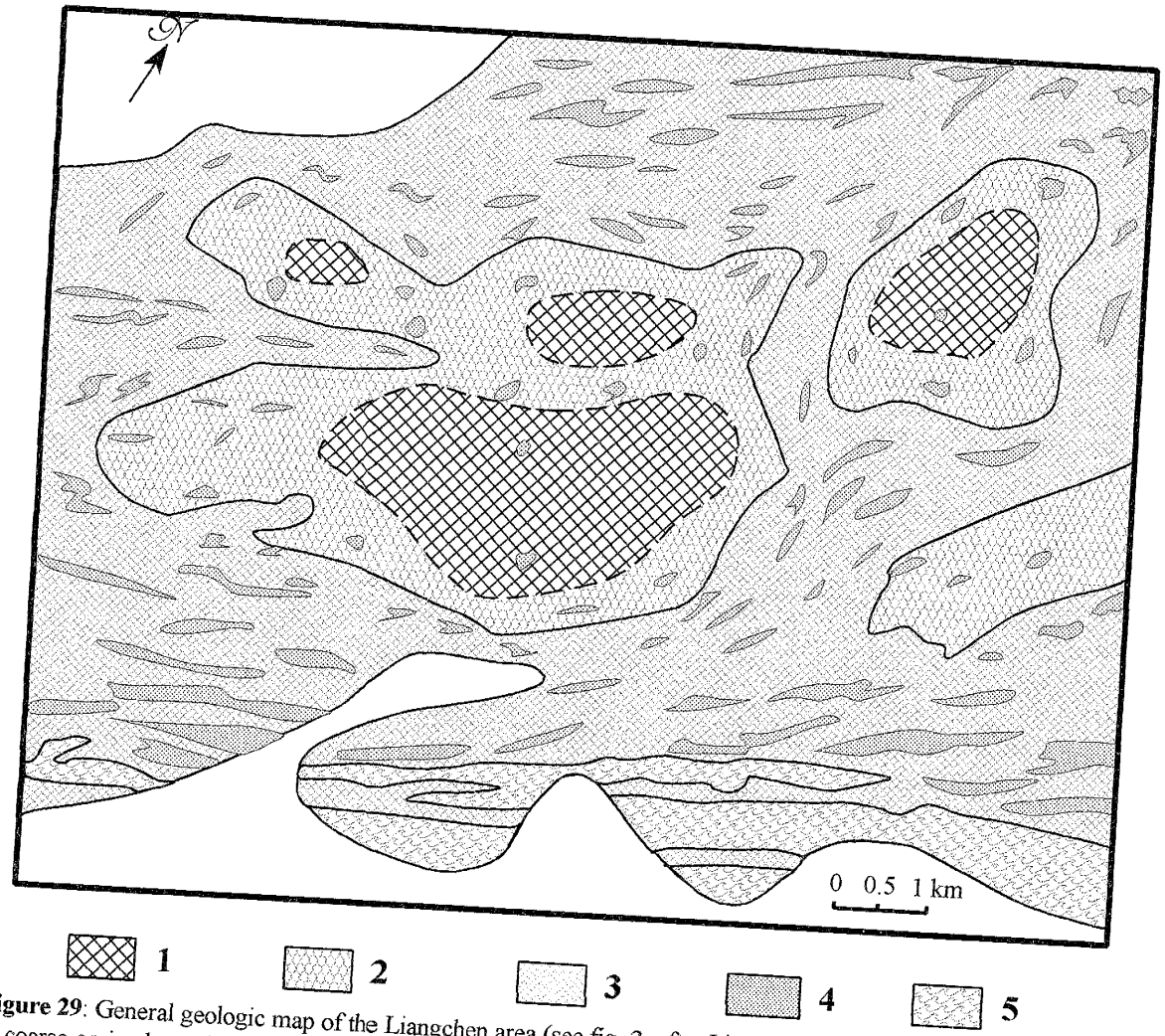

Figure 29: General geologic map of the Liangchen area (see fig. 2; after Liu, 1989). Symbols are as follows. 1: coarse-grained xenolith-bearing granite. 2: coarse-grained xenolith-poor granite. 3: fine-grained granite. 4: khondalite xenolith. 5: khondalite (including migmatite).

form sillimanite and K-feldspar via a reaction such as

$$Ms + Qtz \rightarrow Sill + Kfs + H_2O \qquad \text{Rxn 1}$$

(Essene, 1982)

The absence of muscovite may also indicate the formation of melt by the incongruent reaction

$$Ms + Qtz + Pl \rightarrow Sill + Kfs + M \qquad \text{Rxn 2}$$

(Stevens and Clemens, 1993)

which in the Liangchen area must have proceeded until muscovite was exhausted.

The region preserves evidence for various stages of anatexis. Small (~1 km across) granitoid plutons dominate the landscape. Away from the plutons, the khondalites are banded or interlayered on a scale of centimeters. Some of the banding is related to the development of leucosome. With increasing proximity to the plutons, the proportion of melt to khondalite increases, and the quartz + feldspar leucosomes become thicker. Thin pods and lenses of nearly pure garnet or sillimanite occur as schlieren (Plate 8). At least one of these schlieren is large enough to be considered for evaluation as an economic deposit of garnet. In places, these residual minerals are entrained in the melt. Within the granitoid bodies, garnets sometimes form glomerocrysts up to 1 cm across (Plate 2).

Textures of different granitoid bodies range from fine grained equigranular (average grain size about 4 mm) to pegmatitic (in which feldspar crystals are up to 5 cm in length). Medium- to coarse-grained granodiorites (Group 1) contain abundant mylonitized khondalite xenoliths at their margins. Banding (defined in the granitoids by alignment of feldspars and trains of garnet) is not as well developed as in the surrounding khondalites, and feldspars within the granitoid bodies are often bent or broken.

Petrography

Granitoids of the Liangchen area have mineral assemblages similar to associated khondalites (compare Tables 2 and 4; Appendices C and D). The granitoids can be divided into three groups, based weakly on mineralogical (mainly garnet content) but chiefly on chemical compositions (Tables 4 and 5), epecially the distributions of REE.

Table 4: Ranges of mineralogical composition* in the three granite groups from the Liangchen region.

	Group 1	Group 2	Group 3
# thin sections	5	4	3
Quartz	15-35%	25-60%	30-45%
K-feldspar	5-60%	10-60%	30-65%
Plagioclase	tr-25%	tr-25%	tr-30%
Sillimanite	0-3%	tr-3%	tr-2%
Garnet	10-15%	5%	2-5%
Biotite	tr-10%	tr-3%	tr-1%
Apatite	tr	tr	tr
Zircon	tr	tr	tr
Hercynite	tr	tr	tr
Sphene	tr		tr
Rutile		tr	
Opaques	tr	tr	tr
Sericite	tr	tr	tr
Chlorite		tr	tr

* Abundances based on 400 points counted for each sample.

Most petrographic features are common to all the groups; in the mineralogical descriptions below, differences among groups are noted where appropriate. Group 1 granodiorites (fig. 30, after Le Bas et al., 1986) contain variable proportions of quartz and feldspars; garnet comprises 10-15% and sillimanite is rare. Group 2 granites contain a greater abundance of quartz and variable proportions of feldspars; garnet comprises 5% and sillimanite is present in minor amounts. Group 3 granites are petrographically similar

to Group 1 granodiorites in the abundances of major components (quartz and feldspars), and to Group 2 granites in minor components (sillimanite and garnet).

Quartz that is not hosted in another mineral has undulose extinction and often has fine-grained recrystallized borders (Plate 9). Quartz blebs within garnet *do not* have undulose extinction. A few thin sections contain vein quartz (L18, L30), although visible veins were avoided in pieces analyzed geochemically. K-feldspar in the granitoids is generally perthitic, and its grain size varies from <1 mm to 6 mm across. Myrmekite is common although not pervasive. Plagioclase (An_{10-30}) is often much smaller in size than K-feldspar, usually measuring ≤3 mm across. Bent and broken pericline twins are common, but in very few plagioclase grains, albite twins are present. Plagioclase is often slightly to moderately cloudy and K-feldspar is often partially sericitized, indicating an influx of fluid after crystallization (Plate 9).

Garnet is generally equigranular and poikiloblastic, containing inclusions of quartz. Inclusions of sillimanite are rare (absent in Group 1) within garnet; when present, they occur as strings of tiny needles. Sillimanite strings are continuous through a single garnet crystal, suggesting that garnet growth may have overgrown an earlier fabric, but the strings arediscontinuous between garnets, indicating that the garnets have since moved. Elsewhere sillimanite is larger (up to 5 mm long), needle-like (never fibrous) and occurs in trains within the granitoids (Plate 10). Biotite usually occurs as a retrograde metamorphic alteration product surrounding garnet, and rarely occurs without garnet. It is always reddish-brown, suggesting that it is Ti-rich.

Accessory minerals include opaques, apatite, zircon, rare chlorite (as a retrograde metamorphic alteration product of garnet or biotite), sericite (as a retrograde metamorphic alteration product of feldspar), sphene and rutile (although sometimes too metamict to distinguish; rutile was found only in Group 2), and hercynite (Plate 11). The hydrous phases are scarce in the granitoids: most samples contain <3% biotite, although one sample contains 5%.

The following incongruent metamorphic reactions appear to be responsible for the formation of the granitic liquids in the Liangchen area:

$$Ms + Qtz + Pl \rightarrow Sill + Kfs + M \qquad \text{Rxn 2}$$

(Stevens and Clemens, 1993)

$$Bio + Sill + Qtz \rightarrow Kfs + Grt + M \qquad \text{Rxn 3}$$

(Powell and Downes, 1990; Watt and Harley, 1993)

Reaction 2 must have proceeded until muscovite was exhausted, as indicated by the absence of muscovite and the abundance of sillimanite in both khondalites and granites. Petrographic evidence for Reaction 3 includes the following. 1) Biotite is present in the granitoids only as a retrograde metamorphic alteration product of garnet. Reduction in abundance of primary biotite and sillimanite from khondalites to granitoids suggests that these minerals were consumed in the reaction that formed the melts. 2) The dramatic increase in size of K-feldspar from khondalite to granitoid suggests that K-feldspar grew during the reaction forming the granitoids. 3) Inclusions in garnet (Plates 9, 10): large garnet grains have inclusions of sillimanite and quartz, and smaller garnets have only strain-free quartz blebs, suggesting that larger garnet grains may have shielded sillimanite from the melt-forming reaction. 4) The presence of garnet-rich zones

bordering leucosomes (Plate 12; sample L23A, B, Appendix D) and the presence of garnet glomerocrysts within granitoids (Plate 2) suggest that garnet was refractory, and was sometimes carried by the melt as the melt separated from the khondalites. Reaction 3 is a vapor-absent melting reaction expected at the pressure and temperature conditions of metamorphism in the Liangchen the area (~10 kb and 850°C; Liu, 1989), and proceeds to the right as temperature and pressure increase (e.g., Le Breton and Thompson, 1988; Vielzeuf and Holloway, 1988; Powell and Downes, 1990; Patiño Douce and Johnston, 1991; Stevens and Clemens, 1993; McDermott et al., 1996).

Geochemistry

The granitic rocks have been divided into the three groups based on their petrographic characteristics and rare earth element distributions. Although there are differences among them, these groups form a continuum, corresponding to granodiorites (Group 1) and granites (Groups 2 and 3) (fig. 30, after Le Bas et al., 1986). Analyses are presented in Table 5.

Major elements

Liangchen granitoids are chemically similar to partial melts derived from pelitic rocks (Johannes and Holtz, 1990; Pitcher, 1993; Williamson et al., 1996). All samples are peraluminous (molecular A/CNK > 1.1) and Al_2O_3 shows a strong negative correlation with SiO_2 (fig. 31a). Unlike many S-type granites, the Liangchen samples are

Table 5: Major and trace element data for granitoids from the Liangchen region.

	Group 1					Group 2			
	L18	L41	L36	L40	L15	L35	L42	L30	L29
SiO_2	63.42	64.86	65.84	67.18	70.64	73.48	74.66	78.85	79.13
TiO_2	0.82	1.47	1.03	0.70	0.63	0.37	0.12	0.22	0.45
Al_2O_3	16.94	15.39	15.57	15.34	15.34	13.56	15.62	12.26	11.16
Fe_2O_3T	7.84	7.00	6.94	6.32	5.64	2.52	0.95	1.04	2.73
MnO	0.11	0.09	0.08	0.12	0.07	0.04	0.03	0.02	0.04
MgO	2.27	1.79	2.52	2.38	2.21	0.81	0.18	0.84	1.21
CaO	3.32	3.55	3.10	2.06	1.07	1.88	1.02	1.08	1.61
Na_2O	2.74	2.42	1.83	2.09	1.89	2.69	3.27	1.70	1.88
K_2O	1.85	1.52	2.35	2.71	3.14	4.12	4.55	3.94	1.55
P_2O_5	0.08	0.41	0.13	0.07	0.07	0.08	0.15	0.07	0.06
LOI	0.46	0.36	0.43	0.03	0.28	0.09	0.21	0.37	0.41
Total	99.84	98.87	99.82	99.00	100.98	99.63	100.74	100.37	100.23
Rb	60.3	43.1	90.6	72.9	88.9	119.5	152.9	97.4	37.5
Ba	439	1086	557	700	790	377	469	792	375
Cs	0.35	0.20	0.18	0.28	0.44	0.25	0.13	0.16	0.28
Sr	205	267	182	223	161	142	347	247	170
Pb	19.6	17.6	13.5	22.9	21.7	20.0	28.7	27.3	14.0
Th	23.1	2.49	17.1	15.9	9.29	7.33	1.69	1.22	1.43
U	0.72	0.24	0.48	0.88	1.05	0.63	0.84	0.20	0.43
Sc	24.20	17.47	19.10	21.03	14.27	5.91	2.20	1.37	6.13
V	74.1	112	95.2	109	76.7	35.3	10.7	35.2	50.0
Cr	76	30	80	138	92	29	17	32	64
Co	15.4	13.3	12.9	16.0	13.6	5.1	0.7	2.4	6.3
Ni	24.5	28.1	23.5	42.3	15.8	12.3	9.2	15.3	9.3
Y	53.7	45.2	37.2	43.5	25.1	16.5	10.3	5.60	13.0
Zr	274	247	270	467	213	115	82.0	97.9	188
Nb	12.9	19.5	10.7	6.5	9.5	6.3	5.1	6.7	13.3
Hf	7.19	7.08	9.60	14.7	7.85	4.73	2.40	1.89	5.90
Ta	0.54	0.78	0.37	0.39	0.59	0.23	0.17	0.08	0.46
Ga	20.4	16.3	17.5	9.4	13.3	15.5	18.7	6.5	9.4
Zn	67	31	67	53	52	29	21	18	40
Cu	15.6	30.2	47.1	11.3	4.6	1.8	nd	4.5	3.5
La	69.2	51.4	54.9	66.7	51.7	36.7	16.6	28.3	39.0
Ce	140	110	115	131	97.8	72.5	30.9	50.3	80.5
Nd	62.0	52.4	51.6	57.2	35.7	25.8	10.9	16.8	32.3
Sm	11.4	11.3	10.1	10.6	7.3	5.1	2.3	2.5	4.5
Eu	1.45	2.18	1.27	2.11	1.67	1.11	0.36	0.72	1.15
Tb	1.85	1.14	1.29	1.46	0.99	0.58	0.28	0.23	0.44
Yb	7.36	5.23	3.50	6.46	3.06	1.06	0.62	0.40	1.59
Lu	1.08	0.78	0.50	0.96	0.44	0.17	0.08	0.07	0.25
K/Na	0.68	0.63	1.29	1.30	1.66	1.53	1.39	2.31	0.82
A/CNK	1.35	1.27	1.39	1.52	1.81	1.10	1.29	1.36	1.45
Eu/Eu*	0.39	0.70	0.42	0.65	0.75	0.75	0.52	1.08	0.93
$(La/Yb)_N$	5.7	6.0	9.5	6.3	10.3	21.1	16.1	43.1	14.8
$(Gd/Yb)_N$	1.2	1.3	2.0	1.2	1.7	3.1	2.5	3.5	1.6

$Eu^* = \sqrt[3]{(Sm_N^2 \times Tb_N)}$; N subscript denotes chondrite-normalized value.

Table 5 continued: Major and trace element data for granites from the Liangchen region.

	Group 3 Granites				Other samples					
	L23B	L3	L7	L33	L6	L23A	L17	L22	L39	L38
SiO_2	67.99	69.70	74.31	74.81	62.69	75.43	72.95	73.21	75.89	76.49
TiO_2	0.38	0.35	0.41	0.06	2.20	0.51	0.16	0.10	0.02	0.01
Al_2O_3	17.41	16.80	13.76	15.05	13.98	13.49	15.26	15.71	15.20	15.07
Fe_2O_3T	3.20	1.86	2.83	0.50	13.51	2.60	1.05	0.55	0.25	0.24
MnO	0.04	0.02	0.03	0.02	0.16	0.05	0.02	0.02	0.02	0.02
MgO	1.57	0.98	1.04	0.37	1.64	1.13	0.40	0.27	0.02	0.17
CaO	2.42	2.21	1.15	1.24	4.56	1.22	1.39	1.68	0.73	0.60
Na_2O	3.58	2.68	2.41	1.97	1.38	2.64	3.92	3.36	2.83	2.19
K_2O	3.32	3.90	4.59	4.56	0.41	3.60	3.62	4.62	4.31	4.49
P_2O_5	0.07	0.07	0.04	0.09	0.95	0.08	0.07	0.08	0.08	0.11
LOI	0.60	0.74	0.82	0.84	-0.04	0.20	0.18	0.24	0.33	0.26
Total	100.56	99.29	101.40	99.49	101.44	100.93	99.02	99.84	99.68	99.64
Rb	72.9	84.4	133	98.1	13.8	98.2	63.7	81.3	197	182
Ba	920	1085	1211	661	1138	731	686	126	125	46
Cs	0.97	0.75	0.47	0.37	0.21	0.30	0.06	0.11	0.88	0.24
Sr	514	533	309	267	317	229	751	437	62.6	45.4
Pb	22.5	24.7	24.6	22.4	11.3	20.3	18.3	21.6	36.9	38.3
Th	0.33	0.18	0.40	0.37	5.28	1.52	0.25	0.14	0.24	0.06
U	0.54	0.27	0.44	0.12	0.77	0.45	0.32	0.54	0.43	0.17
Sc	8.18	3.91	6.33	1.62	33.0	6.82	2.20	0.82	0.40	0.33
V	54.6	58.6	72.3	17.0	53.1	58.9	27.4	8.1	6.0	2.0
Cr	46	16	73	14	14	70	20	24	15	13
Co	7.1	3.9	5.4	0.7	17.7	6.3	1.3	0.9	0.4	0.2
Ni	20.7	20.6	18.5	5.8	51.5	15.9	6.9	6.0	7.5	5.5
Y	14.8	6.40	16.6	6.18	84.4	17.1	5.43	1.31	6.52	6.94
Zr	273	227	233	45.4	397	187	99.0	60.4	18.4	16.7
Nb	23.0	6.6	5.0	2.4	25.4	7.4	1.1	4.2	3.0	3.0
Hf	9.89	6.27	10.2	1.19	11.9	7.33	2.41	2.08	0.87	0.34
Ta	3.22	0.53	0.25	0.01	1.23	0.26	0.10	0.28	0.01	0.05
Ga	17.2	15.9	13.2	12.3	14.3	10.3	19.4	20.0	17.8	18.2
Zn	29	24	28	7	80	33	28	53	7	11
Cu	8.0	6.0	38.4	2.1	103	6.8	5.2	3.0	2.8	1.4
La	56.6	41.3	25.3	14.0	46.5	44.0	13.8	8.09	2.49	1.51
Ce	99.3	73.3	34.5	23.2	111	81.9	23.4	15.6	4.20	2.45
Nd	35.2	27.5	9.84	9.37	63.5	30.2	9.82	6.26	1.28	1.37
Sm	4.5	2.9	1.9	1.2	16.8	4.3	1.5	1.3	0.4	0.3
Eu	2.22	1.75	2.62	0.51	3.27	1.53	0.43	0.44	0.22	0.09
Tb	0.54	0.24	0.59	0.15	3.00	0.52	0.20	0.09	0.09	0.10
Yb	1.20	0.51	1.36	0.23	8.42	1.89	0.50	0.08	0.38	0.32
Lu	0.16	0.07	0.18	0.05	1.26	0.29	0.07	0.01	0.05	0.04
K/Na	0.93	1.46	1.90	2.32	0.29	1.37	0.92	1.38	1.52	2.05
A/CNK	1.26	1.33	1.25	1.44	1.27	1.29	1.18	1.16	1.43	1.58
Eu/Eu*	1.68	2.34	3.44	1.40	0.58	1.20	0.96	1.38	1.49	0.81
$(La/Yb)_N$	28.6	49.1	11.2	37.5	3.3	14.1	16.8	61.8	4.0	2.9
$(Gd/Yb)_N$	2.5	2.9	1.7	3.6	1.7	1.5	2.1	7.3	1.1	1.2

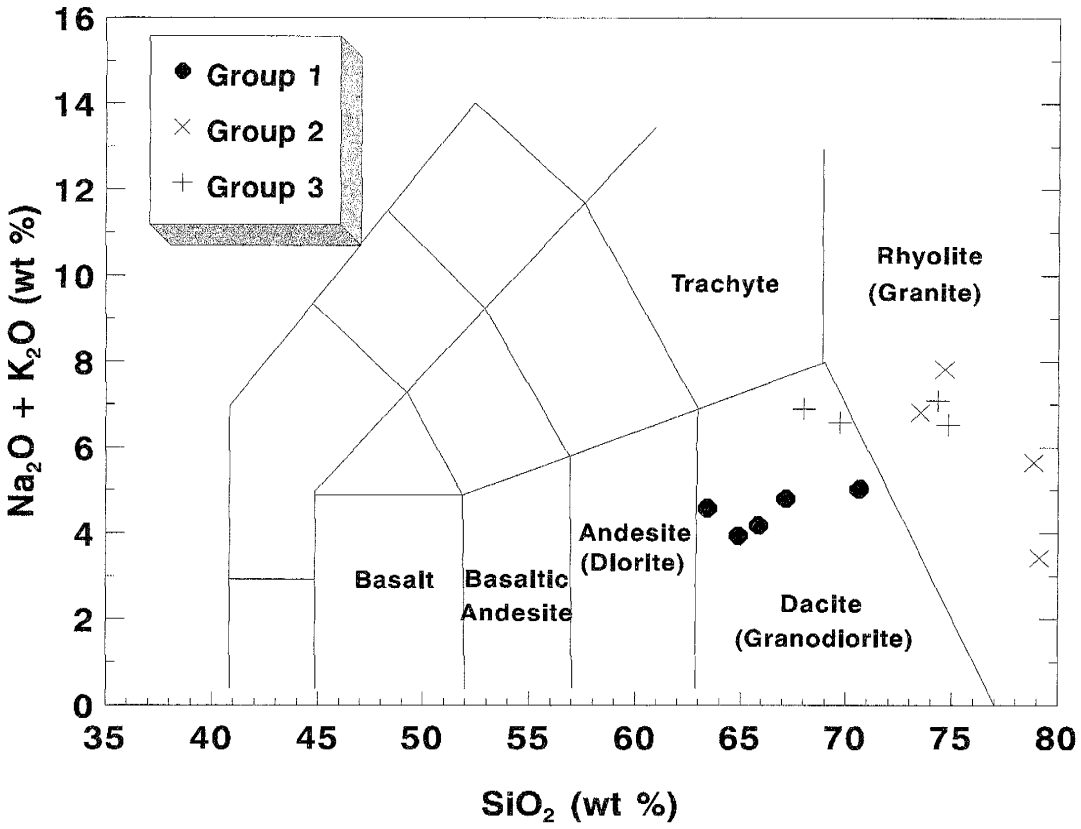

Figure 30: Total alkali - silica chemical classification (Le Bas et al., 1986) shows that Group 1 granitoids are dacitic (granodioritic) and Group 2 and 3 granitoids are rhyolitic (granitic).

relatively anhydrous (2% LOI, very low mica content) (Pitcher, 1993; Williamson et al., 1996).

Group 1 granodiorites have the lowest SiO_2 contents, ranging from 63-67%, and the highest ferromagnesian contents (Fe_2O_3T = 6.3-7.8%, see fig. 31b; MgO = 1.8-2.4%, MnO ≈ 0.1%), TiO_2 (0.7-1.5%) and CaO (2.1-3.5%). These distributions are consistent with the high modal abundances of garnet and (retrogressive) biotite in Group 1. Al_2O_3 and Na_2O are similar to Group 2 and 3 granites (15.3-16.9% and 2.1-2.7%), but K_2O concentrations are low (1.5-2.7%). K_2O/Na_2O averages about 1.0.

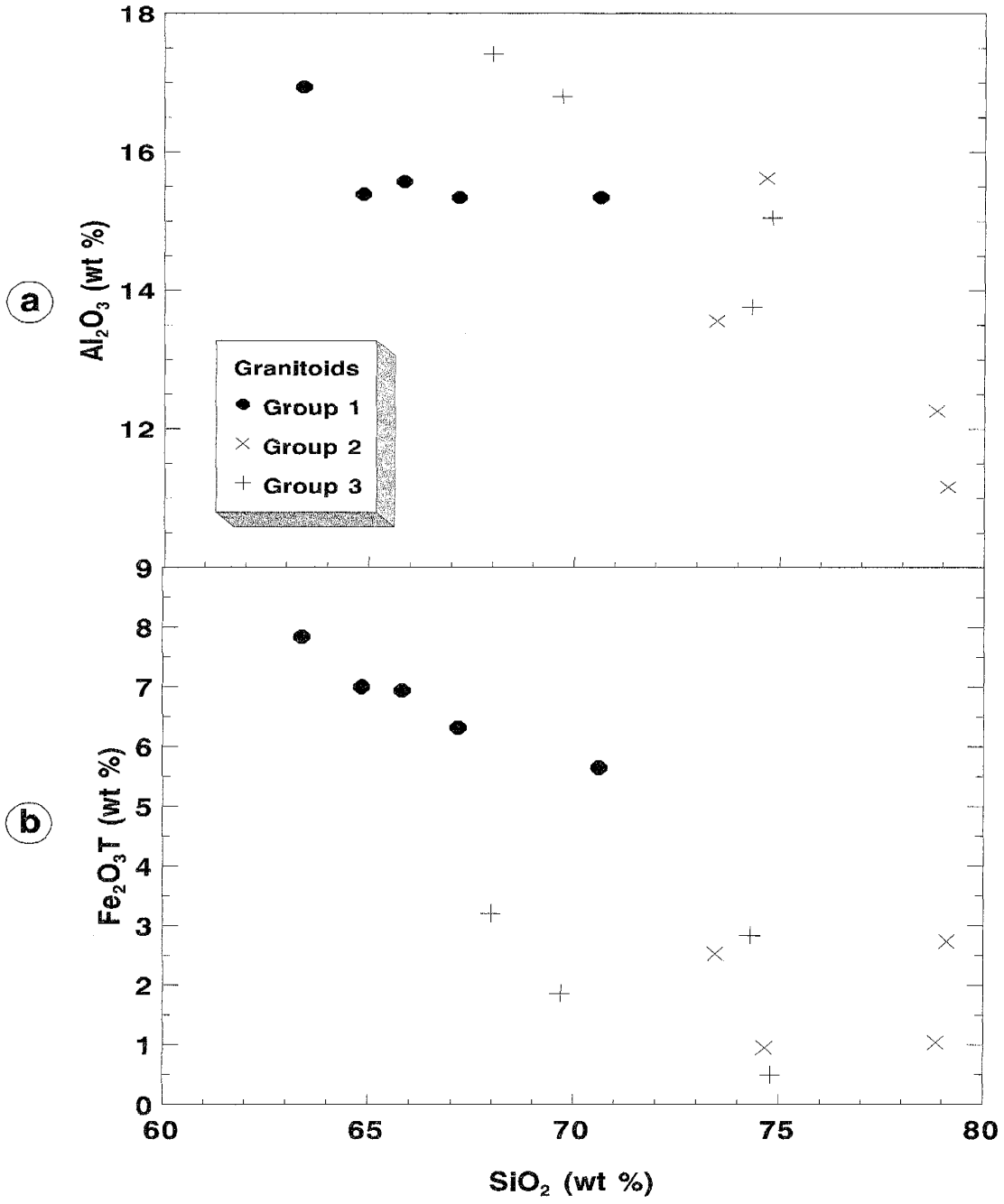

Figure 31: Distributions of (a) Al_2O_3 and (b) Fe_2O_3T relative to SiO_2, Liangchen granitoids. Group 1 granodiorites demonstrate linear correlations among these elements, as expected for cogenetic magmas; Groups 2 and 3 granites are noted for their higher SiO_2 contents and scattered correlations.

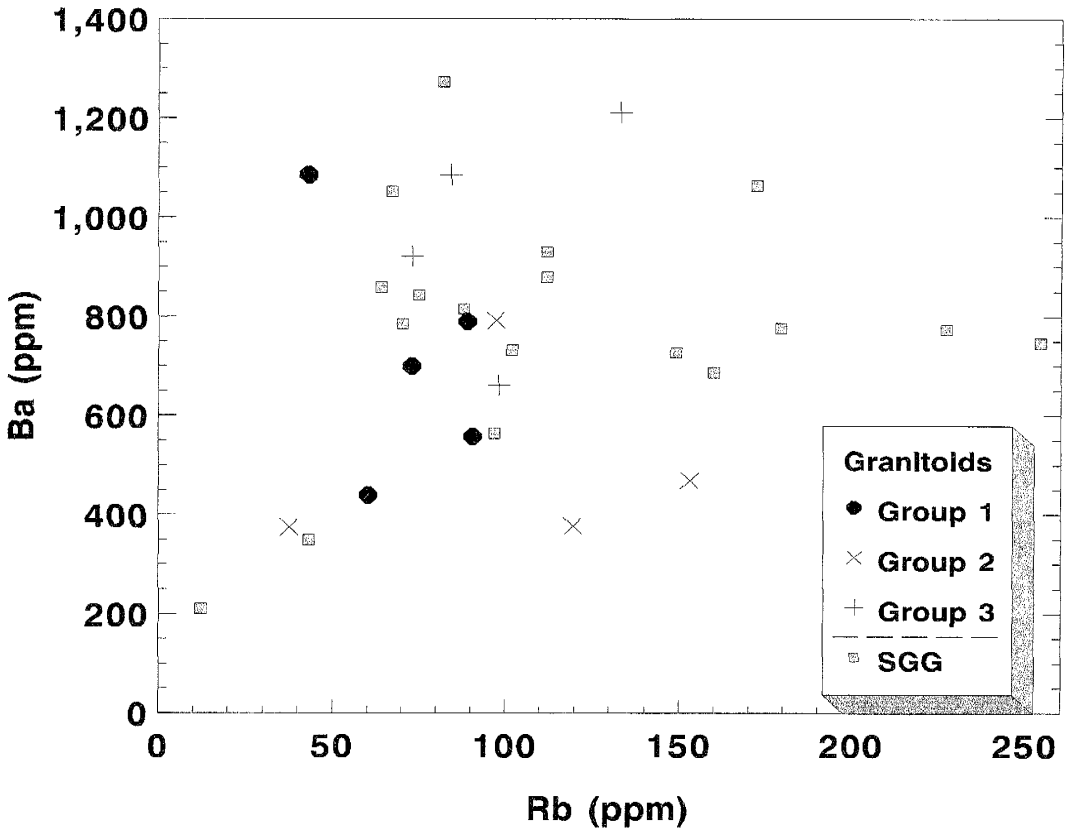

Figure 32: Distribution of Rb vs. Ba for Liangchen granitoids. There are no clear relationships among LILE in these samples. SGG, sillimanite-garnet gneisses from the Datong region for comparison.

Group 2 granites are much more felsic, having higher SiO_2 and K_2O (73.5-79% and 3.9-4.5%, except sample L29 which has only 1.5% K_2O) and lower ferromagnesian concentrations (Fe_2O_3T = 0.95-2.7%, fig. 31b; MgO = 0.2-1.2% and MnO = 0.02-0.04%) than the other groups. Al_2O_3 and CaO contents are also lower (11.1-15.6%, fig. 31a, and 1.0-1.9%) but TiO_2 and Na_2O contents are similar to the other groups. K_2O/Na_2O reflects this felsic composition, averaging about 1.5.

Group 3 granites have major element contents that are intermediate between Groups 1 and 2. SiO_2 varies from 68-74.8%. Ferromagnesian contents do not vary systematically with SiO_2 (fig. 31b). Fe_2O_3T ranges from 0.5-3.2%, MgO ranges from

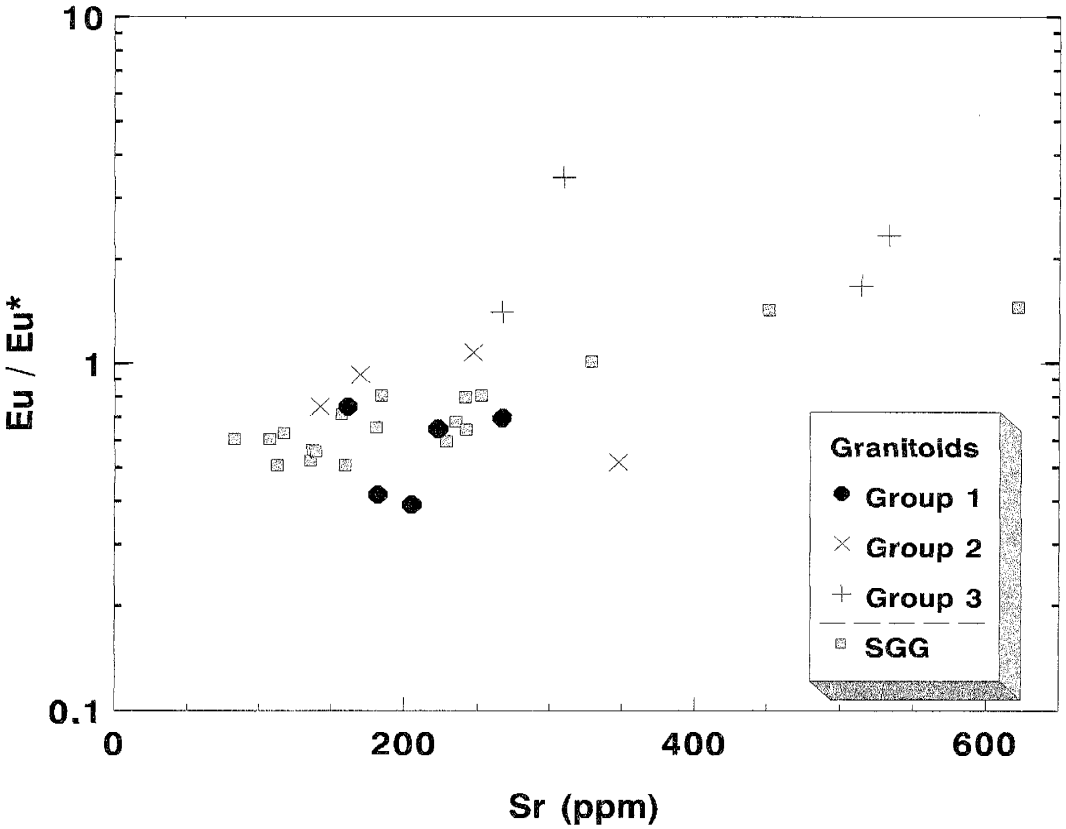

Figure 33: Distribution of Eu/Eu* vs. Sr for Liangchen granitoids. Sr is typically held in plagioclase and Eu is concentrated in feldspars (thereby producing Eu/Eu* > 1), yet there is no clear relationship between Sr and Eu in these samples. SGG, sillimanite-garnet gneisses from the Datong region for comparison.

0.37-1.6%, and MnO from 0.02-0.04%. Al_2O_3 is relatively high, ranging from 13.8 up to 17.4% (fig. 31a), but TiO_2, CaO, Na_2O, and K_2O are similar to concentrations found in the other groups (0.06-0.41%, 1.2-2.4%, 2.0-3.6%, and 3.3-4.6%, respectively). K_2O/Na_2O is similar to that of Group 2 granites, averaging about 1.6.

Large Ion Lithophile Elements (LILE)

Rb and Ba show no correlation in the three Liangchen granitoid groups (fig. 32) nor with respect to SiO_2. This irregular distribution is apparent both within and among each of the groups of granites. Sr, commonly used as an index of plagioclase feldspar

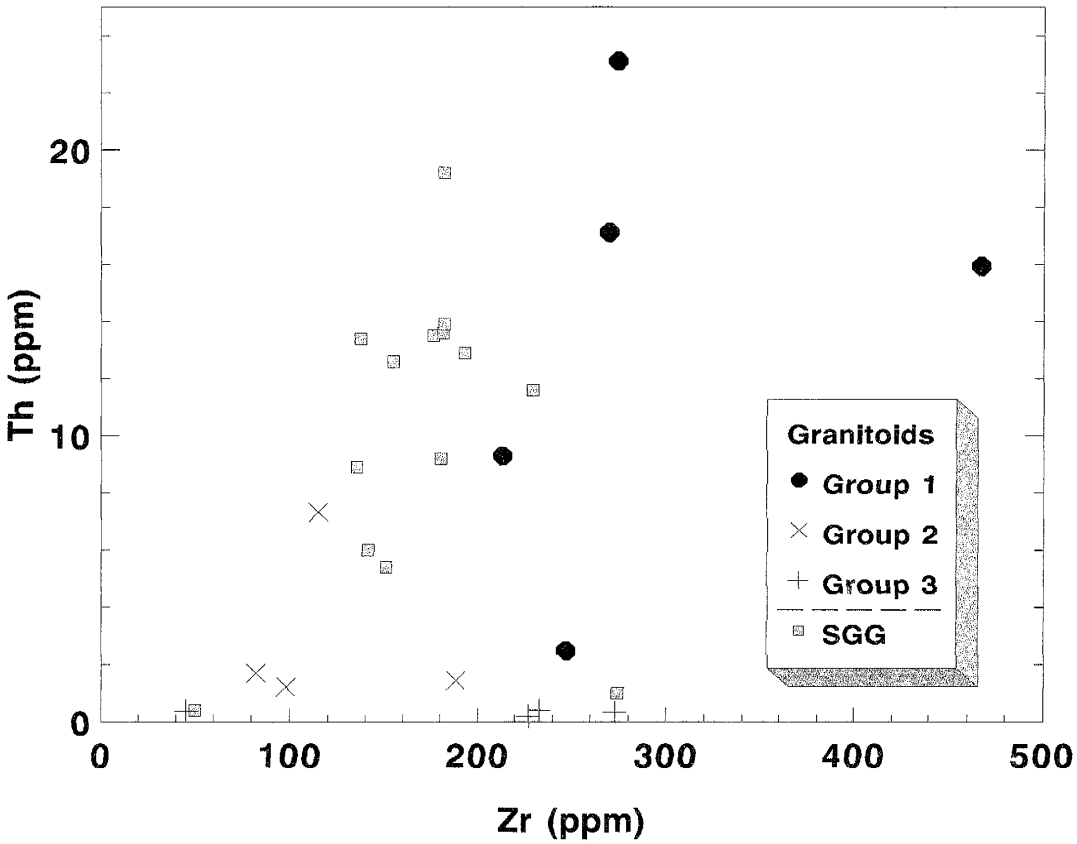

Figure 34: Distribution of Th vs. Zr for Liangchen granitoids. SGG: sillimanite-garnet gneisses from the Datong region for comparison.

fractionation, bears little relationship to normative feldspar or to the size of Eu anomalies (fig. 33). However, such LILE distributions are common among granites derived by partial melting of metasedimentary rocks (e.g., Watt and Harley, 1993). The distributions may be explained by multiple phase control involving feldspars, biotite and trace minerals.

Thorium is different among the LILE in that its concentrations are more group-specific. Group 1 granodiorites generally have higher Th contents (16-23 ppm) than the other groups (fig. 34). Group 2 granites have generally lower Th contents (1.2-1.7 ppm) and Group 3 granites have very low abundances (0.12-0.54 ppm).

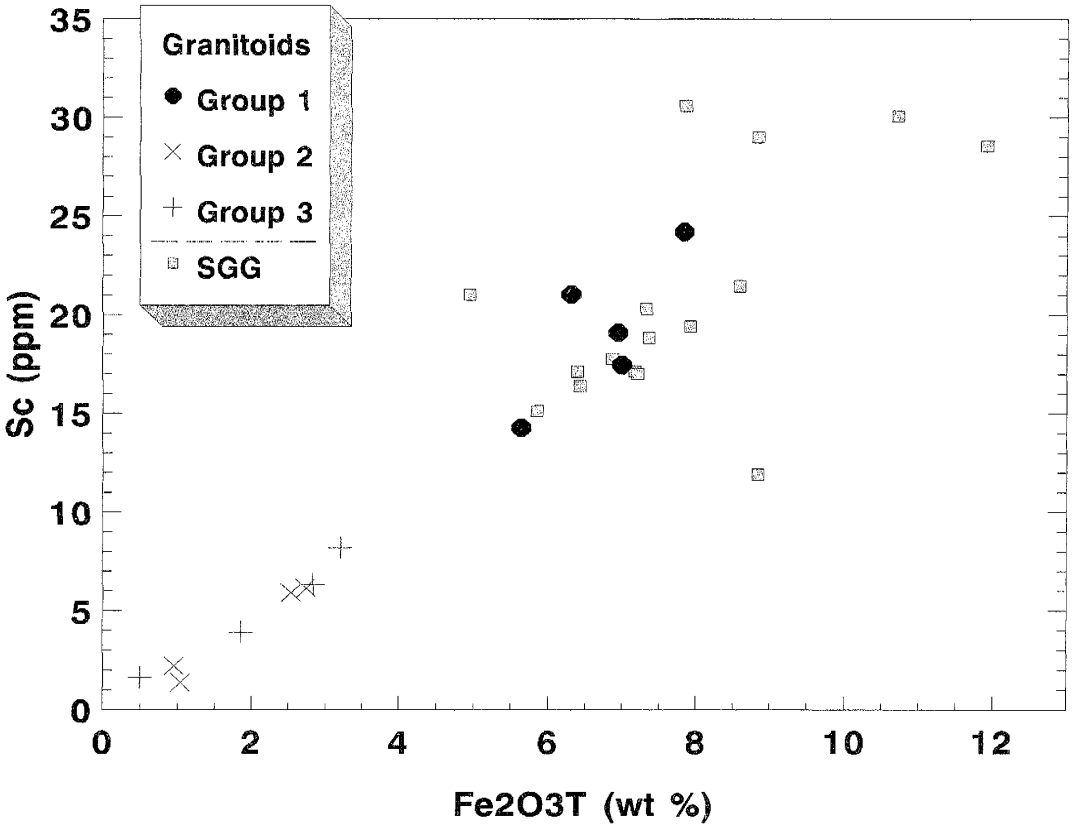

Figure 35: Distribution of Sc vs. Fe_2O_3T for Liangchen granitoids suggests that metals behaved similarly during the igneous and metamorphic processes that affected their formation. SGG: sillimanite-garnet gneisses from the Datong region for comparison.

Trace Metals (Sc, V, Cr, Co, Ni)

Trace metal contents show a negative correlation with SiO_2 and a positive correlation with Fe_2O_3T and MgO (fig. 35), suggesting that these elements are held in mafic phases. The ranges in trace metal contents vary less widely than the LILE, and their ranges are more restricted within individual groups. Sc in Group 1 granodiorites is high, clustering around 20 ppm. In Group 2 and 3 granites, Sc is much lower (1.4-8.2 ppm). V shows a wider range in distribution within each group, but is highest in Group 1 (98 ppm) and lowest in Group 2 (33 ppm). Chromium, cobalt and nickel are similarly distributed.

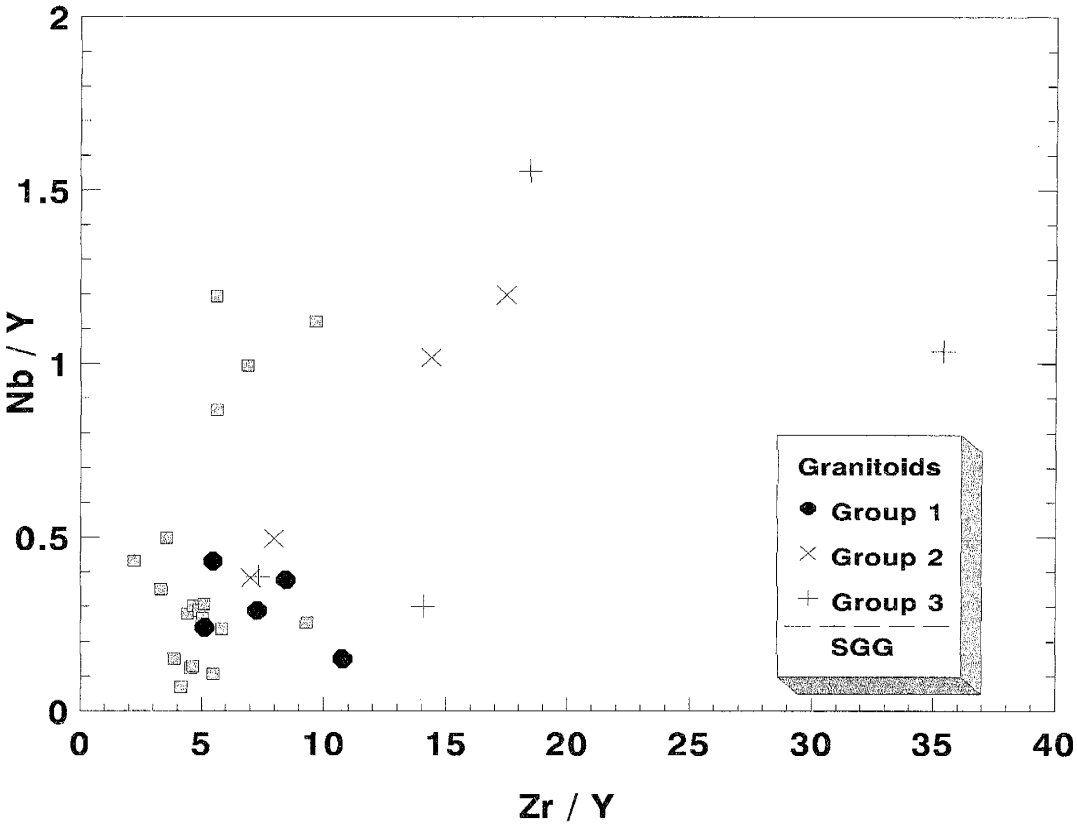

Figure 36: Variation in HFSE ratios Zr/Y vs. Nb/Y. The tight grouping of Group 1 granodiorites within the range of Datong-area sillimanite-garnet gneisses (SGG) supports the proposed model for these granodiorites involving higher degrees of melting of SGG and inclusion of restite. Group 2 granites show a positive correlation of Nb/Y with Zr/Y. Group 3 granites show no correlation between these ratios.

High Field Strength Elements (Zr, Hf, Nb, Ta) and Y

In granitic rocks, high field strength elements are typically held in refractory trace minerals (Watson and Harrison, 1984; Taylor and McLennan, 1985; Watt and Harley, 1995; McDermott et al., 1996; Whitten, 1996). Nb and Ta are geochemically similar to Ti (Green and Pearson, 1987), as seen by the positive correlations with Ti. Zr, Hf and Y constitute major components of zircon, and are positively correlated. Zr does not correlate with Th (fig. 34), indicating no relationship between zircon and monazite. Constant Zr/Hf ratios of around 34 indicate that Hf is controlled by zircon as well. Zr/Y

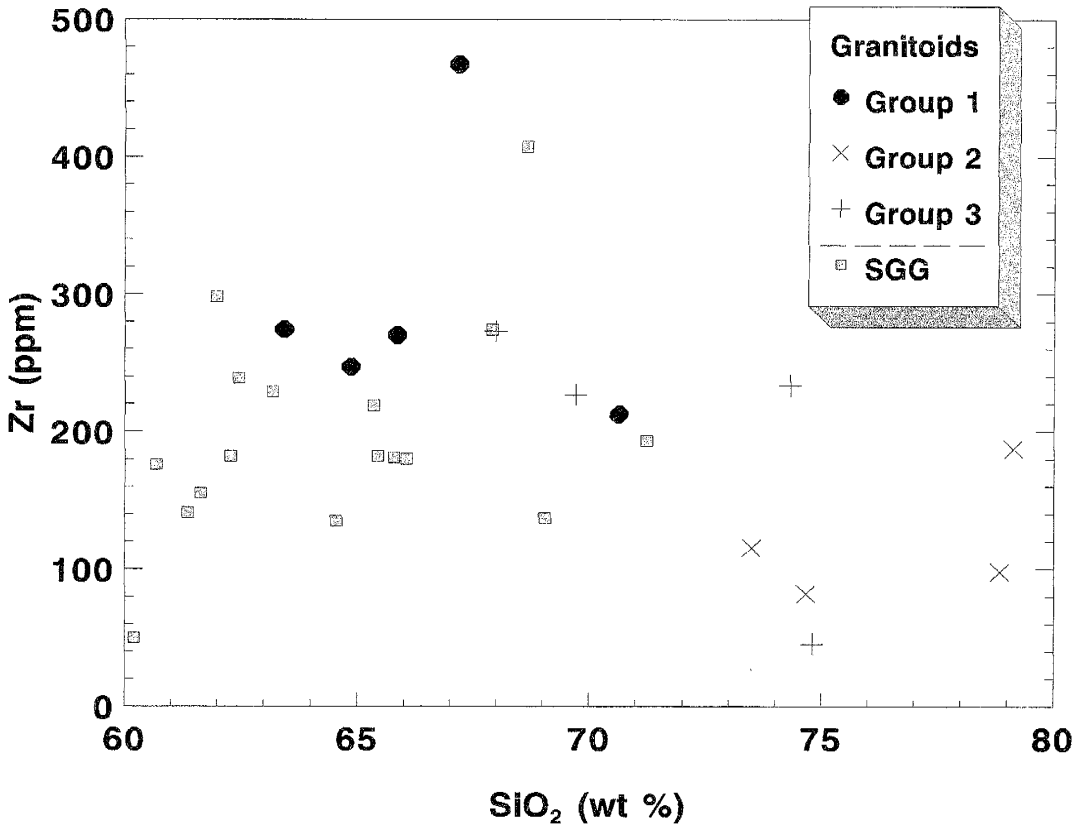

Figure 37: Variation of Zr with SiO_2 in Liangchen granitoids. Steep negative correlations have been used (Watt and Harley, 1993; Fitzsimmons, 1996) to suggest that incorporation of residual zircon controls Zr contents. Zr contents in Groups 1 and 3 granitoids reach levels expected for Zr saturation in magmas of appropriate compositions (Watson and Harrison, 1983, 1984). SGG: sillimanite-garnet gneisses (SGG) of the Datong region, for comparison.

shows more variation (fig. 36), indicating multiple phase control of Y, which is partitioned into garnet as well as zircon (Taylor and McLennan, 1985). Zr is approximately saturated in granitoid compositions of Groups 1 and 3 (Watson and Harrison, 1983; fig. 37). In Group 2 granites, Zr contents are lower than saturated concentrations (except for sample L29) for the estimated temperature of 850°C (Watson and Harrison, 1983; fig. 37).

Rare Earth Elements

Group 1 granodiorites have REE distributions (fig. 38) similar to Phanerozoic shales and to sillimanite-garnet gneisses (SGG) of the Datong region (compare fig. 21): enriched LREE (150× chondrite), flat HREE and significant negative Eu anomalies (Eu/Eu* ranges from 0.4-0.7). $(La/Yb)_N$ ranges from 5.5-9.5.

Group 2 granites have more highly fractionated REE distributions ($(La/Yb)_N$ = 15-40) and small or no Eu anomalies (Eu/Eu* = 0.75-1.1, except sample L42 which has Eu/Eu* = 0.52). Overall REE are slightly less enriched than in Group 1.

Group 3 granites have REE patterns similar to Group 2 except with positive Eu anomalies (Eu/Eu* = 1.4-3.4).

Discussion

Introduction

The formation of granite by partial melting of crustal rocks is a complex process. Typically, a large number of minerals take part in the melt-forming reactions (e.g., see reactions 2 and 3, p. 85), including those minerals that form the bulk of the rock as well as those that are found in only trace amounts. Further complicating the process is the presence of six common minerals (quartz, K-feldspar, plagioclase, garnet, biotite and sillimanite) the Liangchen granitoids, five of which may vary in composition with metamorphic grade and bulk rock composition. Major elements such as Fe, Ti and Ca are

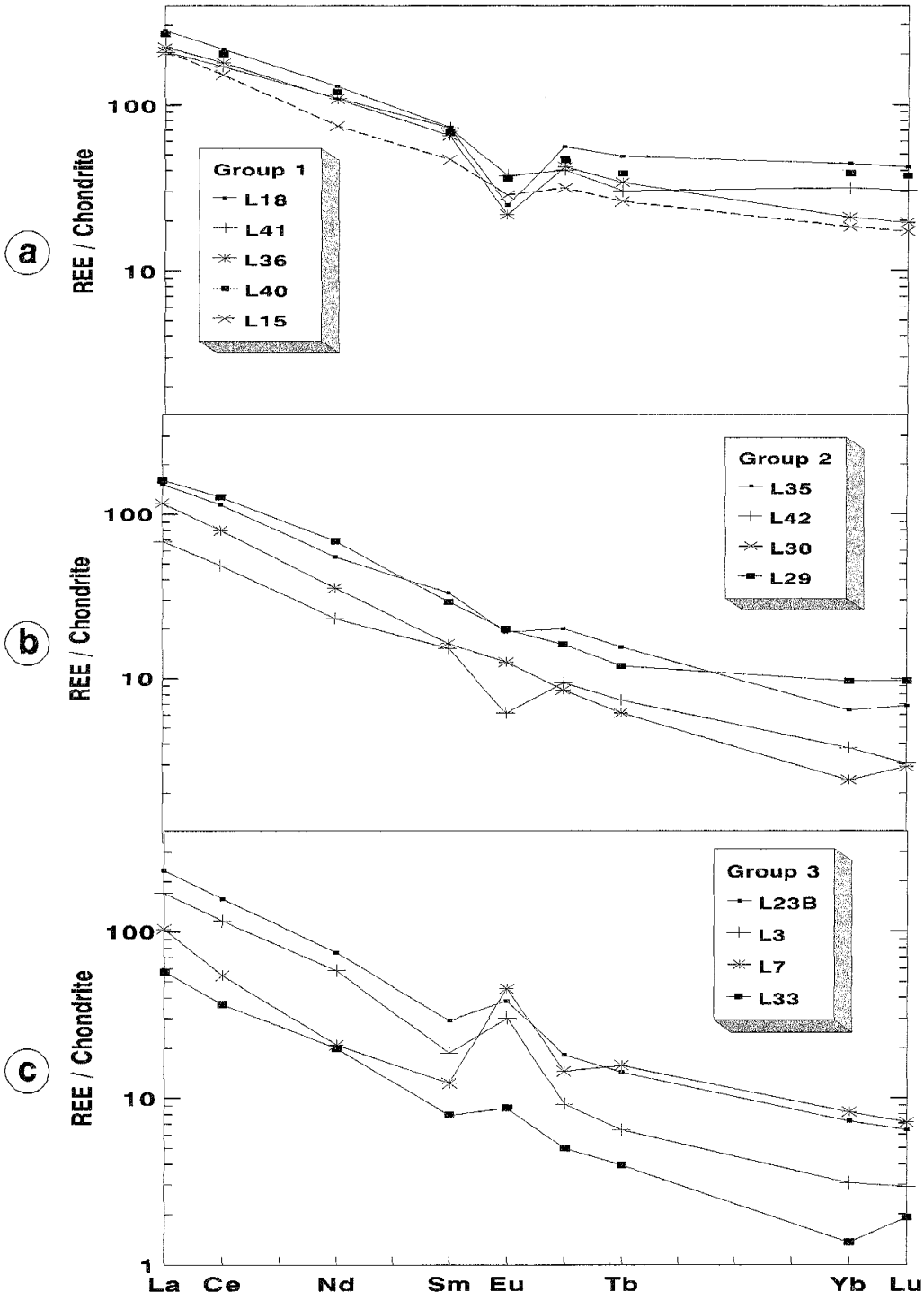

Figure 38: Chondrite-normalized REE distributions of (a) Group 1 granodiorites and (b) Group 2 and (c) Group 3 granites from the Liangchen region.

controlled by up to three of these phases, and Al is contained in all but quartz. Compositions of these phases in Liangchen granitoids have not been determined.

Trace-element controls on geochemical modelling are also not well constrained. Accessory minerals that concentrate trace elements may be distributed unevenly throughout a magma, possibly resulting in unrepresentative characterization of the body (Evans and Hanson, 1993). An accessory mineral might commonly compose 0.1 % of a granitic rock, yet it can contain the bulk of key elements such as Zr, REE, Th, and Nb (McLennan and Taylor, 1985; Evans and Hanson, 1993; Whitten, 1996). Accessory minerals take part either by breaking down to release elements into the melt (dissolving), by exchanging elements with the melt, or by becoming selectively included or excluded from the melt during migration from the source (Wall et al., 1987; Evans and Hanson, 1993). Hence, without accurate modal mineral constraints, *detailed* geochemical modeling is not possible.

Most models that are appropriately constrained use equations for batch or incongruent melting followed by fractional or equilibrium crystallization to explain the compositional variation found in suites of granitic rocks that have separated from their source (Ashworth and Brown, 1990; Evans and Hanson, 1993; Watt and Harley, 1993; Barbey et al., 1995; Claesson and Lundqvist, 1995; McDermott et al., 1996; Williamson et al., 1996). These models differ in the emphasis placed on the presence of residual crystals and on the effects of melt-forming reactions (vapor-present vs. vapor-absent, breakdown of muscovite vs. biotite, non-modal vs. incongruent melting; Pitcher, 1993). Melt-forming reactions control the geochemical signatures of the magma and the restite,

and hence have important implications for the overall processes of crustal formation and subsequent differentiation. If a model is reasonable (i.e., fits all geochemical and field data), then it can be extrapolated to constrain the composition of the source. Usually the source is unavailable or is present in the form of xenoliths that may have been altered from their original composition while within the magma, and thus there is no external check on the validity of these models.

Several studies have rigorously determined the mineralogical and chemical changes accompanying both synthetic (e.g., Le Breton and Thompson, 1988) and naturally occurring metasedimentary rocks (Fourcade and Allègre, 1981; Johannes, 1988; Holtz and Johannes, 1990; Patiño Douce and Johnston, 1991; Watt and Harley, 1993). In rocks with more than three phases involved in the melting process, low proportions of melt tend to have the greatest difference in major element composition compared to their source. Alternatively, higher melt fractions rapidly approach the character of the source (e.g., Defant and Nielsen, 1990). Additionally, greater melt fractions will have a greater capacity to incorporate residual minerals (sillimanite, garnet, zircon, apatite, etc.) (White and Chappell 1977, 1983; Wickham, 1987; Williamson et al., 1996), a model known as the *restite model.*

Origin of the Liangchen Group 1 Granitoids

Field evidence (Liu, 1989) suggests that the entire suite of granitoid rocks formed by melting of the khondalite suite. Group 1 granodiorites have compositions that are remarkably similar to SGG (compare figs. 18, 21, 31, 38; Tables 3 and 5). Evans and

Hanson (1993) have investigated the effect of saturation of trace minerals on elemental abundances. They found that "in a suite of related melts saturated in zircon the concentration of Zr will show less variation than incompatible or compatible trace elements" (Evans and Hanson, 1993, p. 73). Group 1 Zr contents vary from 213-274 ppm (except sample L40), which is in the saturation range for compositions and temperatures of melting in the Liangchen area. Sample L40 is slightly supersaturated with respect to zircon, suggesting that residual zircon has become entrained in this melt. Hence, Group 1 granodiorites must represent either 1) relatively large melt fractions, or 2) melt fractions large enough to carry residue as a "crystal mush." Watt and Harley (1993) have noted that zircon saturation or supersaturation is common for melts in excess of 40%, which allows for either of the interpretations. Reaction 3 above (p. 85) is expected to produce very low fractions of melt at temperatures below 850°C (Le Breton and Thompson, 1988; Vielzeuf and Holloway, 1988; Patiño Douce and Johnston, 1991; Stevens and Clemens, 1993), but reactions 2 and 3 together may produce the quantities of granite observed. Hence it is not possible to discriminate further between these two models with the data at hand.

Origin of the Liangchen Group 2 and 3 Granitoids

Peak metamorphic conditions reported for the Liangchen region (800-900°C and 10-14 kbar, Liu, 1989) are consistent with melting according to reactions 2 and 3 above.

Lower degrees of melting are consistent with generation of Group 2 and 3 granites. These granites have major element features resembling minimum melts in the

granitic system (Tuttle and Bowen, 1958; Patiño Douce and Johnston, 1991). Modal proportions are compatible with melting reactions described for Broken Hill, Australia (Powell and Downes, 1990). K-feldspar is produced by the melting reaction, and also should crystallize from the melt upon solidification. Group 3 granites have the highest proportions of this mineral and also the largest grains, resulting in the highest K_2O contents. K-feldspar preferentially captures Eu (Taylor and McLennan, 1985), and K correlates well with positive Eu anomalies (except L33) in Group 3 (fig. 38). It is therefore possible that Group 3 granites contain both generations of K-feldspar.

Group 2 granites have Zr and Th concentrations similar (82-188 ppm and 1.2-7.3 ppm, respectively) to LG1 leucogranites of the Brattstrand Bluffs, Australia (Watt and Harley, 1993; Fitzsimmons, 1996), but REE distributions (high $(La/Yb)_N$) similar to LG2. These data suggest that Group 2 granites result from separation of the magma during which garnet and zircon, but not monazite, are left behind in the residue. This model is further supported by the low Sc, Fe, Mg, Ca and modal garnet contents of Group 2 granites. Group 3 granites have Th concentrations even lower than Group 2 but Zr reaches saturation levels. REE distributions are similarly fractionated but a significant Eu anomaly is developed. These data suggest that Group 3 granites evolved by separation from the source, leaving most of the garnet in the residue but accumulating K-feldspar, as indicated above. This group (except L33) probably remained in contact with the khondalite source long enough to become saturated in Zr.

Conclusions to Part III

Field and petrographic relationships are used to support general geochemical models for the formation and evolution of three granitoid groups from the Liangchen region of Nei Mongol.

1. Khondalites in the Liangchen region have undergone partial melting to form three distinct groups of granites. Melt formed by the incongruent reactions:

$$Ms + Qtz + Pl \rightarrow Sill + Kfs + M$$

and

$$Bio + Sill + Qtz \rightarrow Kfs + Grt + M$$

2. Field and geochemical evidence indicate that Group 1 granodiorites formed by degrees of partial melting high enough that the resulting magma incorporated unmelted phases from the source, resulting in compositions that are nearly identical with the khondalites.

3. Field evidence also indicates that Group 2 and 3 granites formed by lower degrees of partial melting. These melts were incapable of carrying large proportions of residual phases or products of the melt-forming reaction such as garnet and

zircon. They have minimum melt compositions and trace element signatures, such as low total REE, Zr, Sc and highly fractionated La/Yb ratios, that are controlled by separation from those phases.

4. Group 3 granites have high K contents, consistent with the initial compositions of experimentally derived anatectic melts (Powell and Downes, 1990). This group is also rich in K-feldspar. Positive Eu anomalies result from accumulation of K-feldspar.

5. The suite of granitoids is chemically diverse, but requires no input from sources other than the khondalites.

Summary

The structural and geochemical survey of the central portion of the granulite belt has enhanced our understanding of its geological evolution. The data presented here and in the work of Liu (1989) are consistent with the following model:

1. Khondalites represent a suite of metamorphosed sedimentary rocks, not soils, deposited in a passive margin during Late Archean/Early Proterozoic time. It is not clear whether these aluminous sediments were deposited directly on the gray gneisses (TTG) outcropping to the east.

2. Intercalation of three types of khondalites indicates that the source region of the sillimanite-garnet and quartz-garnet gneisses (SGG and QGG) comprised granite and minor basalt. It is not clear whether quartz-feldspar gneisses (QFG) represent metamorphosed igneous deposits or volcaniclastic sediments, but they are related to arc-type magmas. There is no other evidence for a volcanic arc in the immediate area.

3. Mafic dikes intruding the khondalites and gray gneisses were derived from heterogenous mantle sources underlying the region. These sources include depleted, variably-enriched lithospheric and LREE-enriched refractory mantle

sources. The development of such heterogeneity is found in other terranes, including the Scourie complex of Scotland. Metamorphism of the dikes occurred at granulite grade, and structural relationships are consistent with their having intruded the region prior to the peak of metamorphism.

4. At least one intense compressional event caused pervasive deformation in the region north of Datong (Liu, 1989). Associated peak metamorphic temperatures and pressures were about 800-900°C and 10-14 kbar (Qian et al., 1985; Liu, 1989). Although poorly constrained, this event likely occurred around 1965-2450 Ma (J.J. Peucat, written communication, 1989).

5. Probably toward the end of this metamorphic event, vapor-absent partial melting in the khondalites produced a suite of granitoid rocks in the Liangchen region. These can be divided into three groups. Field evidence and geochemical models indicate they are related.

6. Melt probably occurred by the reactions:

$$Ms + Qtz + Pl \rightarrow Sill + Kfs + M$$

and

$$Bio + Sill + Qtz \rightarrow Kfs + Grt + M$$

These reactions are common to metamorphic conditions such as those determined for the Liangchen region. Incongruent dehydration reactions such as these produce only small volumes of melt at temperatures below 850°C, a temperature that is in the middle of the estimates for peak metamorphism of the region. The granitoid bodies vary in size, grading from migmatites intermingled with the host khondalite to small plutons that have separated from the source.

7. Field evidence and geochemical data both suggest that the granitoids are derived by different degrees of partial melting of the khondalites, producing a variety of geochemical signatures.

Suggestions for Future Research

Due to the reconaissance nature of this study and the inaccessibility of key locations in the field, a number of projects remain that may further our understanding of the granulite belt.

1. Isotopic analyses (Sm-Nd, Pb isotope and Rb-Sr) coupled with detailed geochronological study of mafic units may enhance our understanding of the evolution of the mantle beneath this portion of the Earth's crust at the Archean/Proterozoic boundary. REE ratios are less likely to be reset during metamorphism even at granulite-facies conditions, as suggested by the preservation of REE distributions in samples of this study. These isotopic signatures have been shown to be indicative of mantle sources (Zindler and Hart,

1986; Hart and Zindler, 1989) and crustal contamination (DePaolo, 1981). For example, enriched mantle sources have low ϵ_{Nd}, low to intermediate $^{206}Pb/^{204}Pb$ and intermediate to high $^{87}Sr/^{86}Sr$; depleted mantle has high ϵ_{Nd}, low $^{87}Sr/^{86}Sr$, and low to intermediate $^{206}Pb/^{204}Pb$; and HIMU has intermediate ϵ_{Nd}, intermediate $^{87}Sr/^{86}Sr$, and high $^{206}Pb/^{204}Pb$ (Hart and Zindler, 1989).

2. Chemical analyses of a more comprehensive suite of khondalite samples across the area of outcrop may help to elucidate the direction from which the sediments were derived. This should be done using a more detailed geologic map (unavailable at this time) coupled with more intensive structural investigations. Although foliations are well preserved and perhaps well understood in the Datong region, the relationship of this foliation to the nappe structures to the east (Zhangjiakou-Xuanhua region) is not well understood. Such a study may help constrain the extent of the basin in which these sediments were deposited.

3. More detailed analyses of metamorphic pressure and temperature through time (P-T-t) conditions would help to constrain the deformational and metamorphic history of the region. The importance of the P-T-t in partial melting of crustal rocks is paramount to our understanding of suggestion (4).

4. The exposure of the relationships of source and melt products in the Liangchen area is unique in that it preserves the transitional nature of geochemical

signatures during the early stages of partial melting. Detailed mapping, sampling, and analyses are needed to fully exploit the information available here. Future studies should include microanalysis of separate mineral phases for both major and trace elements, especially HFSE and REE, because these are commonly used to portray the composition of unexposed source rocks for many granites.

References

Allen, P., Condie, K.C., and Narayana, B.L., 1985. The geochemistry of prograde charnockite-gneiss reactions in southern India. Geochimica et Cosmochimica Acta, 49: 323-336.

Ashworth, J.R. and Brown, M., 1990. An overview of diverse responses to diverse processes at high crustal temperatures. In: J.R. Ashworth and M. Brown (Editors), High-temperature Metamorphism and Crustal Anatexis. London: Unwin Hyman, pp. 1-18.

Barbey, P. and Cuney, M., 1982. K, Rb, Sr, Ba ,U and Th geochemistry of Lapland granulites (Fennoscandia): LILE fractionation controlling factors. Contributions to Mineralogy and Petrology, 81: 304-316.

Barbey, P., Allé, P., Brouand, M. and Albarède, F., 1995. Rare-earth patterns in zircons from the Manaslu granite and Tibetan Slab migmatites (Himalaya): insights in the origin and evolution of a crustally-derived granite magma. Chemical Geology, 125: 1-17.

Barbey, P., Capdevila, R., and Hameurt, J., 1982. Major and trace element abundances in the khondalite suite of the granulite belt of Lapland (Fennoscandia): evidence for an Early Proterozoic flysch belt. Precambrian Research, 16: 273-290.

Bhatia, M.R., 1983. Plate tectonics and geochemical composition of sandstones. Journal of Geology, 91: 611-627.

Bhatia, M.R. and Crook, K.A.W., 1986. Trace element characteristics of graywackes and tectonic setting discrimination of sedimentary basins. Contributions to Mineralogy and Petrology, 92: 181-193.

Bernard-Griffiths, J., Jahn, B.-M., and Sen, S.K., 1987. Sm-Nd isotopes and REE geochemistry of Madras granulites, India: an introductory statement. Precambrian Research, 37: 343-355.

Beswick, A.E. and Soucie, G., 1978. A correction procedure for metasomatism in an Archean greenstone belt. Precambrian Research, 6: 235-248.

Bickle, M.J., 1990. Mantle Evolution. In: R.P. Hall and D.J. Hughes (Editors), Early Precambrian Basic Magmatism. New York: Chapman and Hall, pp. 111-135.

Boak, J.M. and Dymek, R.F., 1992. A systematic chemical stratigraphy for clastic metasedimentary and metavolcanic rocks from the 3800 Ma Isua supracrustal belt, West Greenland. Unpublished manuscript.

Boryta, M.D., 1988. Geochemistry and origin of igneous rocks from the Archean Beit Bridge Complex, Limpopo Belt, South Africa. Unpublished M.S. thesis, New Institute of Mining and Technology, Socorro, NM, USA. 111 pp.

Boryta, M.D. and Condie, K.C., 1990. Geochemistry and origin of the Archaean Beit Bridge Complex, Limpopo Belt, South Africa. Journal of the Geological Society, London, 147: 229-239.

Cattell, A. and Arndt, N., 1987. Low- and high-alumina komatiites from a Late Archaean sequence, Newton Township, Ontario. Contributions to Mineralogy and Petrology, 97: 218-227.

Cattell, A. and Taylor, R.N., 1990. Archean basic magmas. In: R.P. Hall and D.J. Hughes (Editors), Early Precambrian Basic Magmatism. New York: Chapman and Hall, pp. 11-39

Chappell, B.W. and Hergt, J.M., 1989. The use of known Fe content as a flux monitor in neutron activation analysis. Chemical Geology, 78: 151-158.

Chappell, B.W. and White, A.J.R., 1974. Two contrasting granite types. Pacific Geology, 8: 173-174.

Cheng Y.Q., 1986. The Archean. In: Z.Y. Yang, Y.Q. Cheng and H.Z. Wang (Editors), The Geology of China. Oxford: Clarendon Press, pp. 16-30.

Claesson, S. and Lundqvist, T., 1995. Origins and ages of Proterozoic granitoids in the Bothnian Basin, central Sweden; isotopic and geochemical constraints. Lithos, 36: 115-140.

Compston, W. and Zhong, F.D., 1983. Rb-Sr geochronology of Precambrian rocks from the Yenshan region, North China. Precambrian Research, 22: 175-202.

Condie, K.C., 1981a. Geochemical and isotopic constraints on the origin and source of Archean granites. Geological Society of Australia, Special Publication 7: 469-479.

Condie, K.C., 1981b. Archean Greenstone Belts. Amsterdam: Elsevier, 434 pp.

Condie, K.C., 1991a. Another look at rare earth elements in shales. Geochimica et Cosmochimica Acta, 55: 2527-2531.

Condie, K.C., 1991b. Precambrian granulites and anorogenic granites: are they related? Precambrian Research, 51: 161-172.

Condie, K.C., 1996. Sources of Proterozoic mafic dyke swarms: constraints from Th/Ta and La/Yb ratios. ????

Condie, K.C. and Sinha, A.K., 1996. Rare-earth and other trace element mobility during mylonitization: a comparison of the Brevard and Hope Valley shear zones in the Appalachian Mountains, USA. Journal of Metamorphic Geology, 14: 213-226.

Condie, K.C., Allen, P., and Narayana, B.L., 1982. Geochemistry of the Archean low- to high-grade transition zone, southern India. Contributions to Mineralogy and Petrology, 81: 157-167.

Condie, K.C., Bobrow, D.J., and Card, K.D., 1987. Geochemistry of Precambrian mafic dykes from the southern Superior Province of the Canadian shield. Geological Association of Canada Special Publication 34: 95-108.

Condie, K.C., Boryta, M.D., Liu ,J.Z. and Qian, X.L., 1992. The origin of khondalites: geochemical evidence from the Archean to Early Proterozoic granulite belt in the North China craton. Precambrian Research, 59: 207-223.

Condie, K.C., Dengate, J. and Cullers, K., 1994.

Condie, K.C., Wilks, M., Rosen, O.M. and Zlobin, V.L., 1991. Geochemistry of metasediments from the Precambrian Hapschan Series, eastern Anabar Shield, Siberia. Precambrian Research, 50: 37-47.

Condie, K.C. and Wronkiewicz, D.J., 1988. A new look at the Archean-Proterozoic boundary: sediments and the tectonic setting constraint. In: S.M. Naqvi (Editor), Precambrian Continental Crust and Its Economic Resources. Amsterdam: Elsevier.

Condie, K.C. and Wronkiewicz, D.J., 1990. The Cr/Th ratio in Precambrian pelites from the Kaapvaal Craton as an index of craton evolution. Earth and Planetary Science Letters, 97: 256-267.

Dash, B. and Bowes, D.R., 1991. Reply to "Geochemistry and original nature of Precambrian khondalites in the Eastern Ghats, Orissa: a discussion." Transactions of the Royal Society of Edinburgh, 82: 89-90.

Dash, B., Sahu, K.N., and Bowes, D.R., 1987. Geochemistry and original nature of Precambrian khondalites in the Eastern Ghats, Orissa, India. Transactions of the Royal Society of Edinburgh, 78: 115-127.

Davies, G.F., 1995. Punctuated tectonic evolution of the earth. Earth and Planetary Science Letters, 136: 363-379.

Defant, M.J. and Nielsen, R.J., 1990. Interpretation of open system petrogenetic processes: phase equilibria constraints on magma evolution. Geochimica et Cosmochimica Acta, 54: 87-102.

DePaolo, D.J., 1981. Trace element and isotopic effects of combined wallrock assimilation and fractional crystallization. Earth and Planetary Science Letters, 53: 2517-2522.

Essene, E.J., 1982. Geologic thermometry and barometry. In: John M. Ferry (editor), Characterization of Metamorphism Through Mineral Equilibria, Reviews in Mineralogy, Vol. 10, pp. 153-206.

Evans, O.C. and Hanson, G.N., 1993. Accessory-mineral fractionation of rare-earth element (REE) abundances in granitoid rocks. Chemical Geology, 110: 69-93.

Fitzsimons, I.C.W., 1996. Metapelitic migmatites from Brattstrand Bluffs, East Antarctica - metamorphism, melting and exhumation of the mid crust. Journal of Petrology, 37:395-414.

Fourcade, S. and Allègre, C. J., 1981. Trace element behaviour in granite genesis: a case study. The calc-alkaline plutonic association from the Querigut complex (Pyrenees, France). Contributions to Mineralogy and Petrology, 61: 163-173.

Garrels, R.M. and MacKenzie, F.T., 1971. Evolution of Sedimentary Rocks. New York: Norton, 397 pp.

Gao, S. and Wedepohl, K.H., 1995. The negative Eu anomaly in Archean sedimentary rocks: Implications for decomposition, age and importance of their granitic sources. Earth and Planetary Science Letters, 133: 81-94.

Gibson, L.L. and Jagam, P., 1980. Instrumental neutron activation analysis of silicate rocks and minerals. In: G.K. Muecke (Editor), Short Course in Neutron Activation Analysis in the Geosciences. Ottawa, Ontario: Mineralogical Association of Canada, pp. 109-131.

Green, T.H. and Pearson, N.J., 1987. An experimental study of Nb and Ta partitioning between Ti-rich minerals and silicate liquids at high pressure and temperature. Geochimica et Cosmochimica Acta, 51: 55-62.

Gromet, L.P., Dymek, R.F., Haskin, L.A. and Korotev, R.L., 1984. The "North American shale composite": its compilation, major and trace element characteristics. Geochimica et Cosmochimica Acta, 48: 2469-2482.

Hall, R.P. and Hughes, D.J., 1990. Noritic magmatism. In: R.P. Hall and D.J. Hughes (Editors), Early Precambrian Basic Magmatism. New York: Chapman and Hall, pp. 83-110.

Harnois, L., 1988. The CIW index: a new chemical index of weathering. Sedimentary Geology, 55: 319-322.

Harris, N.B.W., Pearce, J.A. and Tindle, A.G., 1986. Geochemical characteristics of collision-zone magmatism. In: M.P. Coward and A.C. Ries (Editors), Collision Tectonics. Geological Society Special Paper, 19: 67-81.

Hart, S. and Zindler, A., 1989. Constraints on the nature and development of chemical heterogeneities in the mantle. In: W.R. Peltier (Editor), Mantle Convection: Plate Tectonics and Global Dynamics. New York: Gordon and Breach Science Publishers, pp. 261-387.

Haskin, L.A., Haskin, M.A., Frey, F.A. and Wildeman, T.R., 1968. Relative and absolute terrestrial abundances of the REE. In: L.H. Ahrens (Editor), Origin and Distribution of the Elements. New York: Pergamon, pp.889-912.

Holland, H.D., Feakes, C.R. and Zbinden, E.A., 1989. The Flin Flon paleosol and the composition of the atmosphere 1.8 BYBP. American Journal of Science, 289: 362-389.

Huang, T.K., 1978. An outline of the tectonic characteristics of China. Eclog. geol. Helv., 71: 611-635.

Huppert, H.E. and Sparks, R.S.J., 1985. Cooling and contamination of mafic and ultramafic magmas during ascent through continental crust. Earth and Planetary Science Letters, 74: 371-386.

Jacobs, J.W., Korotev, R.L., Blanchard, D.P. amnd Haskin, L.A., 1977. A well-tested procedure for instrumental neutron activation analysis of silicate rocks and minerals. Journal of Radioanalytical Chemistry, 40: 93-114.

Jahn, B.M., 1990a. Origin of granulites: geochemical constraints from Archean granulite facies rocks of the Sino-Korean Craton, China. In: D. Vielzeuf and Ph. Vidal (Editors), Granulites and Crustal Evolution. Amsterdam: Kluwer, pp. 471-492.

Jahn, B.M., 1990b. Early Precambrian basic rocks of China. In: R.P. Hall and D.J. Hughes (Editors), Early Precambrian Basic Magmatism. New York: Chapman and Hall, pp. 294-316.

Jahn, B.M. and Zhang, Z.Q., 1984. Archean granulite gneisses, eastern Hebei Province, China: REE geochemistry and tectonic implications. Contributions to Mineralogy and Petrology, 85: 224-243.

Jahn, B.M., Auvray, B., Cornichet, J., Bai, Y.L., Shen, Q.H. and Liu, D.Y., 1987. 3.5 Ga old amphibolites from eastern Hebei Province, China: field occurrence, petrography, Sm-Nd isochron age and REE geochemistry. Precambrian Research, 34: 311-346.

Jensen, L.S., 1976. A new cation plot for classifying subalkaline volcanic rocks. Ontario Division of Mines Miscellaneous Paper No. 66.

Johannes, W., 1988. What controls partial melting in migmatites? Journal of Metamorphic Petrology, 6: 451-466.

Johannes, W. and Holtz, F., 1990. Formation and composition of H_2O-undersaturated granitic melts. In: J.R. Ashworth and M. Brown (Editors), High-temperature Metamorphism and Crustal Anatexis. London: Unwin Hyman, pp. 87-104.

Johannes, W., Holtz, F. and Möller, P., 1995. REE distribution in some layered migmatites: constraints on their petrogenesis. Lithos, 35: 139-152.

Karsten, J.L., Klein, E.M. and Sherman, S.B., 1996. Subduction aone geochemical characteristics in ocean ridge basalts from the southern Chile Ridge: implications of modern ridge subduction systems for the Archean. Lithos, 37: 143-161.

Keppler, H. and Wyllie, P.J., 1990. Role of fluids in transport and fractionation of uranium and thorium in magmatic processes. Nature, 348: 531-533.

Kronberg, B.I., Fyfe, W.S., Leonardos, O.H. and Santos, A.M., 1979. The chemistry of some Brazilian soils: element mobility during intense weathering. Chemical Geology, 24: 211-229.

Kröner, A., 1991. Tectonic evolution in the Archaean and Proterozoic. Tectonophysics, 187: 393-410.

Kröner, A., Compston, W., Zhang, G., Guo, A. and Cui, W., 1987. Single grain zircon ages for Archaean rocks from Henan, Hebei and Inner Mongolia, China and tectonic implications. International Symposium on the Tectonic Evolution and Dynamics of Continental Lithosphere, Abstracts, Beijing, China.

Le Bas, M.J., Le Maitre, R.W., Streckeisen, A. and Zanettin, B., 1986. A chemical classification of volcanic rocks based on the total alkali-silica diagram. Journal of Petrology, 27: 745-750.

Le Breton, N. and Thompson, A.B., 1988. Fluid-absent (dehydration) melting of biotite in metapelites in the early stages of crustal anatexis. Contributions to Mineralogy and Petrology, 99: 226-237

Lindstrom, D.J. and Korotev, R.L., 1982. TEABAGS: computer programs for instrumental neutron activation analysis. Journal of Radioanalytical Chemistry, 70: 439-458.

Liu D.Y., Page, R.W., Compston, W. and Jaishan, W., 1985. U-Pb zircon geochronology of late Archaean metamorphic rocks in the Taihangshan-Wutaishan areas, north China. Precambrian Research, 27: 85-109.

Liu J.Z., 1989. Study of cratonization of the Archean granulite facies region and a lower crustal cross section, Inner Mongolia. PhD thesis, Peking University, Beijing, 195 pp.

Liu J.Z, Qian X.L. and Chen Y.P., 1989. The tectonic origin of graphite deposits in the khondalite group, the middle part of Inner Mongolia. Geotectonica et Metallogenia, 13: 162-167.

Lundstrom, C.C., Shaw, H.F., Ryerson, F.J., Phinney, D.L., Gill, J.B. and Williams, Q., 1994. Compositional controls on the partitioning of U, Th, Ba, Pb, Sr and Zr between clinopyroxene and haplobasaltic melts: implications for uranium series disequilibria in basalts. Earth and Planetary Science Letters, 128: 407-423.

Martin, H., 1987. Petrogenesis of Archean tonalites, trondhjemites and granodiorites from eastern Finland: major and trace element geochemistry. Journal of Petrology, 28: 921-953.

McCulloch, M.T. and Gamble, J.A., 1991. Geochemical and geodynamical constraints on subduction zone magmatism. Earth and Planetary Science Letters, 102: 358-374.

McDermott, F., Harris, N.B.W. and Hawkesworth, C.J., 1996. Geochemical constraints on crustal anatexis: a case study from the Pan-African Damara granitoids of Namibia. Contributions to Mineralogy and Petrology, 123: 406-423.

McLennan, S.M., 1989. Rare earth elements in sedimentary rocks: influence of provenance and sedimentary processes. Reviews in Mineralogy, 21: 169-200.

Mohr, P.A., 1987. Crustal contamination in mafic sheets: a summary. Geological Association of Canada Special Publication 34: 75-80.

Moore, B.R. and Dennen. W.H., 1970. A geochemical trend in silicon-aluminum-iron ratios and the classification of clastic sediments. Journal of Sedimentary Petrology. 40: 1147-1152.

Mysen, B.O., 1979. Trace-element partitioning between garnet peridotite minerals and water-rich vapor: experimental data from 5 to 30 kbar. American Mineralogist, 64: 274-287.

Nanda, J.K. and Pati, U.C., 1989. Geochemistry and original nature of Precambrian khondalites in the Eastern Ghats, Orissa: a discussion. Transactions of the Royal Society of Edinburgh, 82: 87-88.

Nesbitt, H.W., Markovics, G. and Price, R.C., 1980. Chemical processes affecting alkalis and alkaline earths during continental weathering. Geochimica et Cosmochimica Acta, 44: 1659-1666.

Newton, R.C., 1987. Late Archaean/Early Proterozoic CO_2 streaming through the lower crust and geochemical segregation. Geophysical Research Letters, 14: 287-290.

Norrish, J. and Chappell, B.W., 1977. X-ray Fluorescence. In: J. Zussman (Editor), Physical Methods in Determinative Mineralogy. London: Academic Press, pp. 75-80.

Norrish, J. and Hutton, J.T., 1969. An accurate X-ray spectrographic method for the analysis of a wide range of geologic samples. Geochimica et Cosmochimica Acta, 33: 431-453.

Patiño Douce, A.E. and Johnston, A.D., 1991. Phase equilibria and melt productivity in the pelitic system: implications for the origin of peraluminous granitoids and aluminous granulites. Contributions to Mineralogy and Petrology, 107: 202-218.

Pearce, J.A., 1983. Role of sub-continental lithosphere in magma genesis at active continental margins. In: Continental Basalts and Mantle Xenoliths, 230-249.

Pitcher, W.S., 1993. The Nature and Origin of Granite. New York: Blackie Academic and Professional.

Powell, R. and Downes, J. 1990. Garnet porphyroblast-bearing leucosomes in metapelites: mechanisms, phase diagrams, and an example from Broken Hill, Australia. In: J.R. Ashworth and M. Brown (Editors), High-temperature Metamorphism and Crustal Anatexis. London: Unwin Hyman, pp. 105-123.

Qian X.L., Cui W.Y. and Wang S.Q., 1985. Evolution of the Archean granulite belt in the North China Craton and rule of metallogenesis. Records of Geological Research of Peking University. 24 pp.

Rainbird, R.H., Nesbitt, H.W. and Donaldson, J.A., 1990. Formation and diagenesis of a sub-Huronian saprolith: comparison with a modern weathering profile. Journal of Geology, 98: 801-822.

Roberts, M.P. and Clemens, J.D., 1995. Feasibility of AFC models for the petrogenesis of calc-alkaline magma series. Contributions to Mineralogy and Petrology, 121: 139-147.

Rogers, J.J.W. and Greenberg, J.K., 1990. Late-orogenic, post-orogenic and anorogenic granites: distinction by major-element and trace-element chemistry and possible origins. Journal of Geology, 98: 291-309.

Roser, B.P. and Korsch, R.J., 1988. Provenance signatures of sandstone-mudstone suites determined using discriminant fuction analysis of major-element data. Chemical Geology, 67: 119-139.

Rubie, D.C. and Brearley, A.J., 1990. A model for rates of disequilibrium melting during metamorphism. In: J.R. Ashworth and M. Brown (Editors), High-temperature Metamorphism and Crustal Anatexis. London: Unwin Hyman, pp. 57-86.

Saunders, A.D., Norry, M.J. and Tarney, J., 1988. Origin of MORB and chemically-depleted mantle reservoirs: trace element constraints. In: M.A. Menzies and K.G. Cox (Editors), Oceanic and Continental Lithosphere: Similarities and Differences. Special Volume of the Journal of Petrology: 415-445.

Schau, M. and Henderson, J.B., 1983. Archean chemical weathering at three localities on the Canadian Shield. Precambrian Research, 20: 189-224.

Shackleton, R.M., 1976. Shallow and deep-level exposures of the Archean crust in India and Africa. In: B.F. Windley (Editor), The Early History of the Earth. London: Wiley, pp.317-321.

Sheraton, J.W., 1984/1985. Chemical changes associated with high-grade metamorphism of mafic rocks in the East Antarctic Shield. Chemical Geology, 47: 135-157.

Sheraton, J.W. and Black, L.P., 1981. Geochemistry and geochronology of Proterozoic tholeiite dykes of East Antarctica: evidence for mantle metasomatism. Contributions to Mineralogy and Petrology, 78: 305-317.

Sheraton, J.W., Black, L.P., McCulloch, M.T., and Oliver, R.L., 1990. Age and origin of a compositonally varied mafic dyke swarm in the Bunger Hills, East Antarctica. Chemical Geology, 85: 215-246.

Sigursson, H., 1987. Dyke injection in Iceland: a review. Geological Association of Canada Special Publication 34: 55-64.

Stattegger, K., 1987. Heavy minerals and provenance of sands: modeling of lithologic end members from river sands of northern Austria and from sandstones of the austroalpine Gosau formation (Late Cretaceous). Journal of Sedimentary Petrology, 57: 301-310.

Stevens, G. and Clemens, J.D., 1993. Fluid-absent melting and the roles of fluids in the lithosphere: a slanted summary? Chemical Geology, 108: 1-17.

Sun D.Z., Hu H., Tang M., Zhao F. and Condie, K.C., 1990. Origin of Late Archean and Early Proterozoic rocks and associated mineral deposits from the Zhongtiao Mountains, east-central China. Precambrian Research, 47: 287-306.

Sun D.Z., Zhang H.M., Hu W.X., Liu W.X., Tang M., Zhao F.Q. and Mei H.L., 1988. Excursion guide: Proterozoic geology, geochemistry and mineral deposits of the Zhongtiao Mountains. International Symposium on the Geochemistry and Mineralization of Proterozoic Mobile Belts, Tianjin, China.

Sylvester, P.J., 1989. Post-collisional alkaline granites. Journal of Geology, 97: 261-280.

Tarney, J. and Weaver, B.L., 1987. Geochemistry and petrogenesis of Early Proterozoic dyke swarms. Geological Association of Canada Special Publication 34: 81-94.

Taylor, S.R. and McLennan, S.M., 1985. The Continental Crust: Its Composition and Evolution. Oxford: Blackwell Scientific Publications. 312 pp.

Taylor, S.R., Rudnick, R.L., McLennan, S.M. and Eriksson, K.A., 1986. Rare earth element patterns in Archean high-grade metasediments and their tectonic significance. Geochimica et Cosmochimica Acta, 50: 2267-2279.

Touret, J., 1971. Le facies granulite en Norvège méridionale II: les inclusions fluides. Lithos, 4: 423-436.

Tuttle, O.F. and Bowen, N.L., 1958. Origin of granite in the light of experimental studies in the system $NaAlSi_3O_8$-$KAlSi_3O_8$-SiO_2-H_2O. Geological Society of America, Memoir 74, 153 pp.

Vielzeuf, D. and Holloway, J.R., 1988. Experimental determination of the fluid-absent melting reactions in the pelitic system: Consequences for crustal differentiation. Contributions to Mineralogy and Petrology, 98: 257-276.

Walker, T.L.. 1902. The geology of Kalahandi State, Central Provine. Memoirs of the Geological Survey of India, 33: 1-22.

Wall, V.J., Clemens, J.D. and Clarke, D.B., 1987. Models for granitoid evolution and source composition. Journal of Geology, 95: 731-749.

Watson, E.B. and Harrison, T.M., 1983. Zircon saturation revisited: temperature and composition effects in a variety of crustal magma types. Earth and Planetary Science Letters, 64: 295-304.

Watson, E.B. and Harrison, T.M., 1984. Accessory minerals and the geochemical evolution of crustal magmatic systems: a summary and prospectus of experimental approaches. Physics of the Earth and Planetary Interiors, 35: 19-30.

Watt, G.R. and Harley, S.L., 1993. Accessory phase controls on the geochemistry of crustal melts and restites produced during water-undersaturated partial melting. Contributions to Mineralogy and Petrology, 114: 550-566.

Weaver, B.L. and Tarney, J., 1980. Rare earth geochemistry of Lewisian granulite-facies gneisses, northwest Scotland: implications for the petrogenesis of the Archaean lower continental crust. Earth and Planetary Science Letters, 51: 279-296.

Weaver, B.L. and Tarney, J., 1981a. Lewisian gneiss geochemistry and Archaean crustal development models. Earth and Planetary Science Letters, 55: 171-180.

Weaver, B.L. and Tarney, J., 1981b. The Scourie dyke suite: petrogenesis and geochemical nature of the Proterozoic subcontinental mantle. Contributions to Mineralogy and Petrology, 78: 175-188.

Weaver, B.L. and Tarney, J., 1983. Elemental depletion in Archaean granulite-facies rocks. In: Atherton, M.P. and Gribbles, C.D. (editors), Migmatites, Melting, and Metamorphism. Nantwich: Shiva Publishing Ltd.: 250-263.

Wendlandt, R.F. and Harrison, W.J., 1979. Rare earth partitioning between immiscible carbonate and silicate liquids and CO_2 vapor: results and implications for the formation of light rare earth-enriched rocks. Contributions to Mineralogy and Petrology, 69: 409-419.

Whalen, J.B., Currie, K.L. and Chappell, B.W., 1987. A-type granites: geochemical characteristics, discrimination and petrogenesis. Contributions to Mineralogy and Petrology, 95: 407-419.

White, A.J.R. and Chappell, B.W., 1977. Ultrametamorphism and granitoid genesis. Tectonophysics, 43: 7-22.

White, A.J.R. and Chappell, B.W., 1983. Granitoid types and their distribution in the Lachlan Fold Belt, southeastern Australia. Geological Society of America Memoir, 159: 21-34.

White, A.J.R., Clemens, J.D., Holloway, J.R., Silver, L.T., Chappell, B.W. and Wall, V.J., 1986. S-type granites and their probable absence in southwestern North America. Geology, 14: 115-118.

Whitten, E.H.T., 1996. Molar-ratio and Harker diagrams in portraying the actual chemical variability of granitoid suites. Journal of the Geological Society, London, 153: 121-125.

Wickham, S.M., 1987. The segregation and emplacement of granitic magmas. Journal of the Geological Society, London, 144: 281-297.

Williamson, B.J., Shaw, A., Downes, H. and Thirwall, M.F., 1996. Geochemical constraints on the genesis of Hercynian two-mica leucogranites from the Massif Central, France. Chemical Geology, 127: 25-42.

Wilson, M., 1993. Magmatic differentiation. Journal of the Geological Society, London, 150: 611-624.

Wood, D.A., 1979. A variably veined suboceanic upper mantle—Genetic significance for mid-ocean ridge basalts from geochemical evidence. Geology, 7: 499-503.

Wronkiewicz, D.J. and Condie, K.C., 1987. Geochemistry of Archean shales from the Witwatersrand Supergroup, South Africa: source-area weathering and provenance. Geochimica et Cosmochimica Acta, 51: 2401-2416.

Zbinden, E.A., Holland, H.D., Feakes, C.R. and Dobos, S.K., 1988. The Sturgeon Falls paleosol and the composition of the atmosphere 1.1 Ga BP. Precambrian Research, 42: 141-163.

Zindler, A. and Hart, S., 1986. Chemical Geodynamics. Annual Reviews of Earth and Planetary Sciences, 14: 493-571.

Appendix A: Petrography of Mafic Dikes

Group 1

13: texture: banded equigranular granoblastic; grains are 0.5-3 mm across. Sample conains 35% mildly sericitized plagioclase (An_{55-65}); 35% diopsidic clinopyroxene; 20% brownish green hornblende, partially seen as a retrograde growth around orthopyroxene; 7% orthopyroxene (hypersthene); 2% opaque minerals. Trace minerals include reddish-brown biotite as retrograde alteration of hornblende, and apatite.

16: texture: banded equigranular granoblastic; grains are 0.5-3 mm across. Sample conains 35% moderately sericitized plagioclase (An_{56}); 25% diopsidic clinopyroxene; 25% brownish green hornblende; 12% orthopyroxene (hypersthene); 3% opaque minerals. Trace minerals include reddish-brown biotite as retrograde alteration of hornblende, apatite, and zircon.

30: texture: banded seriate; grains are 0.1-4 mm across. Sample contains about 35% moderately sericitized plagioclase (An_{40}); 35% chlorite as retrograde alteration products of hornblende, clinopyroxene and orthopyroxene;10% diopsidic clinopyroxene; 10% greenish-brown hornblende; 5% orthopyroxene; and 3% opaque minerals. Trace minerals include reddish brown biotite as retrograde alteration around opaque minerals; apatite; and zircon.

32: texture: banded seriate granoblastic; grains are 0.1-4 mm across. Sample contains about 40% moderately sericitized plagioclase (An_{40}); 40% chlorite as retrograde alteration products of hornblende, clinopyroxene and orthopyroxene; 10% greenish-brown hornblende; 5% diopsidic clinopyroxene; and 3% opaque minerals. Trace minerals include apatite and reddish brown biotite as retrograde alteration around opaque minerals.

34: texture: equigranular granoblastic; grains are 1-5 mm across. Sample contains 40% slightly sericitized plagioclase (An_{40-45}); 30% diopsidic clinopyroxene; 15% orthopyroxene; 12% brownish green hornblende, partially seen as a retrograde growth around ortho- and clinopyroxene; and 1% opaque minerals. Trace minerals include reddish-brown biotite as retrograde alteration of hornblende, and apatite.

43: texture: banded seriate granoblastic; grains are 0.5-3 mm across. Sample contains 35% slightly sericitized plagioclase (An_{40-45}); 30% olive brown hornblende partially as retrograde growth around pyroxene; 30% diopsidic clinopyroxene; 5% biotite replacing opaques and hornblende; and 2% orthopyroxene. Trace minerals include apatite and a few granules of epidote.

51: texture: foliated equigranular, grains are 2-4 mm across. Sample contains 35% mildly sericitized plagioclase (An_{45}); 30% brown to olive brown hornblende; 20% diopsidic

clinopyroxene; 10% orthopyroxene; 3% biotite as retrograde alteration around hornblende and opaques; and 2% opaques. Trace minerals include chlorite and apatite.

57: texture: banded granoblastic, grains are 0.5-4 mm across. Sample contains 45% mildly sericitized plagioclase (An_{40}); 30% porphyroblastic brownish olive green hornblende; 20% moderately chloritized diopsidic cliinopyroxene; and 3% opaques. Trace minerals include apatite and relict orthopyroxene.

69: texture: seriate granoblastic; grains are 0.5-5 mm across. Sample contains 35% mildly sericitized plagioclase (An_{45-55}), 25% diopsidic clinopyroxene; 20% slightly chloritized orthopyroxene; 15% green hornblende; and 5% opaques. Trace minerals include apatite, biotite as a retrograde replacement of opaques, and zircon.

70: texture: equigranular granoblastic; grains are 0.8-3 mm across. Sample contains 45% slightly sericitized plagioclase (An_{55-60}); 35% greenish brown hornblende; 12% diopsidic clinopyroxene; 5% orthopyroxene; and 2% biotite as a retrograde replacement of hornblende. Trace minerals include opaques, apatite, and zircon

Group 2

44: texture: seriate granoblastic; grains are 0.4-4 mm across. Sample contains 35% reddish brown hornblende; 25% slightly sericitized plagioclase; 20% diopsidic clinopyroxene; 15% orthopyroxene; and 5% reddish biotite as a retrograde replacement around hornblende. Trace minerals include opaques, apatite, and chlorite.

55: texture: equigranular granoblastic; grains are 3-5 mm across. Sample contains 50% mildly chloritized diopsidic clinopyroxene; 25% greenish brown hornblende; 20% moderately chloritized orthopyroxene; and 5% biotite as a retrograde replacement within hornblende. trace minerals include plagioclase, opaques, apatite, and chlorite. A thin (0.05 mm) vein of calcite cuts across the thin section sample.

59: texture: equigranular granoblastic; grains are 4-5 mm across. Sample contains 50% brownish green hornblende, sometimes with blebs of opaque minerals exolved; 45% moderately sericitized plagioclase (An_{45}); and 5% moderately chloritized diopsidic clinopyroxene. Trace minerals include opaques both as individual grains and as exolution blebs within hornblende; biotite, apatite; zircon, and chlorite.

60: texture: equigranular granoblastic; grains are 2-4 mm across. Sample contains 40% olive green hornblende; 35% highly sericitized plagioclase; 20% holes (!); and 5% moderately

chloritized clinopyroxene. trace minerals include green biotite, chlorite, opaques, apatite, zircon, and sphene.

Group 3

46: texture: equigranular granoblastic; grains are 0.8-3 mm across. Sample contains 30% diopsidic clinopyroxene; 30% highly sericitized plagioclase (An_{55}?); 15% moderately chloritized orthopyroxene; 10% greenish brown hornblende; 10% garnet (!) (see below); 4% biotite. Trace minerals include opaques, chlorite, apatite, and zircon.

Garnet in this sample is much larger than other grains; one grain is 8 mm across. A break in this grain is filled with chlorite and a minute proportion of calcite. Smaller grains occur as round blebs distributed nearby the large grain, and these are in direct equilibrium with clinopyroxene, among other minerals.

49: texture: equigranular granoblastic; grains are 3-5 mm across. Sample contains 30% greenish brown hornblende; 30% highly sericitized plagioclase; 25% garnet as small rounded;blebs; 10% diopsidic clinopyroxene; and 3% highly chloritized orthopyroxene. Trace minerals include opaques, chlorite, biotite, apatite, and zircon.

Appendix B

Parameters used in mafic dike petrogenetic models

Trace-element model calculations were carried out using the equations of DePaolo (1981). Models involve both fractional crystallization (FXL) and combined assimilation and fractional crystallization (AFC). Two starting liquid compositions (C_0) were tested: average komatiite of Cattell and Arndt (1987) and the composition of sample 34 of this study (Table 1). Compositions of assimilate (C_a) include the bulk crust estimate of Taylor and McLennan (1985), average khondalite (SGG) from the Hunyuanyao area (Table 3) and average Archean tonalite (compiled from various sources). These compositions are listed below, along with bulk distribution coefficients (Bulk D) for the crystallization assemblages.

	C_0	Assimilant Compositions (C_a)			Bulk D	
	Komatiite	Bulk Crust	Khondalite	Tonalite	Komatiite	Basalt
Rb	9	32	104	50	0.009	0.096
Sr	33	260	366	460	0.00036	0.487
La	2.52	16	39	30	0.00004	0.495
Ce	3.74	33	82	50	0.00004	0.422
Nd	3.15	16	35		0.00006	0.0597
Sm	1.17	3.5	6.9	2.9	0.00052	0.0687
Eu	0.47	1.1	1.4	0.7	0.00074	0.5327
Tb		0.6	0.85	0.28	0.001	0.0769
Yb	1.21	2.2	2.77	0.5	0.0175	0.0646
Lu	0.18	0.3	0.434	0.1	0.03	0.0608
Y	13	20	30	7	0.00767	0.049
Nb	2	11	8.9	6	0.079	0.0097
Ta	0.1	1	0.62	0.5	0.107	0.0344
Zr	29	100	200	140	0.028	0.0291
Hf	1	3	6.63	3.5	0.076	0.0354
Sc	38	30	16	5	0.193	0.5659
Ti	3031	5400	4500	2100	0.768	0.1175
Cr	2320	185	108	40	5.57	1.18
Mg	19.9	5.3	2.8	1.1	1.48	1.1
Mn	0.22	0.18	0.08	0.04	0.5	0.66
Fe	12.3	10.11	6.65	3	0.59	0.2039
Co	110	29	14	10	2.132	0.6626
Ni	2000	105	21	15	4.089	6.58

Crystallizing modes used in the calculations are listed below. Individual mineral/melt distribution coefficients are combined in the proportions noted to calculate the bulk distribution coefficients above.

	Assemblage	Temperature	r_a/r_c
Komatiite Model	Olivine (90%) Spinel (10%)	1350°C	0.40
Basalt Model (C_0 = sample 34)	Olivine (10%) Clinopyroxene (20%) Plagioclase (70%) Magnetite (0.1%)	1100°C	0.25

Appendix C: Petrography of Khondalites

Petrographic analyses of khondalite samples preceded by a K are given below.

Sillimanite-Garnet Gneisses

11: texture: banded seriate; grains are 0.1-6 mm across. Microperthitic K-feldspar (30%) is mildly sericitized and has bent or broken twin planes and cleavage traces. Quartz (25%) occurs both as larger (up to 4 mm) strained grains with embayed or cuspate boundaries, and as small unstrained blebs within garnet. Sillimanite (20%) occurs as trains of crystallites within garnet porphyroblasts and in bands of larger grains (up to 4 mm long). Garnet (20%) occurs as subrounded porphyroblasts containing sillimanite, quartz, rutile, zircon, and biotite. Trace minerals include rutile, zircon, apatite, and biotite.

20: texture: banded seriate; grains are 0.1-5 mm across. Microperthitic K-feldspar (30%) is moderately sericitized and has bent or broken twin planes and cleavage traces. Quartz (30%) occurs both as larger (up to 4 mm) strained grains with embayed or cuspate boundaries, and as small unstrained blebs within garnet. Highly fractured garnet (20%) occurs as larger, subrounded porphyroblasts containing sillimanite, quartz, rutile, zircon, and biotite, and as smaller rounded grains that are relatively inclusion-free. Sillimanite (15%) occurs as trains of crystallites within garnet porphyroblasts and in bands of larger grains (up to 4 mm long); in one case it appears to have replaced chiastolite. Trace minerals include rutile, zircon, apatite, and biotite.

42: texture: banded seriate; grains are 0.1-3 mm across. Microperthitic K-feldspar (45%) is mildly sericitized and has bent or broken twin planes and cleavage traces. Highly fractured garnet (20%) occurs as subrounded porphyroblasts containing sillimanite, quartz, rutile, zircon, and biotite. Sillimanite (15%) occurs surrounded by either garnet or plagioclase. Quartz (15%) occurs both as larger (up to 4 mm) strained grains with embayed or cuspate boundaries, and as small unstrained blebs within garnet. Trace minerals include rutile, zircon, apatite, and biotite.

48: texture: banded seriate; grains are 0.1-3 mm across. Microperthitic K-feldspar (40%) is highly sericitized. Quartz (30%) occurs both as larger (up to 4 mm) strained grains with embayed or cuspate boundaries, and as small unstrained blebs within garnet. Garnet (20%) occurs as subrounded porphyroblasts containing sillimanite, quartz, rutile, zircon, and biotite. Sillimanite (5%) only occurs surrounded by garnet. Biotite (2%) is present as a retrograde alteration of garnet; sometimes it contains needles of rutile. Trace minerals include opaques, plagioclase, rutile, chlorite, muscovite/sericite, zircon, and apatite.

62: texture: coarse-grained granoblastic; grains are 3-5 mm across. Microperthitic K-feldspar (60%) is moderately sericitized. Highly fractured garnet (30%) occurs as subrounded porphyroblasts containing quartz, rutile, zircon, and biotite. Plagioclase (5%) is moderately sericitized. Quartz (1%) occurs only as small unstrained blebs within garnet. Biotite (1%) is present as a retrograde alteration of garnet; sometime it contains needles of rutile. Sillimanite is notably absent. Trace minerals include rutile, chlorite, muscovite/sericite, zircon, and apatite.

64: texture: seriate porphyroblastic; grains are 0.1-6 mm across. Microperthitic K-feldspar (35%) is moderately sericitized. Quartz (30%) occurs both as larger (up to 4 mm) strained grains with embayed or cuspate boundaries, and as small unstrained blebs within garnet. Garnet (20%) occurs as subrounded porphyroblasts containing sillimanite, quartz, rutile, zircon, and biotite. Sillimanite (10%) occurs as large single grains and smaller grains surrounded by either garnet or plagioclase. Trace minerals include opaques, plagioclase, rutile, chlorite, muscovite/sericite, zircon, and apatite.

65: texture: banded seriate porphyroblastic; grains are 0.1-6 mm across. Quartz (35%) occurs both as larger (up to 4 mm) strained grains with embayed or cuspate boundaries, and as small unstrained blebs within garnet. Microperthitic K-feldspar (25%) is moderately sericitized. Garnet (20%) occurs as subrounded porphyroblasts containing quartz, rutile, zircon, and biotite. Sillimanite (15%) occurs as large single grains defining a folded banding. Trace minerals include rutile, zircon, and apatite.

77: texture: seriate porphyroblastic; grains are 0.1-4 mm across. Quartz (30%) occurs both as larger (up to 4 mm) strained grains with embayed or cuspate boundaries, and as small unstrained blebs within garnet. Microperthitic and mesoperthitic K-feldspar (30%) is mildly sericitized. Garnet (15%) occurs as subrounded porphyroblasts containing sillimanite, quartz, rutile, zircon, and biotite. Sillimanite (15%) occurs as large single grains and as crystallites within garnet. Plagioclase (5%) is also mildly sericitized. Trace minerals include opaques, rutile, chlorite, muscovite/sericite, biotite, zircon, and apatite.

Sillimanite-Garnet Gneiss Subgroup

21: texture: seriate granoblastic; grains are 0.2-6 mm across. Plagioclase feldspar (50%; An_{30}?) occurs as large (4 mm across)grains and is moderately sericitized. Quartz (25%) occurs mainly in a band (vein?) but also thoroughout the sample. Garnet (20%) occurs as large irregular porphyroblasts and also as smaller hypidiomorphic grains; porphyroblasts contain inclusions of

quartz. Perthitic K-feldspar (5%) is moderately sericitized. Sillimanite is notably absent. Trace elements include opaques, chlorite, rutile, muscovite/sericite, zircon, and apatite.

Quartz-Garnet Gneisses

23: equigranular granoblastic; grains are 2-3 mm across. Quartz (65%) occurs as strained grains with embayed or cuspate boundaries, and rarely as small unstrained blebs within garnet. Plagioclase (15%; An_{45}?) is mildly sericitized. Microperthitic K-feldspar (10%) is also mildly sericitized and sometimes has tartan twinning (microcline). Garnet (5%) occurs as small irregular grains with rounded margins; often there are unstrained quartz blebs within. Trace minerals include rutile, zircon, and apatite.

45: equigranular granoblastic; grains are 2-3 mm across. Quartz (65%) occurs as strained grains with embayed or cuspate boundaries, and rarely as small unstrained blebs within garnet. Plagioclase (15%; An_{45}?) is mildly sericitized. Microperthitic K-feldspar (10%) is also mildly sericitized and sometimes has tartan twinning (microcline). Garnet (5%) occurs as small irregular grains with rounded margins; often there are unstrained quartz blebs within. Trace minerals include biotite, rutile, zircon, and apatite.

47: equigranular granoblastic; grains are 2-3 mm across. Quartz (50%) occurs as strained grains with embayed or cuspate boundaries, and rarely as small unstrained blebs within garnet. Plagioclase (25%) is highly sericitized, as is microperthitic K-feldspar (10%). Garnet (5%) occurs as small irregular grains with rounded margins; rarely there are unstrained quartz blebs within, and only one grain in the slide contains sillimanite crystallites. Trace minerals include rutilated chlorite, biotite, opaques, rutile, zircon, and apatite.

Quartz-Feldspar Gneisses

38: equigranular granoblastic; grains are 2-3 mm across. Microperthitic K-feldspar (50%) is highly sericitized. Quartz (25%) occurs as strained grains with embayed or cuspate boundaries, and rarely as small unstrained blebs within garnet. Plagioclase (15%) is highly sericitized. Garnet (5%) occurs as small irregular grains with rounded margins; often there are unstrained quartz blebs within. Trace minerals include biotite, chlorite, opaques, rutile, zircon, and apatite.

Other samples analyzed and reported by Liu, 1989.

Appendix D: Petrography of Granitic Rocks

Group 1

L15: equigranular granoblastic; grains are 1-3 mm across. Microperthitic K-feldspar (50%) is mildly sericitized and has non-perthitic boundaries. Quartz (35%) is mostly recrystallized to very small grains (mortar texture); otherwise it is found in garnet as strain-free blebs. Garnet (10%) occurs as small rounded grains, either with quartz inclusions, or associated with quartz in an "open sieve" or poikiloblastic texture. Sillimanite (3%) appears as randomly-distributed aggregates (glomerocrysts?). Trace minerals include reddish-brown biotite, rutile, opaques, and zircon.

L18: seriate; grains are 0.1-8 mm across. Microperthitic K-feldspar (50%) is moderately sericitized. Sodic plagioclase (20%; An_{10}) is mildly sericitized and often micrographic texture can be seen. Feldspars have bent and broken cleavage traces/twin planes. Quartz (15%) occurs in several varieties: vein or bull quartz is very coarse-grained (6-8 mm across) and shows highly undulose extinction, and recrystallized unstrained grains that are much smaller (0.3-0.5 mm across). Garnet (10%) occurs as subhedral grains with sparse inclusions of zircon and sphene. Trace minerals include sphene, hercynite, zircon, opaques, reddish-brown biotite and apatite.

L36: seriate; grains are 0.1-6 mm across. Microperthitic K-feldspar (40%) and sodic plagioclase (15%; An_{10}) are moderately sericitized and have bent/broken cleavage traces/twin planes. Quartz (20%) occurs in several varieties: very coarse-grained (up to 4 mm across) showing highly undulose extinction, and recrystallized unstrained grains that are much smaller (0.3-0.5 mm across). Garnet (15%) occurs as subhedral and anhedral grains with sparse inclusions of unstrained quartz. Reddish-brown biotite and chlorite (2%) occur as retrograde alterations of garnet. Trace minerals include opaques, hercynite, zircon, and apatite.

L40: foliated equigranular; grains are 0.5-1.5 mm across. Quartz (30%) occurs in several varieties: coarse-grained (up to 2 mm across) showing highly undulose extinction, and recrystallized unstrained grains that are much smaller (0.3-0.5 mm across). Sodic plagioclase (25%) and microperthitic K-feldspar (25%) are mildly sericitized; plagioclase shows complex twinning. Reddish-brown biotite (10%) delineates the foliation and also occurs as a retrograde alteration of garnet.Garnet (8%) contains inclusions of unstrained quartz, zircon, sphene, and opaques. Sillimanite (2%) is found in association with foliation planes. Trace minerals include opaques, hercynite, sphene, zircon, and apatite.

L41: seriate; grains are 0.1-4 mm across. Microperthitic K-feldspar (60%) and sodic plagioclase (10%; An_{10}) are moderately sericitized and have bent/broken cleavage traces/twin planes. Quartz (15%) occurs in several varieties: very coarse-grained (6-8 mm across) showing highly undulose extinction, and recrystallized unstrained grains that are much smaller (0.3-0.5 mm across). Garnet (10%) occurs as subhedral and anhedral grains with sparse inclusions of unstrained quartz. Trace minerals include reddish-brown biotite as a retrograde alteration of garnet, opaques, hercynite, zircon, and apatite.

Group 2

L29: equigranular granoblastic; grains are 0.5-1 mm across. Quartz (60%) occurs in several varieties: larger (up to 1.5 mm across) showing highly undulose extinction, and recrystallized unstrained grains that are much smaller (0.3-0.5 mm across). Sodic plagioclase (25%) is mildly sericitized and has bent or broken twin planes. Microperthitic K-feldspar (10%) often displays tartan twinning (microcline) and is mildly sericitized. Garnet (5%) occurs as rounded or amoeboid grains along a foliation. Trace minerals include opaques, rutile, sillimanite (2 grains), zircon, reddish-brown biotite, and a very limited thin vein of calcite.

L30: foliated seriate granoblastic; grains are 1-5 mm across, although most are 1.5-1.8 mm. Perthitic K-feldspar (60%) is mildly sericitized and forms the grains larger than 2 mm. Quartz (30%) has interlobate and polygonal borders. Garnet (5%) is amoeboid or stretched and has inclusions of quartz, rutile, opaques, and zircon. Sillimanite (3%) is fractured and strung out wih garnet along a foliation. Reddish-brown biotite (2%) occurs both as primary grains and as retrograde alteration of garnet. Trace minerals include opaques, rutile, zircon, and a single grain of hercynite.

L35: seriate, coarse-grained foliated; grains are 6-11 mm across. Perthitic K-feldspar (40%) is slightly sericitized and accounts for the largest grains. Sodic plagioclase (25%; An_{12}) is also slightly sericitized and has bent and broken twin planes. Feldspars rarely show micrographic texture. Quartz (25%) occurs mostly as large undulose grains with recrystallized boundaries. Garnet (5%) contains rutile needles, opaques, biotite and, very rarely, quartz blebs. Reddish-brown biotite (3%) defines a faint foliation and often occurs as a retrograde alteration of garnet. Trace minerals include opaques, zircon, rutile, chlorite,and apatite.

L42: no thin section is available.

Group 3

L3: seriate; grains are 1-6 mm across. Perthitic K-feldspar (38%) is moderately sericitized, as is sodic plagioclase (30%; An_{30}), and micrographic intergrowths are sometimes present. Quartz (30%) occurs as large broken crystals with recrystallized boundaries. Garnet (2%, but possibly underestimated due to plucking) appears skeletal and has strongly embayed boundaries. Trace minerals include sillimanite, sphene, opaques, zircon, and a single grain of hercynite enclosed in sillimanite.

L7: seriate, faintly banded; grains are 1-6 mm across. Quartz (45%) occurs as large broken grains with recrystallized borders. Perthitic K-feldspar (27%) is moderately sericitized. Sodic plagioclase (25%) is highly sericitized. Feldspars rarely show micrographic texture. Garnet (2%) is either skeletal and stretched, or equant, with inclusions of quartz, opaques, rutile, and zircon. Biotite (1%) occurs as unaltered flecks within quartz grains and partially altered to chlorite otherwise. Trace minerals include opaques, chlorite, muscovite, sillimanite, zircon, sphene, and apatite.

L23B: see below*

L33: foliated seriate; grains are 0.3-5 mm across. Perthitic K-feldspar (65%) is highly sericitized and forms the largest grains; twin planes are bent or broken. Quartz (30%) occurs as large broken crystals with recrystallized borders. Sillimanite (4%) occurs in anastomosing trains, commonly as glomerocrysts. Trace minerals include garnet, opaques, muscovite (which is pseudomorphic after sillimanite), zircon, and rutile.

Other Granitoids

L6: equigranular, fractured; grains are 1-2 mm across. perthitic K-feldspar (50%) is mildly sericitized and has bent or broken twin planes. Quartz (25%) has undulaose extinction and recrystallized borders. Garnet (25%) is skeletal. Trace minerals include abundant opaques, apatite, and zircon, and minor calcite.

L17: no thin section is available.

L22: no thin section is available.

L38: foliated, seriate; grains are 0.3-1 mm across. Mesoperthite (58%) is only slightly sericitized; exolution lamellae show a swirling pattern, and twin planes are bent or broken. Quartz (30%) occurs as large broken crystals with small recrystallized borders. Sillimanite (10%) occur in clusters of needles that define the foliation. Garnet (2%) occurs as equant grains with inclusions of

quartz, fibrous sillimanite, and hercynite. Trace minerals include opaques, hercynite, zircon, rutile, and apatite.

L39: foliated, seriate; grains are 0.3-6 mm across. Mesoperthite (55%) is mildly sericitized; twin planes are bent or broken. Quartz (40%) occurs as large broken crystals with small recrystallized borders. Sillimanite (4%) occur in clusters of needles that define the foliation. Garnet (1%) occurs as stretched grains with inclusions of quartz, fibrous sillimanite, and hercynite. Trace minerals include opaques, hercynite, zircon, rutile, and apatite.

* L23 is an example of the migmatitic zone, where "liquid" granitic magma (and any residual material it was carrying) appear to be escaping from the khondalite host. The sample from which the slide was made is divided into these two separate portions: L23A is the khondalite residue portion, and L23B is the escaping magma portion.

Plates

Plate 1: Compositional banding in khondalites is preserved within moderately-developed quartz + feldspar leucosome. Note segregation and enlargement of garnet crystals (small round dark blebs) in leucosome.

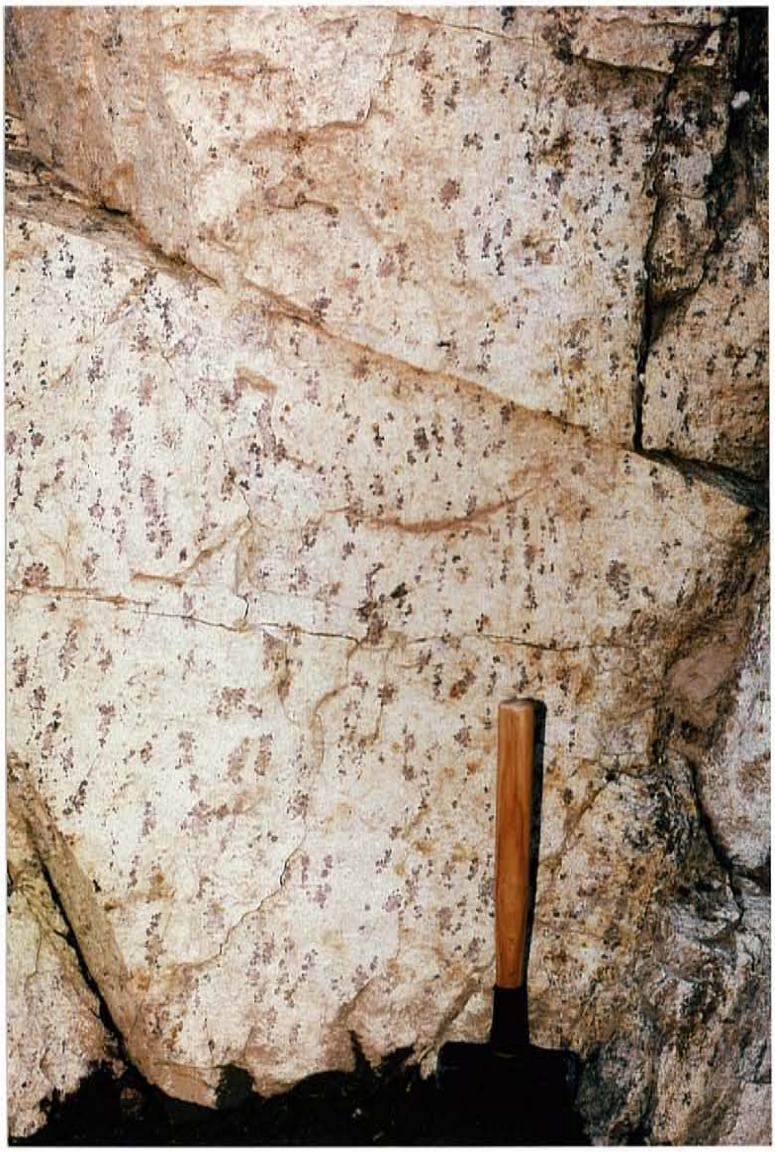

Plate 2: Glomerocrysts of garnet developed in a medium-grained granite body, Liangchen area, Nei Mongol, China.

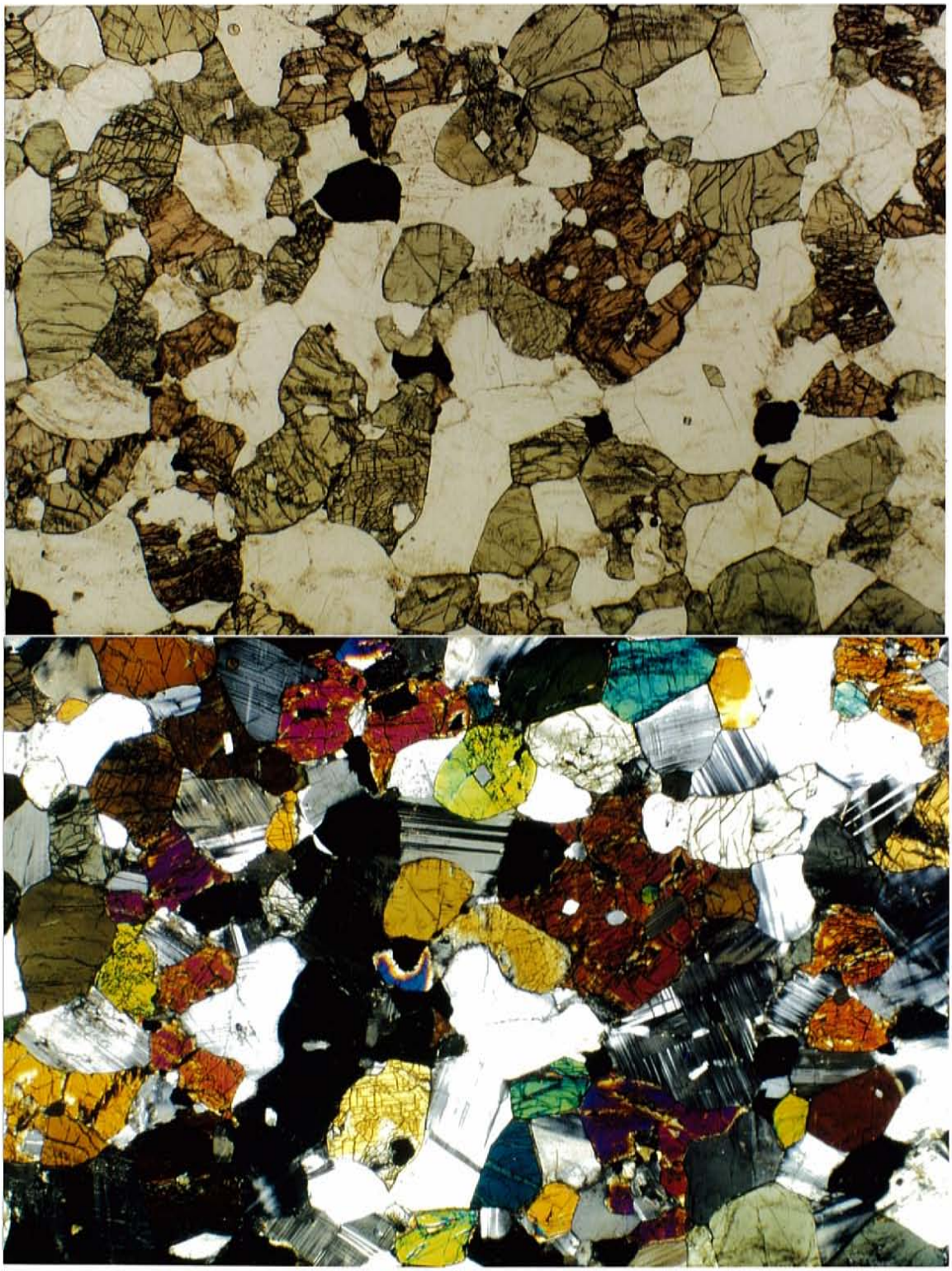

Plate 3: Photomicrograph of typical Group 1 mafic dike under (a) plane polarized light (top) and (b) crossed nichols (bottom). Minerals include orthopyroxene (light greenish yellow, with low birefringence, 90° cleavage, straight extinction), clinopyroxene (light green, moderate birefringence, 90° cleavage, inclined extinction), hornblende (dark green and brown, 120° cleavage, pseudomorphic after pyroxene), plagioclase feldspar (clear; slightly sericitized), and opaque minerals. Field of View = 6.5 mm × 4.33 mm.

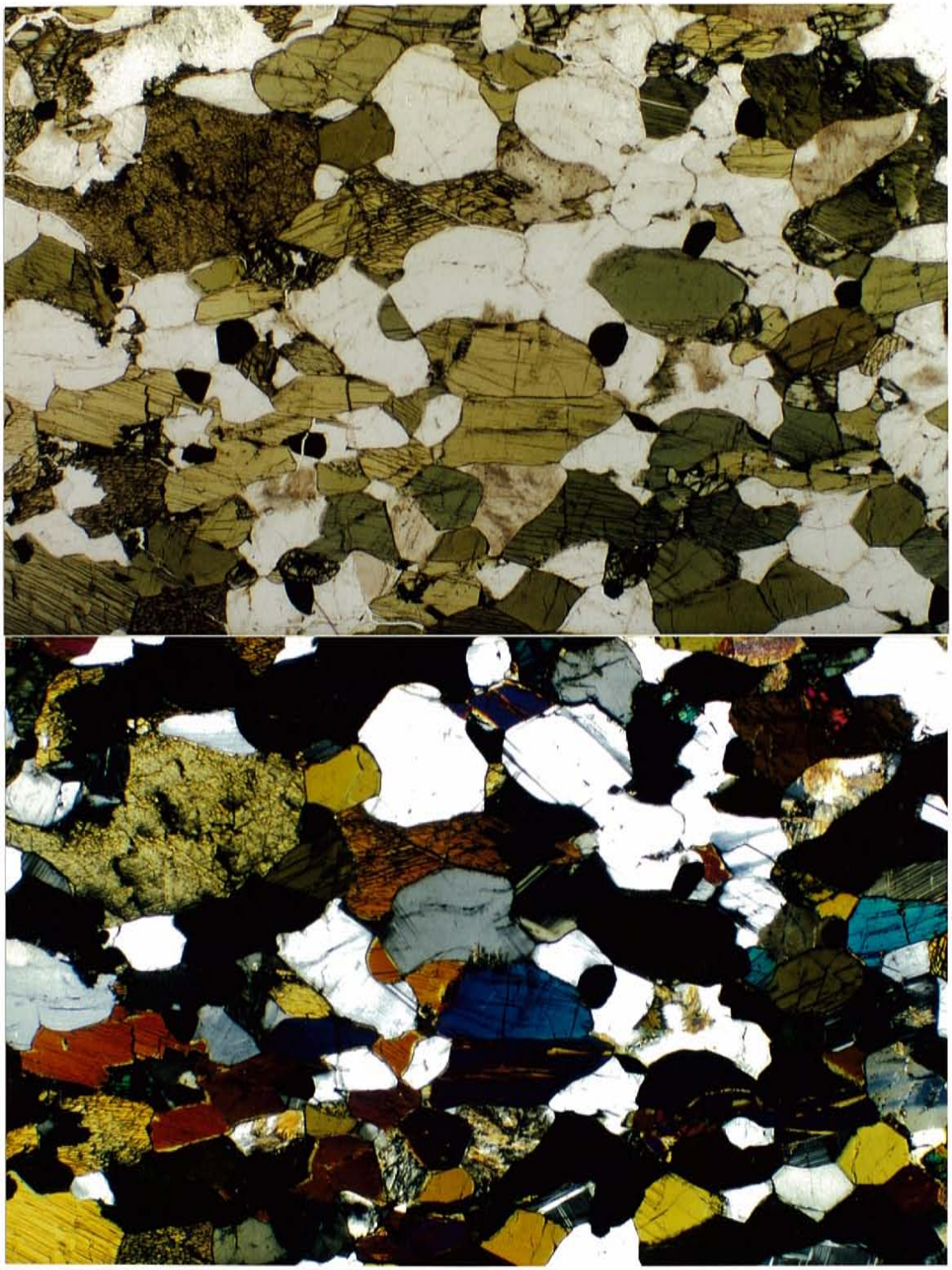

Plate 4: Photomicrograph of typical Group 2 mafic dike under (a) plane polarized light (top) and (b) crossed nichols (bottom). Minerals include orthopyroxene (light greenish yellow, with low birefringence, 90° cleavage, straight extinction; see upper right corner), clinopyroxene (light green, moderate birefringence, 90° cleavage, inclined extinction), hornblende (dark green and brown, 120° cleavage, pseudomorphic after pyroxene), plagioclase feldspar (clear; slightly to strongly sericitized), and opaque minerals. Field of View = 6.5 mm × 4.33 mm.

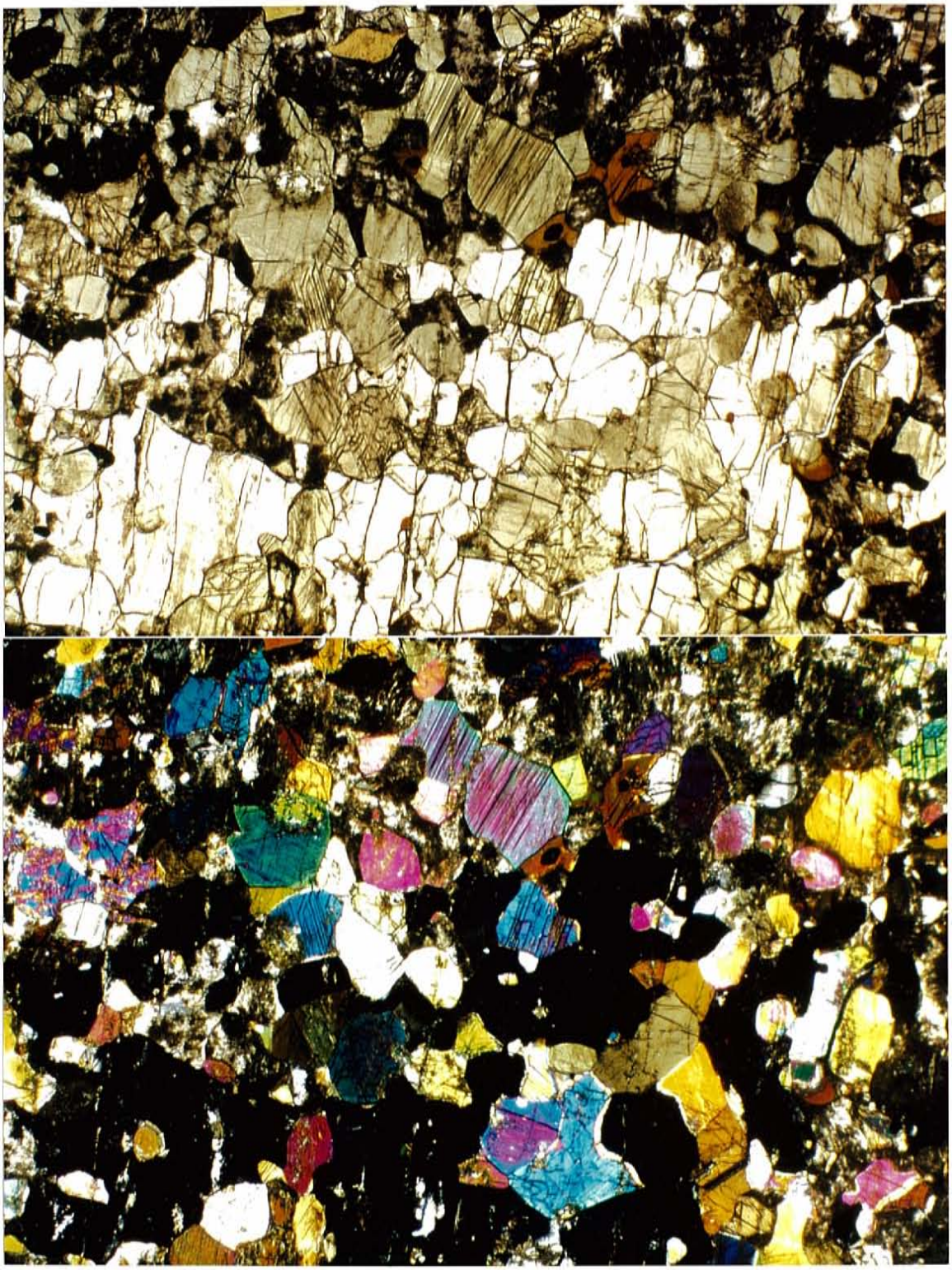

Plate 5: Photomicrograph (note: slide is thick) of Group 3 mafic dike under (a) plane polarized light (top) and (b) crossed nichols (bottom). Minerals include orthopyroxene (not found in this view), clinopyroxene (light green, moderate birefringence, 90° cleavage, inclined extinction, see upper right), hornblende (dark green and brown, 120° cleavage, pseudomorphic after pyroxene, partially replaced by biotite), plagioclase feldspar (cloudy; strongly sericitized), garnet (clear, uniaxial) and opaque minerals. Field of View = 6.5 mm × 4.33 mm.

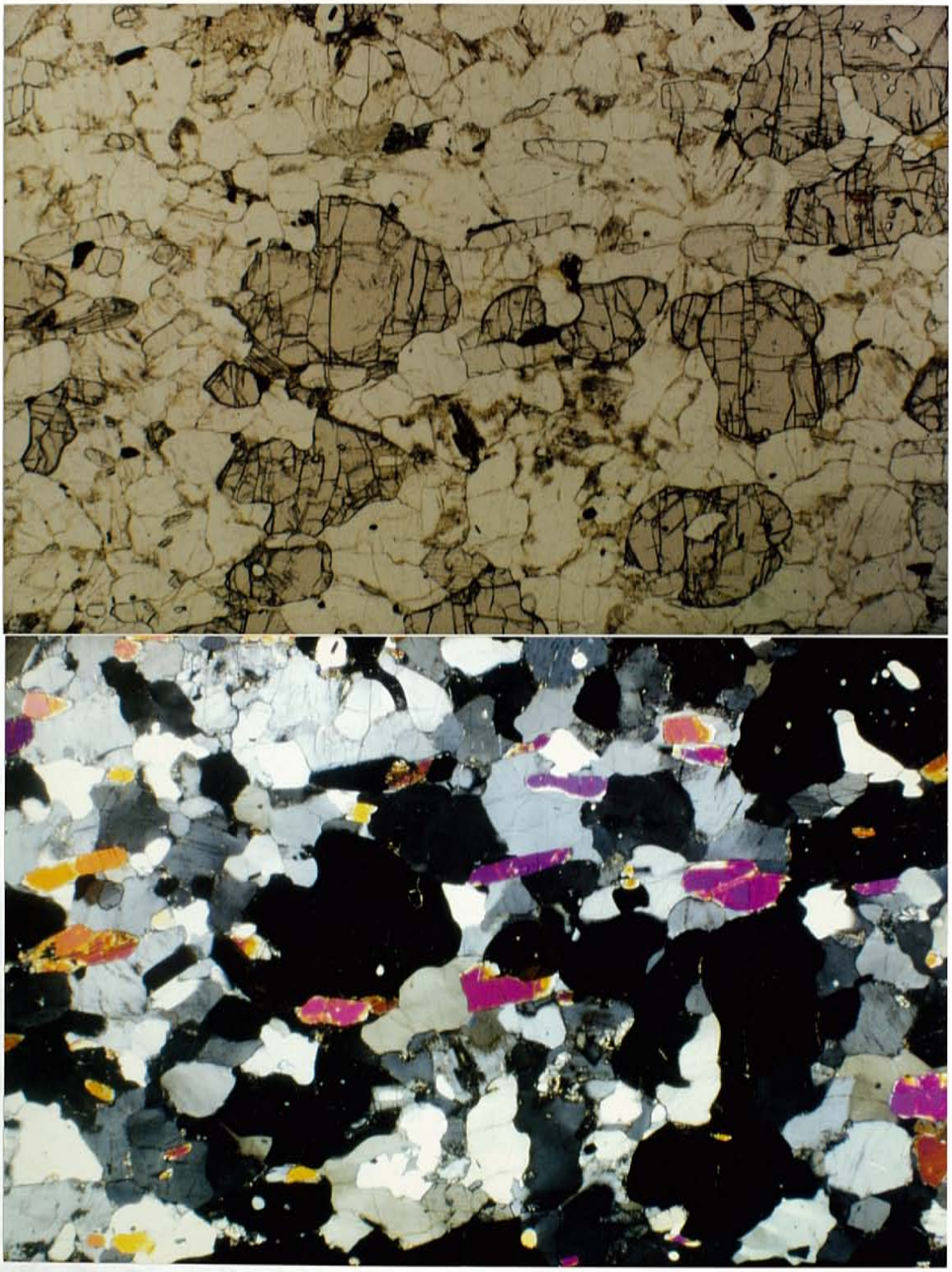

Plate 6: Photomicrograph of sillimanite-garnet gneiss (SGG) under (a) plane polarized light (top) and (b) crossed nichols (bottom). Minerals include quartz and feldspar (clear, low refractive index; feldspars are slightly sericitized), sillimanite (clear, elongated, high refractive index and moderate birefringence), garnet (pink, uniaxial), and opaque minerals. Trace minerals include sphene (dark brown), apatite and zircon. Field of View = 6.5 mm × 4.33 mm.

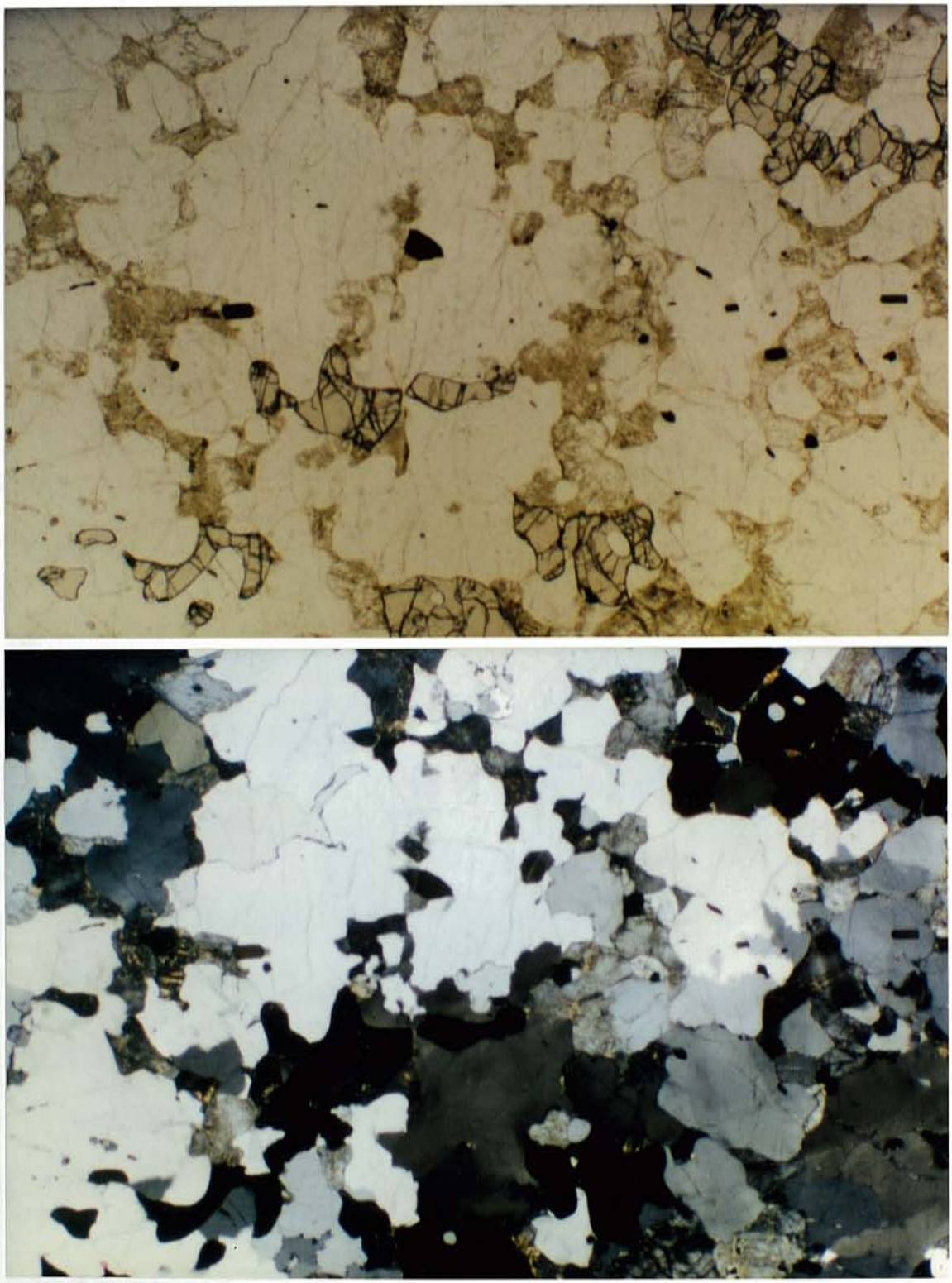

Plate 7: Photomicrograph of quartz-garnet gneiss (QGG) under (a) plane polarized light (top)and (b) crossed nichols (bottom). Minerals quartz and feldspars (clear, low refractive index; feldspars are moderately sericitized), garnet (pink, uniaxial), and opaque minerals. Trace minerals: sphene (dark brown), apatite and zircon. Sillimanite is virtually absent in this view. Field of View = 6.5 mm × 4.3 mm.

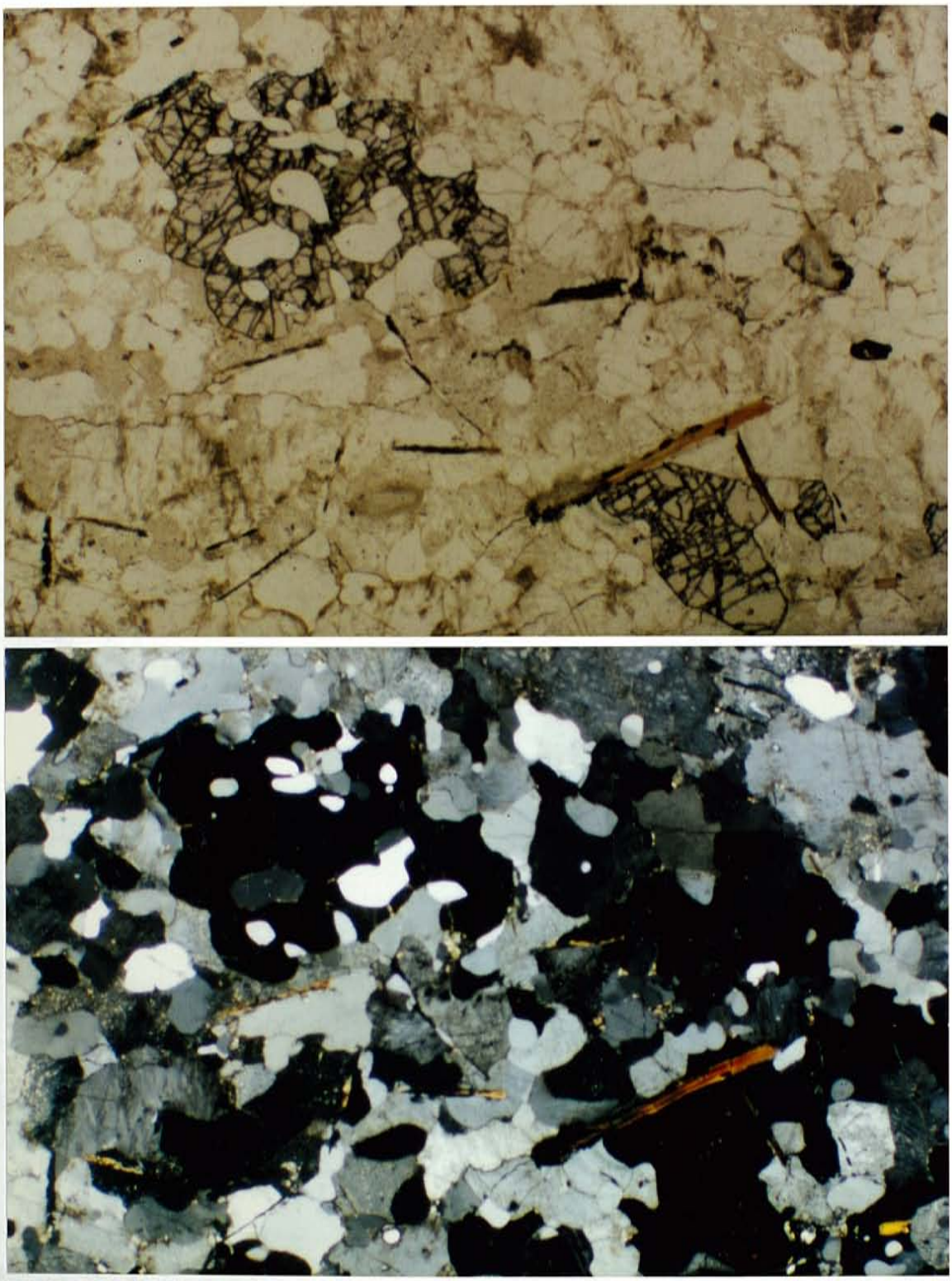

Plate 8: Photomicrograph of typical quartz-feldspar gneiss (QFG) under (a) plane polarized light (top) and (b) crossed nichols (bottom). Minerals include quartz and feldspars (clear, low refractive index; feldspars are moderately sericitized), garnet (pink, uniaxial), and opaque minerals. Biotite appears in this view as long brown laths. Field of View = 6.5 mm × 4.33 mm.

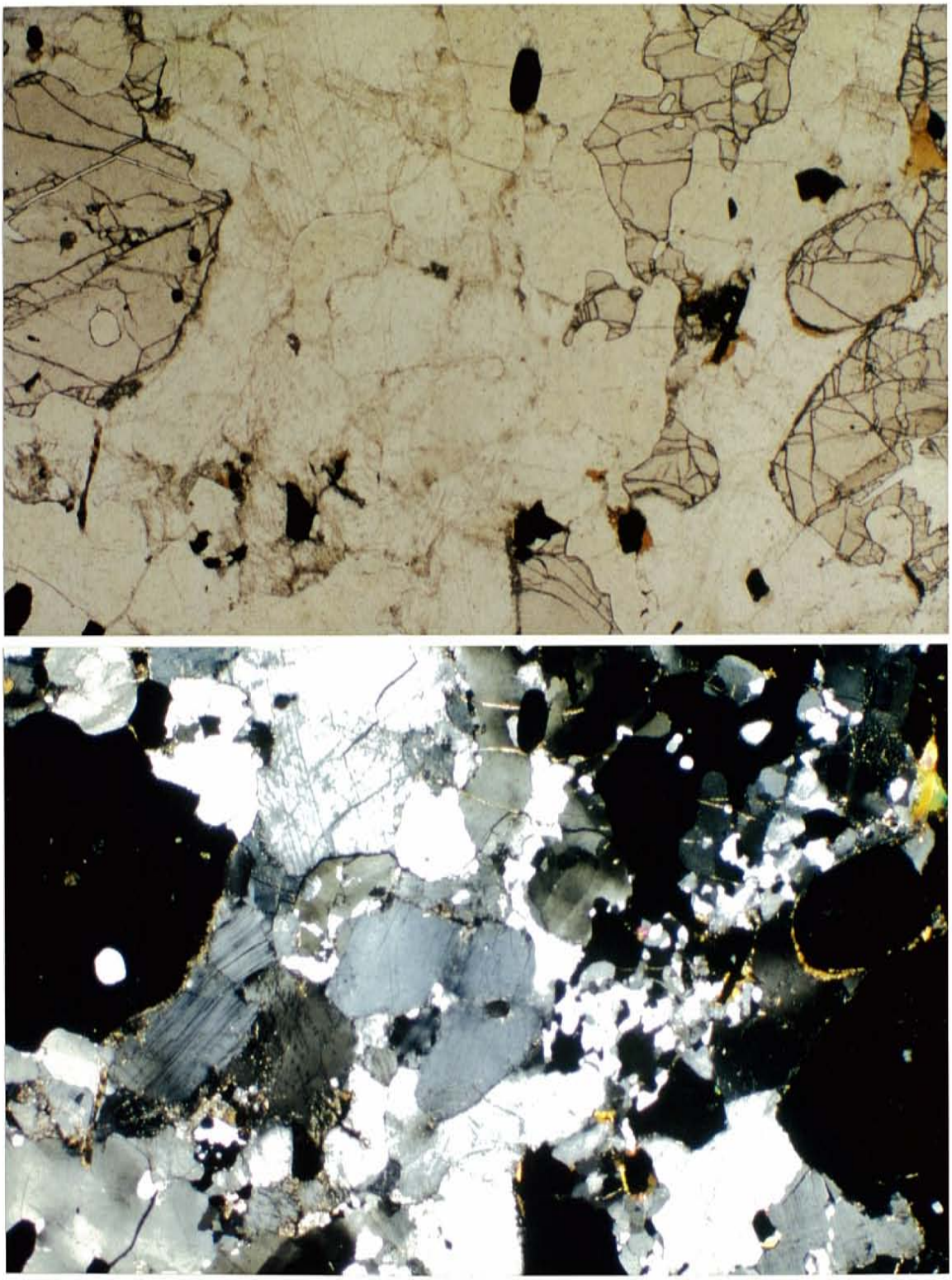

Plate 9: Photomicrograph of typical granitoid under (a) plane polarized light (top) and (b) crossed nichols (bottom). Minerals include quartz and feldspar (clear; feldspars are slightly sericitized, with bent/broken cleavage traces), garnet (pink, uniaxial), and opaque minerals; biotite occurs as alteration product around opaques and garnet. Field of View = 6.5 mm × 4.33 mm.

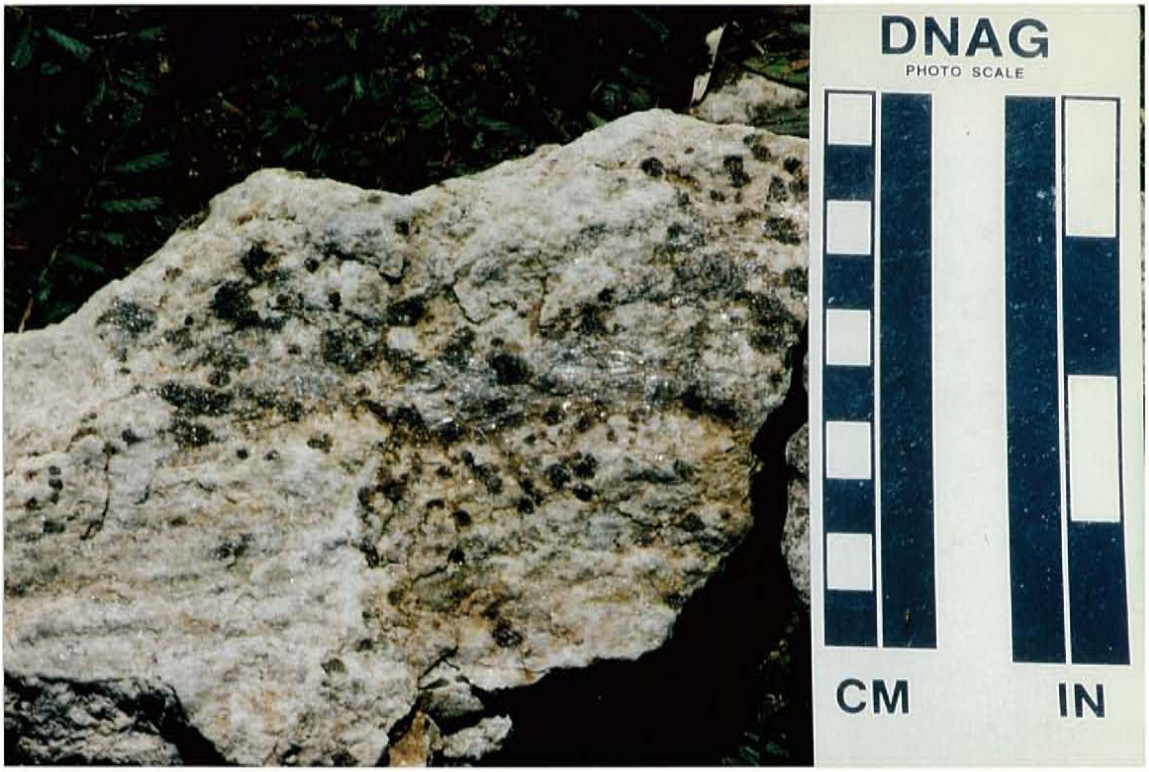

Plate 10: Concentration of residual garnet (dark red blebs) and sillimanite (silvery streak in center of sample) from schlieren in partial melting zone of the Liangchen region.

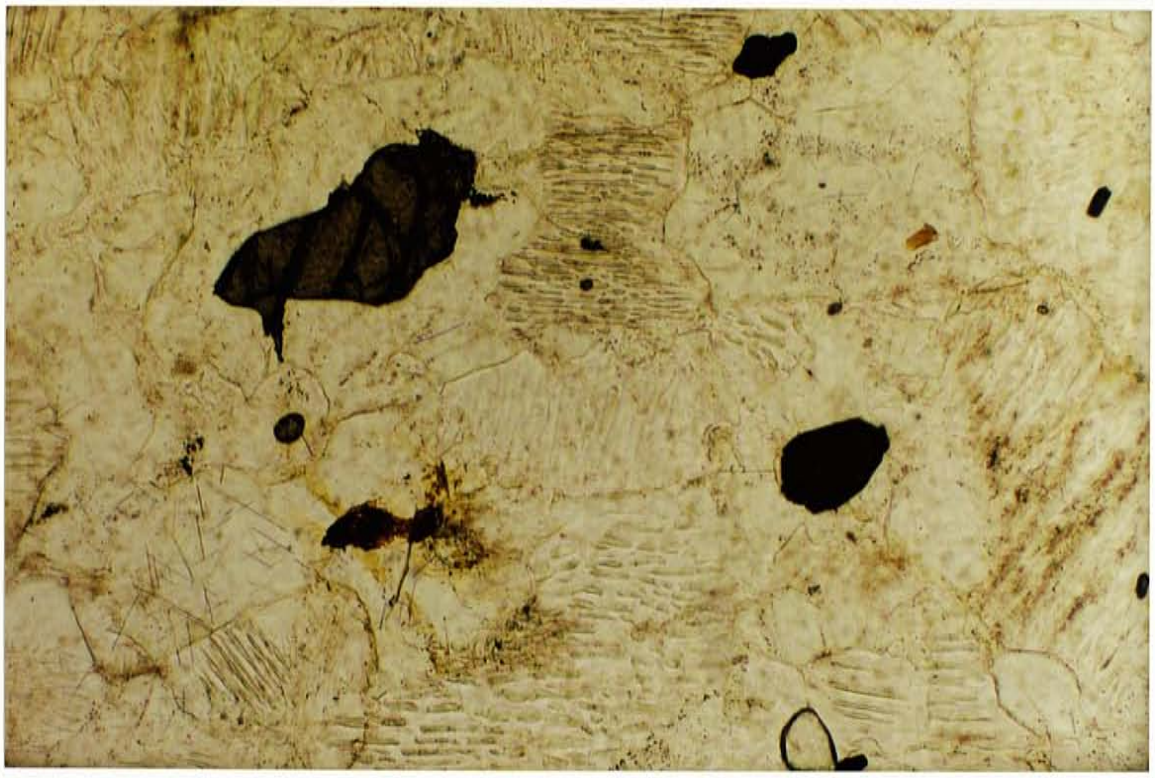

Plate 11: Photomicrograph of trace minerals hercynite (large green bleb), zircon (small bleb beneath hercynite), rutile (opaque-looking terminated prism, just above center of right edge, and as needles, lower left) and apatite (clear, very high refractive index, lower right) with perthitic feldspar in granitoids. Field of View: 1.30 mm × 0.87 mm.

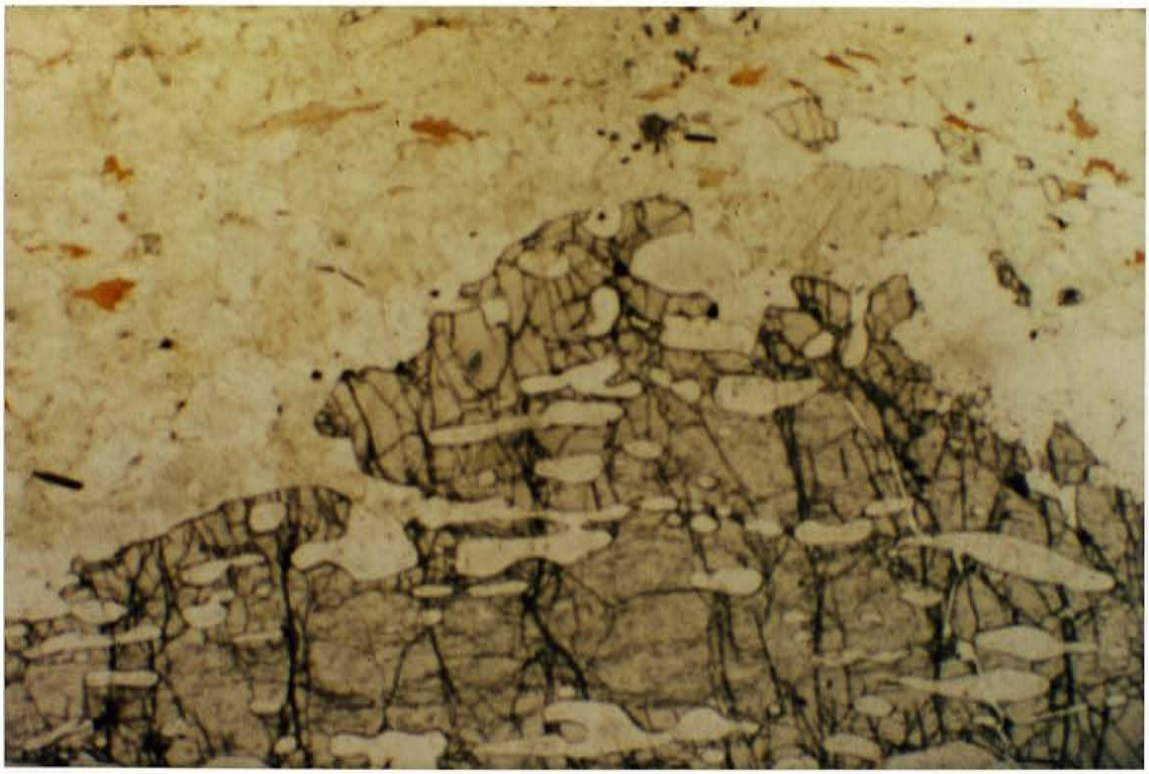

Plate 12: Photomicrograph of garnet-rich border (bottom) of leucosome (top). Garnet contains quartz. Leucosome contains quartz and feldspar (clear groundmass), sillimanite (high refractive index, good cleavage) and minor biotite (reddish-brown). Field of View = 6.5 mm × 4.33 mm.